The impact of raw material selection on damring formation and pre-reduction during ferrochrome production

Y Van Staden

orcid.org 0000-0002-6145-7640

Thesis submitted in fulfilment of the requirements for the degree *Doctor of Philosophy in Chemistry* at the North-West University

Promoter: Prof JP Beukes

Co-promoter: Prof PG van Zyl

Graduation October 2018

20667744

Preface

This thesis was submitted in fulfilment to the exit level outcomes, as prescribed by the A-rules of the North-West University. Additionally, the results from Chapter 4 and 5 were published as an article in Materials and Metallurgical Transaction B, a high impact factor, internationally accredited, peer reviewed journal. The published paper is included in the appendix. Additionally, it is the intention of the candidate to also publish the results from Chapter 6 in a high impact factor, internationally accredited peer reviewed journal.

Acknowledgements

"I have set the Lord continually before me; because He is at my right hand, I will not be shaken. Therefore my heart is glad and my glory [my innermost self] rejoices" – Ps. 16:8-9

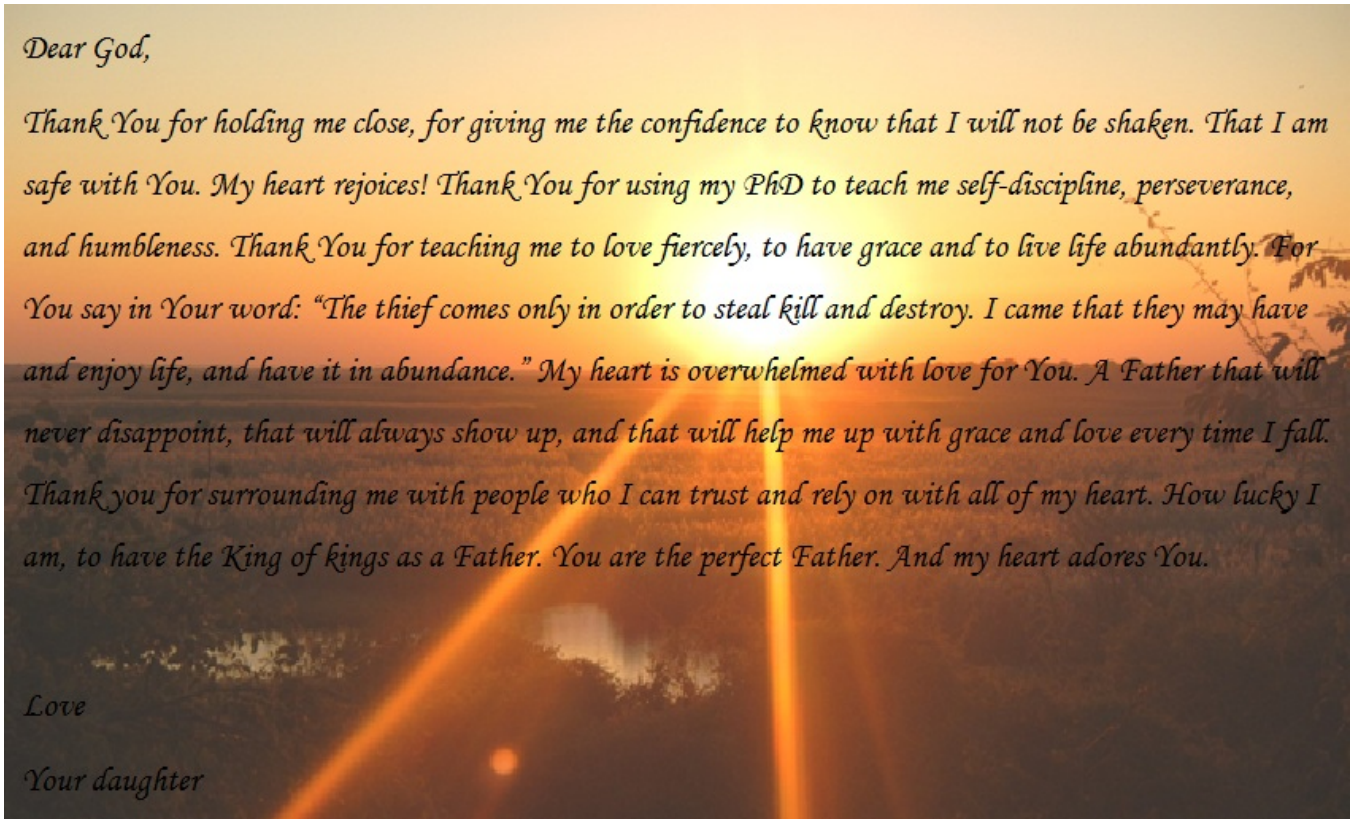

Prof Paul Beukes, I hardly have the words to convey my gratitude for all you have done for me. Thank you for all your support and being a committed supervisor and also a committed “academic father”. I have learned so much from you. Thank you for caring not only about my work, but caring about me as a person. The life lessons I have learned from you are more value than any academic degree I could receive.

I would also like to thank my co-supervisor, Prof Pieter van Zyl for you for all your guidance and support through the years.

My husband, Marco Coetsee, thank you for the amazing support you have given me. I have never met anyone with such a beautiful character. Your patience, love and support overwhelm me and I am so grateful. You are my favourite!

I would also like to thank Retha Peach for being my cheerleader, for all the lunch time conversations and encouragement during the last couple of years. Thank you for being my voice of reason and for making my life so much more exciting and filled with adventure.

To my fellow students, Ralph Glastonbury, Kerneels Jaars and Faan du Preez, thank you for always being willing to listen and help, even at times when it annoyed you! Sharing an office with you has been a privilege.

A special thanks to my parents Schalk van Staden and Lani Joubert, for all the years you have supported and encouraged me. And to my siblings, Schalk van Staden (Jnr) and Leani van Staden for all the years filled with of tears and laughter. Thank you that we can always stick together.

Tanya Pienaar, my best friend. Thank you for all the voice notes, prayers and encouragement over our 11 (and counting) years of friendship. We messed up together, grew together, and today we stand not only as best friends, but as sisters in Christ.

I would also like to acknowledge the National Research Foundation (NRF) for providing financial assistance towards this PhD study (Grant UID: 89398).

Abstract

Electricity consumption is the largest cost component in the production of ferrochrome (FeCr). Currently the pelletised chromite pre-reduction process (solid-state reduction of chromite) is the process option with the lowest specific electricity consumption (MWh/ton). In this process, composite chromite pellets are pre-reduced at approximately 1300 °C in a rotary kiln. Excessive damring formation (material build-up) in the rotary kiln requires routine shutdowns to remove it, which cause damage to the kiln refractory and result in loss of revenue due to the break in the production of pre-reduced pellets. Damring formation can be caused by: i) melting of the ash of the pulverised fuel (PF) coal, which is used to fire the kiln, and/or ii) partial melting of the chromite pellets and/or pellet fragments.

Ash fusion temperatures (AFT) of twenty different carbonaceous samples were evaluated to assess the temperature at which the PF coal ash will start to contribute to damring formation. The softening temperature (T_{soft}), as determined with AFT analysis, was assumed to be the lowest temperature at which PF coal ash could start contributing to damring formation. The results indicated that the reducing and oxidising T_{soft} of the carbonaceous materials differ substantially from one another, with many of these being below the typical material temperature in the pre-reduction kiln (~ 1300 °C). Therefore, PF coal ash can contribute significantly to damring formation. Multiple-linear regression (MLR) analysis was used for derive optimum MRL equations that could be used to relatively accurately calculate/predict reducing T_{soft} and oxidising T_{soft}. The equations will enable FeCr producers to select PF coals, in order to limit damring formation. The mathematical information obtained by the MLR analyses were also converted into a chemical context, by considering the relatively importance of the independent parameters included in the optimum MLR equations. This indicated that the PF ash composition, which is currently not considered by FeCr producers when selecting PF coals, is very important to minimise damring formation.

Sessile drop tests were used to assess the softening behaviour of seven different fine chromite ores, as well as the softening behaviour of composite chromite pellets (containing the afore-mentioned ores) and the other pellet components (a carbonaceous reductant and a clay binder). The first sign of deformation detected during the sessile drop tests (deformation temperature), was taken as the lowest temperature at which the pellets and/or pellet components could start contributing to damring formation. The results proved that the composite pellet mixtures had significantly lower deformation temperatures than the ores alone. However, the deformation temperatures of the ores and pellet mixtures were above the typical material temperature expected in a pre-reduction rotary kiln (~ 1300 °C), therefore these materials are expected to contribute less significantly to damring formation than PF coal ash. Actual damrings were also analysed using scanning electron microscopy (SEM) with energy dispersive x-ray spectroscopy (EDS), which indicated that the damrings contained significant amounts of Cr and Fe (chromite or chromite derived particles). However, the matrix that bound these particle together most likely originated from PF coal ash. Interestingly, the sessile drop results also demonstrated that UG2 ore will not necessarily contribute more to damring formation than metallurgical grade chromite ore (which is currently assumed by FeCr producer). In order to assess the possible contribution of ores to damrings, the liberation of gangue minerals need to be considered, rather than the chemical composition of the ores.

In addition to investigating damring formation, it was also attempted to correlate thermo-dimensional changes of composite chromite pellets to pre-reduction. This was done by first designing, constructing, commissioning and testing (to verify the accuracy thereof) a large mass thermo-gravimetric analyser (TGA). This was necessary, since the gas environment inside the pre-reduction rotary kiln is partially oxidising to allow for PF combustion, but also partially reducing due to the partial positive CO pressure inside the composite pellets (creating a reducing atmosphere inside the pellets themselves and in the pellet bed). This complex environment could not be recreated using a small mass commercial TGA. The results from the large mass TGA compared very well with the thermo-mechanical analysis (TMA) measurements, with both instruments

indicating maximum rate of Fe and Cr reduction at 780 and 1380 °C, respectively. Therefore, it was concluded that thermo-dimensional changes can indeed be used to follow chromite pre-reduction.

Keywords: Damring formations; solid-state reduction of chromite; chromite pre-reduction; ash fusion temperatures; sessile drop test; thermo-gravimetric analysis (TGA); thermo-mechanical analysis (TMA)

Table of contents

List of Tables

List of Figures

List of abbreviations

Only less commonly known abbreviations are listed. Well known subject specific abbreviations (e.g. C, H, Fe etc.) are not listed below, but are still defined in the text.

AC	Alternating current
AFT	Ash fusion temperature (°C)
CDR	Chrome Direct current
CMI	Consolidated Metallurgical Industries
CV	Calorific value
Cr/Fe	Chrome to iron ratio
DC	Direct current
DTG	Differential mass loss
DTMA	Differential dimensional change
FC	Fixed carbon
FeCr	Ferrochrome
ICP	Inductively Coupled Plasma
LG6	Lower group 6
MC	Moisture content
MLR	Multiple-linear regression
MG1	Middle group 1
MG2	Middle group 2
OES	Optical emission spectrometry
PF	Pulverised fuel
PGM's	Platinum group metals
RMSE	Root mean square error
SAF	Submerged arc furnace
UG2	Upper group 2
XRD	X-ray diffraction
SABS	South African bureau of standards
SEC	Specific electricity consumption (MWh/ton)
SEM	Scanning electron microscope
SRC	Solid-state reduction of chromite
TGA	Thermo-gravimetrical analysis
TMA	Thermo-mechanical analysis
T_{indef}	Initial deformation temperature (°C)
T_{hem}	Hemispherical temperature (°C)
T_{soft}	Softening temperature (°C)
T_{fluid}	Fluidised temperature (°C)
UG 2	Upper group 2
VM	Volatile matter
XRD	X-ray diffraction
XRF	X-ray fluorescence

Chapter 1

Background, motivation and objectives

In this chapter, a brief background of the chromite and ferrochrome (FeCr) industry in South Africa is discussed. There after the motivation for this study is presented, which led to the main aims being identified (Section 1.1). The general aims are again stated in Section 1.2, together with the specific objectives and the strategies of how these objectives were approached.

1.1 Background and motivation

Chromite is a mineral with a spinel crystalline structure with $FeCr_2O_4$ being the theoretical pure chemical composition (Edwards and Atkinson, 1986). However, chromite is rarely pure, therefore it is usually characterised by the formula $[(Mg,Fe^{2+})(Al,Cr,Fe^{3+})_2O_4]$ (Haggery, 1991). Chromite is an essential mineral, since it is the only commercially recoverable source of new chromium (Cr) units (Murthy *et al*., 2011; Riekkola-Vanhanen, 1999). Chromium has many uses in metallurgical, chemical and refractory applications. The application of importance in this study is the production of alloys and more specifically the production of ferrochrome (FeCr). FeCr is a relatively crude alloy used mainly in the production of stainless steel, which is a vital alloy in modern day society. Cr contributes to the hardness of stainless steel and makes it corrosion resistant due to the formation of a strong dense, nonporous chromium(III)oxide (Cr_2O_3) surface layer that forms when it comes in contact with atmospheric oxygen (Jacobs and Testa, 2005). According to Rao (2010), approximately 90% of all mined chromite is consumed in the production of FeCr.

South Africa holds approximately three quarters of the world's viable chromite reserves and was the world's leading FeCr producer in 2011 with 36% market share of the global annual high carbon FeCr production. However, since 2012 China has been the leading producer (ICDA, 2013). South Africa's reduced FeCr production can largely be ascribed to the shortage and steep price increases of electricity (Kleynhans *et al.*, 2012), which is the single largest cost component in FeCr production (Daavittla *et al*., 2004). It is therefore important

for FeCr producers to use processes to minimise energy consumption. Several of these processes have been developed and commercialised (McCullough *et al*., 2010; Naiker and Riley, 2006; Takano *et al*., 2007). One of these processes was developed by Showa Denko in the 1970's, i.e. solid-state reduction of chromite (SRC), or otherwise known as pelletised chromite pre-reduction. This process was modified and is being applied by Glencore Alloys at two large smelters in South Africa (i.e. Lydenburg operations and the Lion Ferrochrome smelter) (Naiker, 2007). With increasing FeCr production in China, FeCr smelters applying this process have also been developed there (Basson and Daavittila, 2015). However, information regarding these smelters was not yet available in the public peer reviewed domain when this thesis was written. Glencore Alloys refers to their application of pelletised chromite pre-reduction as the Premus process (Naiker, 2007). This process has the lowest specific electricity consumption (SEC) (i.e. MWh/ton FeCr) and is associated with high Cr recovery. It is also more environmentally friendly than the conventional process in some respects, e.g. lower Cr(VI) generation and availability of CO rich off-gas as energy source (Naiker, 2007).

In the pelletised chromite pre-reduction process raw materials (chromite ore, reductants and binder clay) are dry milled, pelletised, as well as dried and pre-heated, where after the pellets are fed to a counter current rotary kiln where chromite pre-reduction takes place. These hot, pre-reduced pellets are fed directly into a closed submerged arc furnace (SAF). Feeding the hot, pre-reduced pellets into the SAF further reduces the amount of energy required for the smelting process (Beukes *et al*., 2010; Naiker, 2007). The pre-reduction level achieved, which related to metallisation of up to 90% for iron (Fe) and 50% for Cr, in combination with the heat energy transferred from the kiln, reduce SEC during the smelting process by up to 40% (McCullough *et al*., 2010). The process also enables the consumption of fine chromite ores and reductants (which are less expensive that the coarse materials), and allows for operational control of the SAF that enables a low silicon (Si) and sulphur (S) containing FeCr alloy to be produced (Takano, 2007). Both the afore-mentioned elements are usually indicated as key FeCr specifications by stainless steel producers. According to Naiker (2007), another advantage is the low lumpy coke consumption during the smelting step and replacement of coke with less expensive reductants such as anthracite. Disadvantages associated with this process are the higher capital cost (Naiker, 2007) and extensive operational control that is required due to variation in pre-reduction levels and carbon (C) contents of the pre-reduced pelletised furnace feed material (Mohale *et al*., 2017).

Several studies have been conducted on different aspects of chromite pre-reduction, with just a few mentioned here. Dawson and Edwards (1986) indicated that the overall reduction process could be enhanced by the addition of a fluorspar (CaF_2), as a fluxing agent, to cause disruption in the formation of a magnesia-chromite spinel. Several other fluxes and/or additives have also been investigated (e.g. Weber and Eric, 2006; Nunnington and Barca, 1989). Neizel *et al.* (2013) proved that the addition of $CaCO_3$, which is used as a flux in the SAF smelting of pre-reduced pellets, could enhance chromite pre-reduction. However, this addition decreased the compressive and abrasion strengths of the pre-reduced pellets to such an extent that it is not feasible. Kleynhans *et al.* (2012 and 2017) investigated the effects of clay binder and carbonaceous reductant selections. Several studies have also focussed on the fundamental reaction mechanisms of chromite pre-reduction (e.g. Takano et al, 2007).

In this study several remaining research questions with regard to chromite pre-reduction will be considered. Chromite pre-reduction applied on an industrial scale takes place in a counter current rotary kiln. Pellets are fed into the kiln and heated to approximately 1300 °C. Cross- and longitudinal sectional cut illustrations of a typical rotary kiln with pelletised feed that is used in the chromite pre-reduction process is presented in Figure 1.1

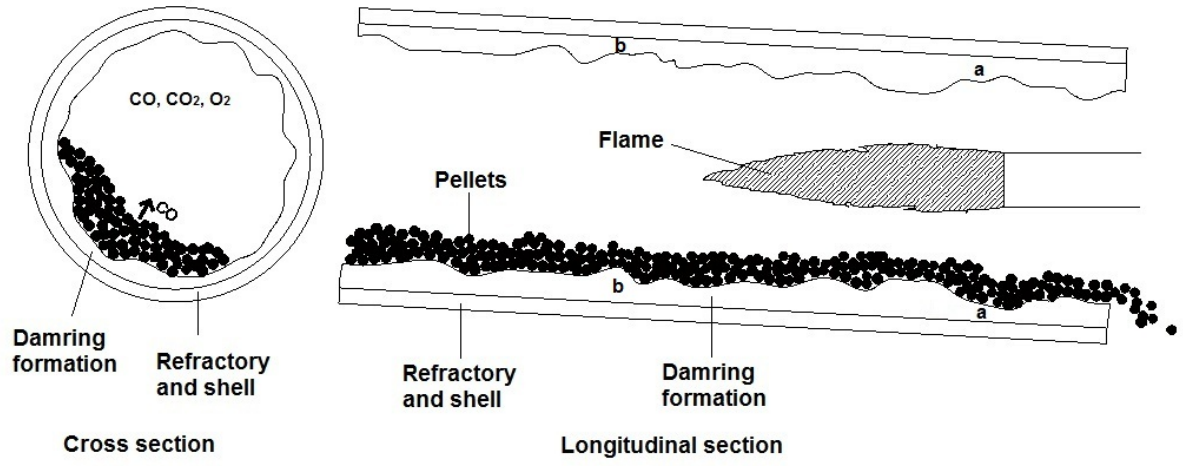

Figure 1.1: Illustration of the cross and longitudinal sections of a rotary kiln used in pelletised chromite pre-reduction.

During chromite pre-reduction, damrings (material build-up) are formed in the kiln (Figure 1.1). These damrings can have positive and/or negative impacts on the process. Limited damring formation can protect the refractory lining of the kiln. It is also known that limited damring formation in strategic areas (e.g. marked with "a" in Figure 1.1) can increase the retention time of the pellets in the kiln hot zone, therefore enhancing pre-reduction levels.

However, if damring formation is too extensive it compromises material throughput. Also, excessive damring formation in certain areas (e.g. marked with "b" in Figure 1.1) can actually increase the effective slope that the chromite pellets experience in the kiln, which will lead to shorter retention time and lower pre-reduction levels. Currently, routine shutdowns have to be performed on chromite pre-reduction kilns to break out the damrings in order to maintain the desired throughput. This mechanical breaking of the damrings can cause extensive damage to the refractory of the rotary kiln. Figure 1.2 presents a photo taken during a relatively recent shutdown of a chromite pre-reduction kiln. In the photo, the extent of damring formation inside the kiln can be seen.

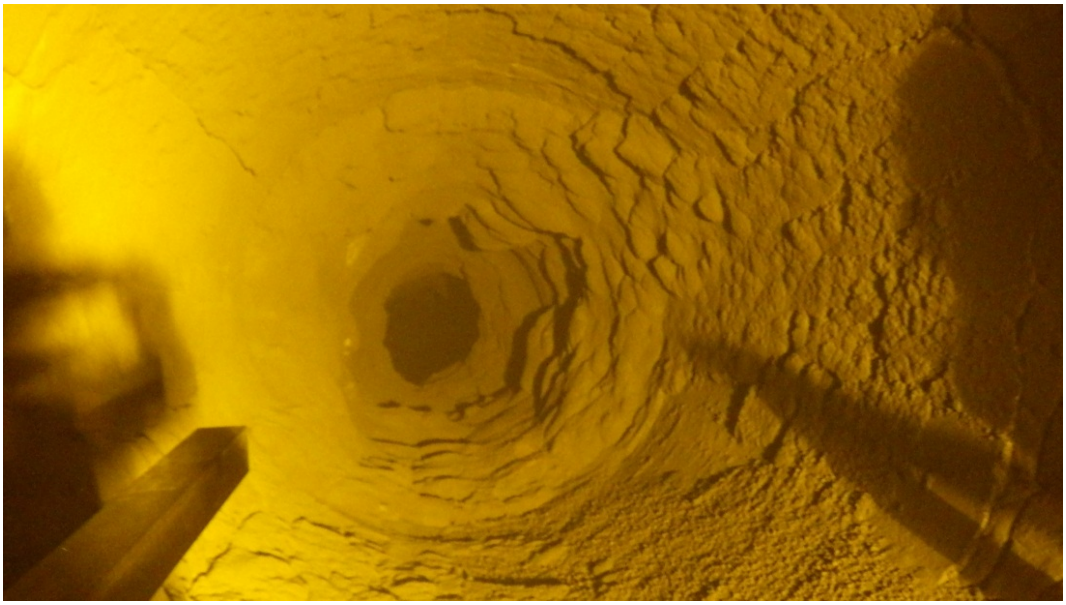

Figure 1.2: A picture of damrings inside a pelletised chromite pre-reduction kiln.

Considering the negative impacts of excessive damring formation in chromite pre-reduction kilns, conducting research relevant to this aspect was identified as one of the general aims of this study. One of the possible reasons for damring formation is melting of pulverised fuel (PF) coal ash that originates from the coal used to fire (heat) the kiln. Therefore, the ash fusion temperatures (AFTs) of the PF coal ash can be used as an indication of the temperature at which the ash will start to contribute to damring formation. AFTs, i.e. initial deformation (T_{indef}), softening (T_{soft}), hemispherical (T_{hem}) and fluid (T_{fluid}) temperatures can be determined experimentally (Nel *et al.*, 2014). However, AFTs are not always readily available, since AFT analyses are time-consuming and special instrumentation is needed. In contrast proximate, ultimate, total S, calorific value (CV) and ash composition analyses are routinely conducted in industry. Therefore, there have been a number of studies done on the

prediction of AFT based on chemical composition. Previously Liu *et al*. (2007) predicted AFT for steam boiler operations of power plants based on chemical composition. These authors used a neural network method, i.e. ACO-BP neural network based on ant colony optimisation, to predict the AFT. Chakravarty *et al.* (2015) used thermodynamic modelling to predict and understand ash fusion behaviour, and Winegartner and Rhodes (1975) used regression analysis to calculate AFT of coal ash from chemical composition. However, none of the afore-mentioned studies considered chromite pre-reduction kilns specifically.

The possibility exists that damring formation can also be caused by partial melting of pellets being fed into the kiln and/or pellet fragments formed in the kiln, e.g. due to pellet breakup. Extensive sessile drop test work has been conducted for Manganese-ores (Gaal *et al*., 2007; Safarian *et al*., 2009; Ringdalen *et al*., 2010) in order to observe their behaviour during heating. The sessile drop test, which is a very high temperature measurement method, is used to measure the melting and reduction temperatures of materials (Ringdalen *et al*., 2010). As far as the authors could assess, no such work has been published for chromite ores, therefore the possible contributions of ores and/or pellet fragments cannot be assessed at present.

Another general aim of this study was to identify if a technique other than thermo-gravimetric analysis (TGA) can be used to follow chromite pre-reduction, occurring specifically in composite chromite pellets. TGA analysis has been used extensively to study chromite pre-reduction (Niayesh and Dippenaar, 1992; Kekkonen *et al*., 1995; Weber and Eric, 2006; Khan, 2013). Kleynhans *et al*. (2016a) suggested the possibility to relate pre-reduction of chromite to the dimensional changes that occurs upon heating, as measured with a thermo-mechanical analyser (TMA). However, as far as the candidate could assess from literature, this has never been attempted. Kleynhans *et al*. (2016a) did prove that TMA measurement can be used to at least partially investigate the thermal strength of composite chromite pellets that are pre-reduced in a rotary kiln. Such thermal strength would be important within the context of damring formation considered in this study.

1.2 Aims and Objectives

Considering the project background and motivation presented in Section 1.1., the general aims of the study were to investigate damring formation and to assess if a method other than TGA can be used to follow chromite pre-reduction occurring in pelletised composite pellets. The specific objectives were to:

i) Assess the possible contribution of PF coal ash to damring formation in chromite pre-reduction kilns. The strategy to fulfil this objective was to obtain a wide range of different PF coal samples, which could then be characterised in detail. It was assumed that the softening temperature, determined with AFT analysis, could be used to indicate possible contribution to damring formation. However, ATFs are not routinely determined by the FeCr industry, therefore a multivariate statistical method will be used to related more commonly measured PF coal characteristics to its ash softening behaviour.

ii) Evaluate the possible contribution of chromite ore, as well as composite chromite pellet fragments to damring formation in chromite pre-reduction kilns. In order to achieve this, several typical chromite ores will be obtained from FeCr producers, as well as a typical clay binder and carbonaceous reductant used in the production of composite chromite pre-reduced pellets. These raw materials will be characterised in detail. The thermal softening behaviours of the composite chromite pellets and individual raw materials will then be evaluated by performing sessile drop tests, which will be related to possible damring formation contribution. It is also foreseen that actual damrings will be analysed to verify conclusions made from Objectives i) and ii).

iii) Compare TMA and TGA measurements of chromite composite pellets, in order to assess if TMA can also be used to follow chromite pre-reduction occurring in such pellets. The pelletisation method presented by Kleynhans *et al*. (2012) and Neizel *et al.* (2013) will be used to simulate the formation of green (uncured) pellets for the purpose of further experimentation. However, the atmosphere in a pre-reductions kiln is partially oxidising to allow PF combustion, while a partial positive CO pressure existing inside the pellets themselves, causes a reducing atmosphere inside and around the pellets. To recreate this environment, it would be better to be able to perform TGA measurements on a couple of pellets in a packed bed, which will not be possible

with a commercial TGA since the typical maximum sample mass is usually 50 mg. Therefore as part of this study, a large mass TGA (able to analyse approximately 100 g) will be designed, constructed, commissioned and tested. The results from this large mass TGA will then be compared to TMA measurements conducted on full size pellets.

Chapter 2

Literature review

In this chapter relevant literature is reviewed. A general introduction to chromite ore is presented in Section 2.1, followed by an overview of ferrochrome processes applied in South Africa (Section 2.2). A more in depth discussion of chromite pre-reduction is presented in Section 2.3, while damring formation in a chromite pre-reduction kiln is considered in Section 2.4. Finally, conclusions are presented in Section 2.5.

2.1 An overview of chromite

2.1.1 Importance of chromite

Chromite, (chromium ore) is a dark grey, blackish oxide mineral. A photo of a lumpy chromite ore piece is presented in Figure 2.1.

Figure 2.1: A photo of a lumpy chromite ore piece.

Chromite occurs as a spinel mineral (Kotz *et al*., 2006) in ultramafic igneous rocks (Nriagu, 1988). Chromite spinel contains magnesium (Mg) iron (Fe), aluminium (Al) and chromium (Cr) and can be characterised by the following formula $[(Mg,Fe^{2+})(Al,Cr,Fe^{3+})_2O_4]$. The ratios of these elements can vary significantly depending on the deposit (Motzer, 2005; Haggerty, 1991). Figure 2.2 presents an image of the complex crystalline structure of

chromite spinel. The spinel has a stable, compact, cubic coordination structure and substitutions of Fe(II) by Mg(II), as well as Cr(III) by Al(III) or Fe(III), can take place.

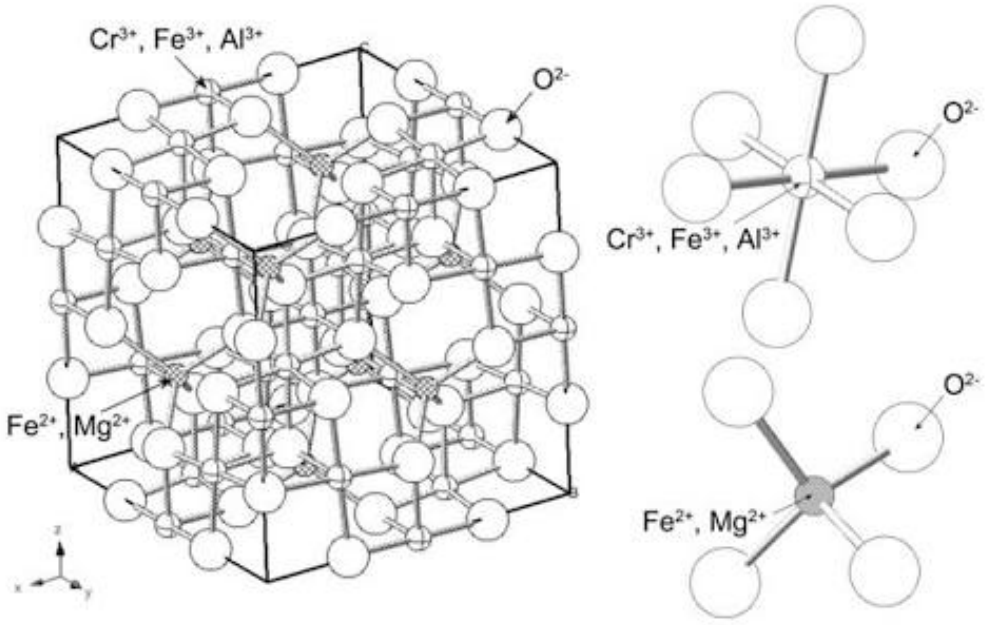

Figure 2.2: Crystalline structure of chromite spinel as proposed by Zhao and cited by Zhang *et al*. (2016)

Chromite is one of 82 known Cr-containing minerals within the earth's crust; however it is the only commercially viable source of new Cr units (Motzer, 2005; Riekkola-Vanhanen, 1999). This makes it an extremely important resource since Cr is an essential material used in chemical, metallurgical and refractory industries (Papp, 2004). Cr is a transition element that exists in various oxidations states forming brightly coloured compounds used in dyes, paint pigments, leather tanning etc. Cr is also widely used as a catalyst and in various other chemical applications. It is a hard, brittle shiny metal with high melting (1907 °C) and boiling points (2671 ° C). Cr metal forms a strong, nonporous Cr_2O_3 surface oxide layer when coming in contact with oxygen and is therefore corrosion resistant. This makes Cr ideal for applications such as metal plating (Jacobs and Testa, 2005). However, the most important application of Cr is in the production of stainless steel, which is produced from stainless steel scrap, ferrochrome (FeCr) and additions of metals in smaller quantities. More than 90 % of all mined chromite is used for the production of FeCr (Rao, 2010). In addition to making stainless steel corrosion resistant, Cr enhances the steel's resistance to impact (Jacobs and Testa, 2005).

2.1.2 History of chromite

The discovery of chromite was put in motion in 1761 when Johann Gottlob Lehmann obtained samples of an orange-red mineral while he was visiting a Siberian gold mine in the Ural Mountains. He called this mineral "Siberian red lead". It was later discovered that this mineral was a lead chromate ($PbCrO_4$), also referred to as crocoisite or crocoite (Jacobs and Testa, 2005). Years later in 1798, Louis Nicolas Vauquelin managed to isolate an oxide of an unknown metal from the crocoite. Given the many colours produced by the compounds of this metal, it was called Cr which is Greek for colour. In the following year Cr was also discovered in a dark, heavy mineral, which was more common in the Ural Mountains. This mineral was named chromite (Papp and Lipin, 2006). Chromite was mainly used in the chemical industry (paint, textile dying, leather tanning etc.) until 1827. The use of Cr in alloys started developing in the early 1800's after the French scientist Pierre Berthier discovered that mixing Cr with iron (Fe) resulted in a corrosion resistant alloy (Roza, 2008). The first patent for using Cr in steel was issued in 1865. Thereafter the industrial application for Cr expanded In addition to steel, it was used in chromium plating, refactory bricks, alloys etc. (Nriagu, 1988).

Ever since the applications of Cr became important, chromite has essentially been the only commercially recoverable source of new Cr units. According to Howat (1986) deposit of chromite was discovered in Maryland in the U.S.A. in 1827. This deposit was the only available source of chromite until 1848, when high-grade chromite deposits were discovered in Turkey. Almost sixty years later chromite was discovered in India and Zimbabwe. But the significant expansion of chromite production started in 1932 and thereafter increased by fiftyfold until 1980.

2.1.3 Chromite deposits

Commercial chromite deposits can be of the alluvial, podiform or stratiform types. Alluvial deposits are a result of weathering of chromite-bearing rock with the chromite being gravity concentrated by flowing water. These deposits are relatively small, with the commercial significance thereof being limited (Murthy, 2011). Podiform deposits are relatively small, pouch/pod-shaped deposits that are generally richer in Cr than stratiform deposits (Murthy, 2011; Pohl, 2011). However, the distribution of these deposits is irregular and unpredictable,

making its exploration challenging and costly. Significant podiform deposits are located in Turkey, Kazakhstan, the Philippines, New Caledonia and Russia (Cramer *et al*., 2004). Stratiform deposits occur in parallel seams in large, layered mafic (high silicate mineral rich in magnesium and iron) and ultramafic (low silicate mineral rich in magnesium and iron) rocks, which are formed as a result of underground crystallisation and solidification of magma to form igneous intrusions rich in heavy iron containing minerals. Ores from stratiform deposits tend to be softer and more friable than ores from podiform deposits (Murthy, 2011). The Bushveld complex in South Africa is the largest stratiform chromite deposits. The Great Dyke in Zimbabwe, Stillwater Complex in the U.S.A. and Kemi intrusion in Finland are also igneous rock intrusions containing chromite deposits (Schouwstra and Kinloch, 2000). The stratiform deposits found in India are deformed and faulted and therefore exploration and mining are as costly as that of podiform deposits (Cramer *et al*., 2004). Large commercially viable chromite deposits were also discovered fairly recently (2008) in the Ring of Fire in Canada (Chong; 2014). The Ring of fire is a 5000 km^2 crescent shaped belt of greenstone-hosted chromite and nickel-copper-platinum group metal (PGM) deposits (Williams, 2014). However, before exploration and exploitation of these Canadian deposits can begin, there are a few challenges that need to be overcome. The Ring of Fire is located in the largest peatland in the world and is also located in traditional territories of several First Nations (Chong, 2014; Beukes *et al.*, 2017). Another important challenge is the inaccessibility of the area due to the lack of infrastructure. Therefore, exploitation of these deposits will take considerable planning, negotiations and funding.

2.1.4 Chromite in South Africa

South Africa holds approximately 70 % of the world's viable chromite deposits (James, 2016) and is the largest chromite producer. In Figure 2.3 the world production of chromite for 2017 is presented. As is evident, South Africa was responsible for 49 % of the world's chromite production, followed by Kazakhstan with 18 %.

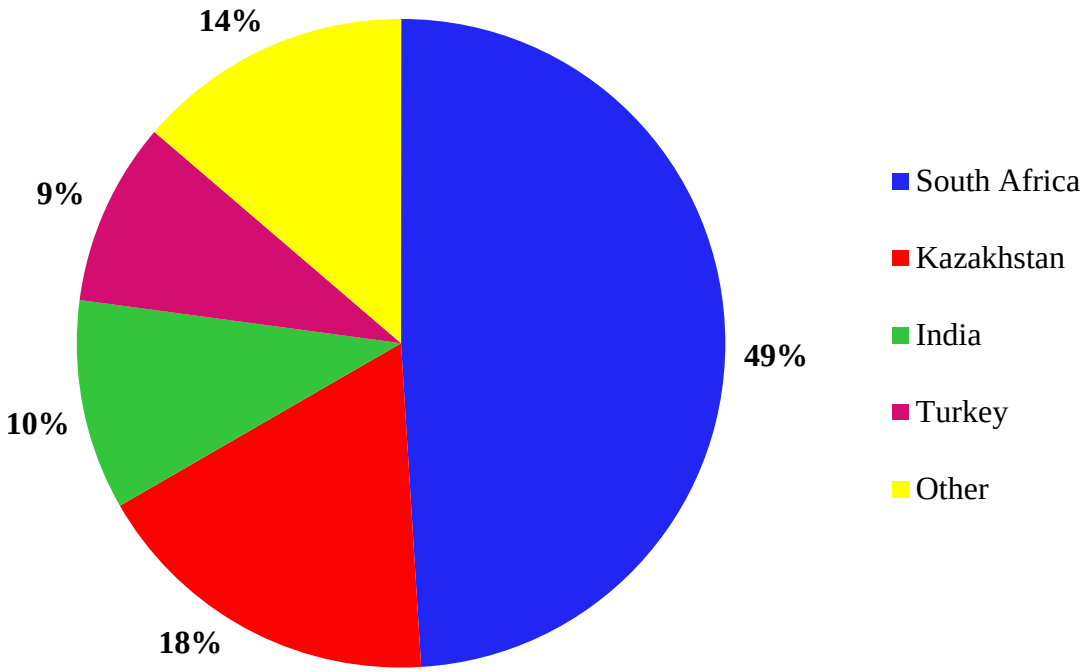

Figure 2.3: World production of Chromite for 2017. Constructed from USGS (2018).

As previously stated, chromite deposits in South Africa are located in the Bushveld Complex, which was discovered in 1865. The Bushveld Complex is a saucer-like geological phenomenon consisting of a layered intrusion of igneous rocks. It is the largest layered intrusion of its kind in the world (Schouwstra and Kinloch, 2000). It is highly mineralised and contains fluorspar (CaF_2), tin (Sn) and titanium (Ti), as well as the largest vanadium (V), platinum group minerals (PGMs) and Cr reserves in the world. It extends about 400 km from east to west and roughly the same distance from north to south, and it is about 9 km thick. It is located in the central and slightly western part of the South African Highveld (Howat, 1994).

A schematic geological map of the Bushveld complex is presented in Figure 2.4. This figure also shows locations of PGM mines discussed by Latypov *et al*. (2015), which is not of interest in this study. However, the figure does show the location and geology of the Bushveld Complex, as well as the different limbs of the complex.

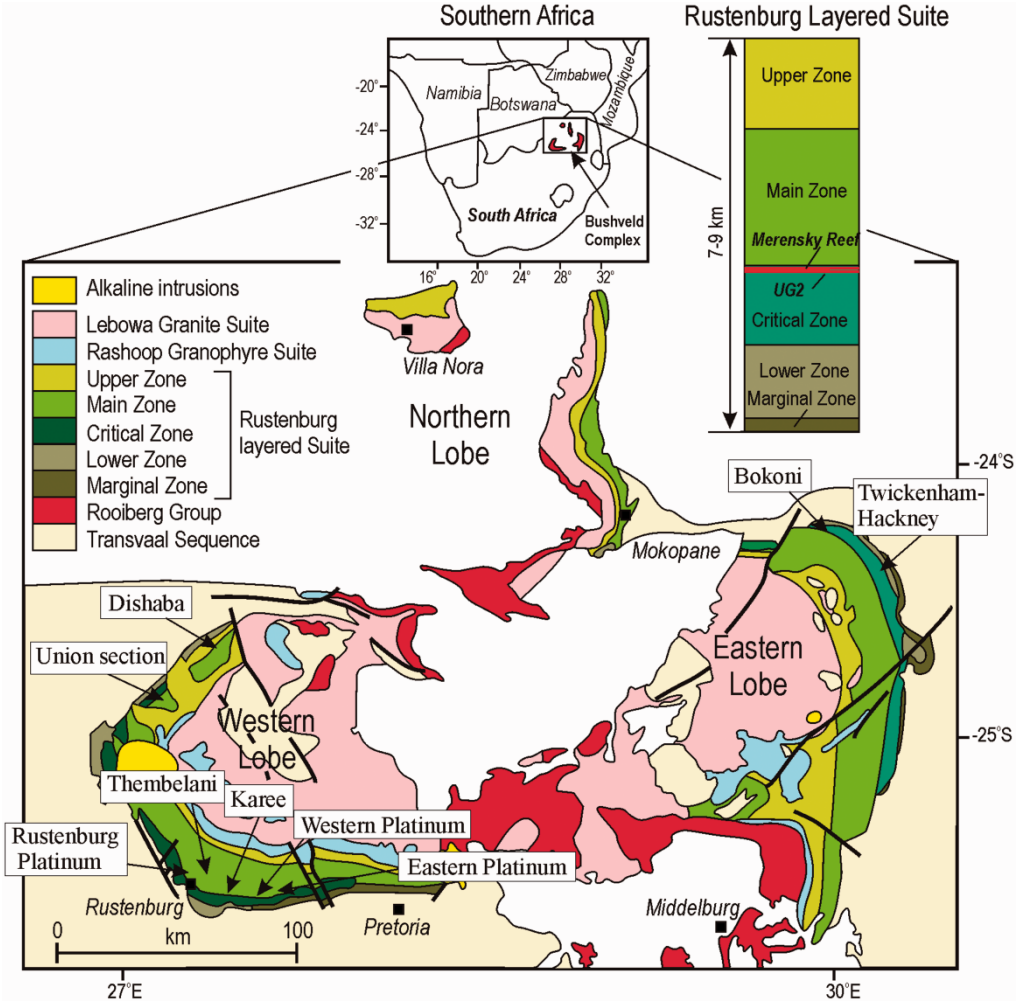

Figure 2.4: Location and schematic geology of the Bushveld Complex, indicating the different limbs as well as the zones it is divided into. The location of PGM mines are also shown, but it is not of interest in this study (Latypov *et al.*, 2015).

The Bushveld complex is divided into a nothern, southern, eastern and western limb (of which the locations can be seen in Figure 2.4) and is made up out of mafic rocks known as Rusterburg Layered Suite, Lebowa Granites and Rooiberg Fesicsi. The Rustenburg Layered Suite is subdivided into five zones. They are the Main, Upper, Lower, Upper Critical and Lower Critical zones. Chromite and PGM deposits are found in the Critical zones (Perrit and Roberts, 2007). Chromite is mainly exploited from the Lower Critical zone because it contains ores with a higher Cr/Fe ratio. The Cr/Fe ratio is significant in the FeCr industry, since it is a primary determinant of the Cr grade in the FeCr product. FeCr with a lower Cr/Fe ratio are not desirable due to the fact the FeCr producers get paid per mass unit of Cr-content in the product (Cramer *et al.*, 2004). The economically exploitable seams in the Critical zone are the lower group 6 (LG6), which is the most important seam containing ore

with a Cr/Fe of 1.5-2, the middle group1 and 2 (MG1 and MG2) with a Cr/Fe ratio of 1.5-1.8 and the upper group 2 (UG2) with a Cr/Fe ratio of 1.3-1.4 (Schouwstra and Kinloch, 2000; Howat, 1986). The UG2 seam is primarily mined as a source of PGMs (Mondal and Mathez, 2007). During the extraction of PGM's from the UG2 ore, chromite is rejected into the tailings stream. The PGM tailings can be beneficiated (via physical separation methods) to the required Cr_2O_3 content and used as a feed material in FeCr production (Cramer *et al*., 2004).

2.2 Ferrochrome industry

2.2.1 Overview of ferrochrome industry

FeCr is a relatively crude alloy, containing principally Cr and Fe (Riekkola-Vanhanen, 1999). The first recorded production of FeCr was in 1893 when Henri Moissan smelted chromite and carbon in an electric furnace. This was followed by large scale production of high carbon FeCr from 1897 utilising an electric furnace. This was the beginning of a rapidly growing global industry, which escalated as the demand for stainless steel increased. As the industry expanded the production of low-carbon FeCr, with reduction achieved by aluminium (Al) or silicon (Si), was developed. This process yielded FeCr with less than 0.06 % carbon. In 1942 South Africa joined the industry with the production of high and medium-low carbon FeCr (Nriagu, 1988; ICDA, 2018). At that time, low-carbon FeCr was the desired product to use in the steel industry, since higher %C created several manufacturing problems. However, with the development of Argon-oxygen-decarburisation (AOD) and vacuum decarburisation stainless steel process in the 1970's high carbon FeCr became the main feed material for stainless steel manufacturing (Bhonde, 2007). South Africa became the world's largest producer of charge grade FeCr in 1999 (ICDA, 2018).

As mentioned in Section 2.1.1, approximately 90 % of Cr is used in the production of FeCr, of which 80 % is used to produce stainless steel (Murthy *et al*., 2011). Therefore, the demand for FeCr is primarily dependant on the stainless steel industry. The use of stainless steel is globally growing and according to SEAISI (2017) stainless steel production reached a global record high in 2017. The market is also expected to grow further in the foreseeable future.

2.2.2 Ferrochrome in South Africa and challenges the industry is facing

At least fourteen FeCr smelters occur in South Africa, of which the locations and capacities are presented in Table 2.1. According to Jones (2018), two of the fourteen listed (Table 2.1) FeCr smelters were not in operation at the time that this study was conducted.

Table 2.1: Production capacities of South African FeCr smelters (Beukes *et al*., 2010 adapted from Jones, 2018).

Ferrochrome smelter	Location	Production capacity (kt/a)
Glencore-Merafe Loin (Phase I and II)	Steelpoort	720
Glencore Wonderkop	Rustenburg	545
Glencore Rustenburg	Rustenburg	430
Glencore Lydenburg	Lydenburg	400
Glencore Boshoek	Boshoek near Rustenburg	240
Samancor Ferrometals	Witbank	550
Samancor ASA Metals	Dilokong	410
Samancor Tubatse Ferrochrome	Steelpoort	380
Samancor Middelburg ferrochrome	Middelburg	285
Samancor TC Smelter	Mooinooi	240
Assmang Chrome	Machadadorp	300
Henric Ferrochrome	Brits/Madibeng	420
Traxys	Richards bay	150
Mogale Alloys	Krugersdorp	130
TOTAL		5 200

As mentioned in Section 1.1, South Africa was the leading producer of high carbon FeCr until 2011. However, in 2012 China became the global leader in FeCr production (ICDA, 2013). According to Creamer (2017), China consumes 90 % of South Africa's exported chromite. In 2016 China produced 43 % of the world's FeCr output, compared to South Africa's 33 %. China is also the world's largest stainless steel producing country with 54 % of the global production. Figure 2.5 presents the FeCr production trends of South Africa and China from 2009 to 2012. South Africa's FeCr production started decreasing after 2010 and China's production started to increase. According to Conradie (2016) South African FeCr

sales to China, the world's largest importer of South African FeCr, are being negatively affected by increased exports of South African chromite that, is enabling the growth of the Chinese FeCr industry.

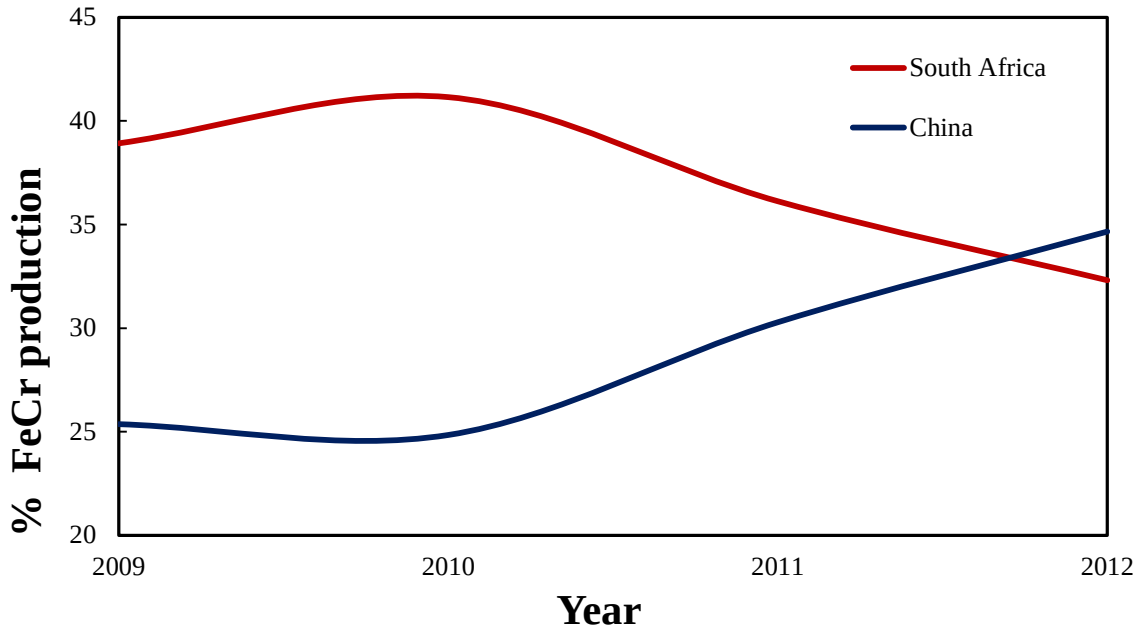

Figure 2.5: The global annual high carbon FeCr production of South Africa and China from 2009 to 2012.

Electricity shortage and increasing costs are the biggest challenges that the FeCr in South Africa are facing (Creamer, 2017). Figure 2.6 presents the rise in real price of electricity in South Africa from 1970 to 2015. As is evident from this figure, after 2008 the price of electricity has increased almost at an exponential rate.

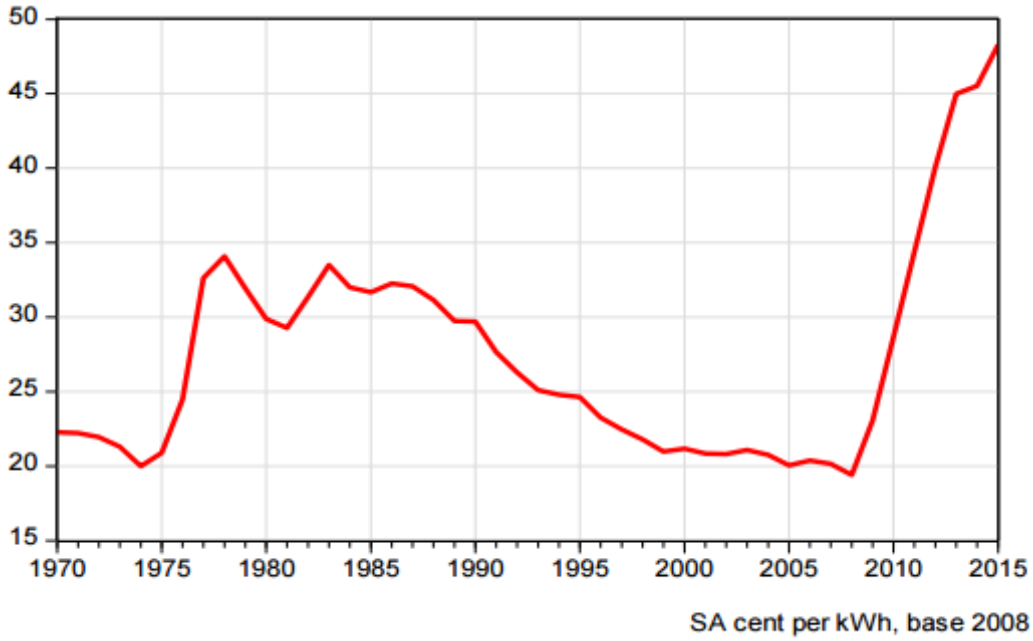

Figure 2.6: Real price of electricity from 1970 to 2015 (https://businesstech.co.za/news/energy/91216/eskoms-shocking-annual-price-hike-since-2007/. Date of access 25 May 2018).

Creamer (2017) pointed out that South Africa's chromite exports to China had grown significantly from 100 000 t/y in 2004, to 6-million tons a year in 2013. Therefore, South Africa is rapidly losing its competitive advantage, with chromite exports to China still growing.

With the continuous market price fluctuation, waste disposal cost factors, increased labour cost and the above-mentioned ongoing electricity crisis, the SA FeCr industry is under huge pressure (Biermann, *et al*., 2012). According to Daavittila *et al*. (2004), the cost distribution for the FeCr industry (in European conditions) can be divided into 4 categories, namely: chromite (30 %), electricity (30 %), reductants (20 %) and other costs that including maintenance, labour and waste disposal (20 %). The current South African situation is probably similar, but is likely to have a higher electricity component. Even though cost distribution for each SA FeCr smelters would vary according to different operational strategies, electricity would likely remain the biggest cost factors. With the major price increases in electricity since 2008, South African FeCr producers are therefore at a major disadvantage.

2.2.3 Processes utilised by the South African ferrochrome industry

2.2.3.1 Chromite beneficiation

Chromite is one of the hardest minerals, but the South African ores are relatively friable and break down into the chromite crystals size fairly easily. With lumpy ore being the ideal smelter feed (at least historically), fine low grade ores must be subjected to beneficiation (increase in grade) and agglomeration (increase in size) before smelting (Murthy *et al*., 2011). During beneficiation valuable minerals are separated form gangue. Different beneficiation practices are applied, depending on factors such as the characteristics of the ore deposit. According to Glastonbury, *et al*. (2010), the friability of South African chromite results in recovery of only 10 to 15 % lumpy ore with a typical size range of 15 mm to 150 mm and 8 to 12 % pebble/chip ores with a typical size range of 6 mm to 15 mm. The remaining ore fraction is usually smaller than 6 mm and requires further beneficiation. Figure 2.7 presents a flow diagram of a typical beneficiation circuit of the < 6 mm ore fraction. The < 6 mm fraction is crushed in two stages by a primary and secondary crusher, as seen on Figure 2.7. Screening produces ores that are typically < 3mm. This fraction is grounded to < 1 mm and upgraded in the concentration section in Figure 2.7, using gravity separation techniques (typically spirals). This upgraded < 1 mm ore fraction is known as metallurgical grade concentrate (Murthy *et al*., 2011).

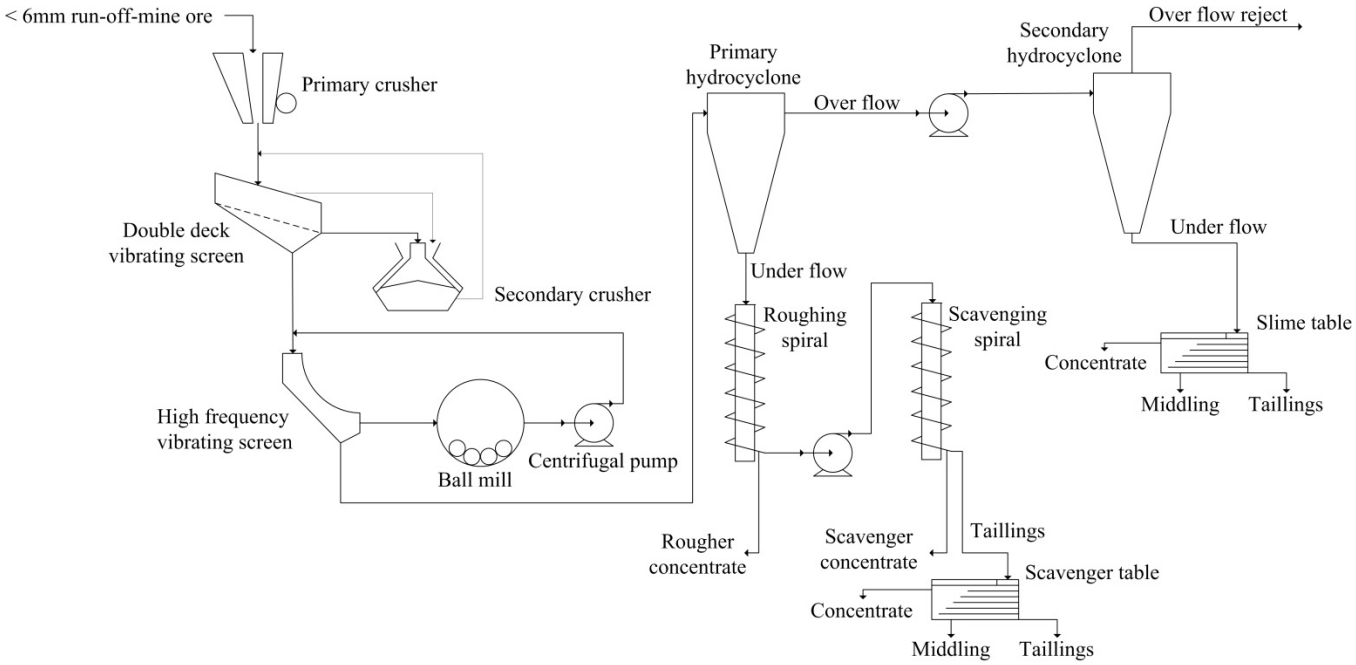

Figure 2.7 Chromite beneficiation process (adapted from Murthy *et al.*, 2011, by Beukes *et al*., 2017).

2.2.3.2 Ferrochrome production

FeCr is produced by carbothermic reduction of chromite (Riekkola-Vanhanen, 1999). High carbon FeCr typically contains 60 to 70 % Cr and 4 to 6 % carbon. In order to achieve this specification ore with a high Cr/Fe ratio is needed (Basson and Daavittila, 2013). South African ores typically have a Cr/Fe ratio of 1.7 or less. With the commercialisation of the AOD process, the use of charge grade FeCr became more acceptable, which can be produced from lower-grade chromite with a Cr/Fe ratio of typically 1.5 to 1.6. FeCr produced from such ores usually have a Cr content of 50 to 55 % and a carbon content of between 6 and 8% (Cramer *et al*., 2004; Basson and Daavittila, 2013).

There are four main process combinations used in the production of FeCr in South Africa and have been described by Basson and Daavittila (2013) and Beukes *et al*. (2010; 2017):

i) The conventional process utilising open/semi-closed submerged arc alternating current (AC) furnaces.

In this process a mixture of chrome ore, reductant and flux is fed directly into the semi-closed submerged arc furnaces with minimum pre-processing. Coarse (lumpy

and chips/pebble ores), as well as a limited fraction of fine ores, are used in this process. This process has a bag filter off-gas treatment. This is the oldest technology applied in South Africa, but it still accounts for a substantial fraction of FeCr produced. The advantages of this process are that it requires the lowest capital investment and it has some flexibility in terms of raw materials that can be used. The disadvantages of this process are that it is a less environmentally friendly process (comparatively more Cr(VI) is generated and CO rich off-gas is combusted on the furnace bed) and it has lower efficiencies (Cr-recovery and specific electricity consumption, SEC) if compared to some of the other processes (Beukes *et al*., 2010; Naiker, 2007). More recently, oxidative pellet sintering plants, as described below (Outotec pelletising process), have been added to older semi-closed furnace operations. Feeding such furnaces with pelletised feed has significantly improved efficiencies.

ii) Outokumpu/Outotec process

In this process, fine ore(s) and a small fraction of carbonaceous material are wet milled, where after the mixture is pelletised using a binder such as bentonite. These pellets are then sintered (oxidative sintering conditions) and air cooled. At some smelters these pellets are then heated together with fluxes and reductants in a preheater, which is located above the furnace bins. All greenfield developments include closed submerged arc furnaces. The furnace off-gas is cleaned in wet venturi scrubbers and the cleaned CO rich off-gas is used as an energy source where required. This process has lower energy consumption and higher chromium recoveries, if compared with the conventional process, due to the use of sintered pellets and preheating (Naiker, 2007). It is the most commonly applied process in South Africa (Outotec, 2018), with a significant number of the FeCr producers listed in Table 2 applying it.

iii) DC arc furnace operation

In this process the furnace uses a single carbon electrode, producing a DC arc to the anode in the bottom of the furnace. Raw materials can be fed directly next to the electrode when a solid electrode is used. A hollow electrode can also be used, in which case the raw material is fed through the electrode. The most significant advantage of this process is that any raw materials can be used, including chromite

fines exclusively. The chromium recoveries are also very high (Naiker, 2007), but the SEC is the highest of all process options.

iv) Premus process (pelletised pre-reduction process)

In the Premus process the furnaces consumes mainly pre-reduced pellets. The composite pellets consist of dry-milled fine chromium ore, a clay binder and a reductant. The pellets are preheated, before being fed into a counter current rotary kiln, where partial pre-reduction of the chromite takes place. The hot pre-reduced pellets are then fed into closed submerged arc furnaces, directly after pre-reduction (to retain heat energy). Venturi scrubbers are used to clean the off-gas, which is then used throughout the plant as an energy source. The main disadvantages of this process, are that the initial capital cost is high and it requires a very high level of operational control. The main advantages this process has over the other processes include low SEC, high Cr-recoveries and the production of a low silicon product (Naiker, 2007). This process is currently used by two smelters in South Africa (Beukes *et al*., 2010).

2.3 Chromite pre-reduction

Since the current study is related to the SRC/Premus process (pelletised pre-reduction process), as introduced in Section 2.2.3.2, aspect related to chromite pre-reduction is further considered in this section.

2.3.1 Fundamental aspects

According Chakraborty *et al*. (2007) the overall reduction of chromite can be presented as indicated below:

$$FeCr_2O_4 + 4C \rightarrow Fe + 2Cr + 4CO \quad [2.1]$$

$$C + CO_2 \rightarrow 2CO \quad [2.2]$$

Barnes *et al.* (1983) suggested certain definitions for terms used in pre-reduction discussions such as extent of reduction and extent of metallisation. The extent of reduction, %R was defined by the following equation.

$$\%R = \frac{Mass\ of\ oxygen\ removed}{Original\ removable\ oxygen}\ x\ 100 \quad [2.3]$$

Solid carbon is used as a reductant in the pre-reduction process, which results in CO being formed as a product in a 1:1 molar relationship with oxygen that is removed from the "oxides" (chromite is not an oxide in the true sense of the definition). Therefore the extent of reduction according to Barnes *et al.* (1983) can also be defined as:

$$\%R = \frac{Mass\ of\ CO\ evolved}{\frac{28}{16}xOriginal\ removable\ oxygen}\ x\ 100 \quad [2.4]$$

The extent of metallisation is defined (Barnes *et al.* 1983) by the following equation

$$\%M = \frac{Cr^0 + Fe^0}{Cr_{tot+} + Fe_{tot}} \quad [2.5]$$

With Cr^0 and Fe^0 being the amount of Cr and Fe reduced to its metal state and Cr_{tot} and Fe_{tot} the total amount of Cr and Fe.

Kleynhans (2016b) recently summarised literature, relating to the fundamental aspect of chromite pre-reduction. Generally, high temperature reduction of chromite with carbon can occur in three ways. It can occur by solid chromite being reduced by a solid or gaseous reductant. It can also occur by direct reaction at the slag or metal interface (where the dissolved chromite in the slag is reduced by dissolved carbon in metal phase) or by direct reaction between dissolved chromite in the slag and carbon particles floating on it (Takano *et al.*, 2007). The latter two methods , will be dominant in furnace smelting. In chromite pre-reduction however, a large portion of chromite is expected to reduce by solid or gaseous reductants before liquid phase is formed. Reduction of oxides is based on the reaction with solid carbon and CO. The relevant CO gas interaction reactions were presented by Niemelä *et al.*, (2004), i.e.:

$$2C + O_2\ (g) \rightarrow 2CO \quad [2.6]$$

$$2CO\ (g) + O_2\ (g) \rightarrow 2CO_2\ (g) \quad [2.7]$$

The formation, characterisation and utilisation of CO-gas formed during the carbothermic reduction of chromite was also investigated by Niemelä *et al.* (2004). Figure 2.8 presents

standard free energies of reduction of metal oxides with carbon and CO (Ellingham diagram). This indicates that solid carbon can reduce Fe_2O_3 to Fe_3O_4 at around 250 °C. The reduction of Fe_3O_4 to FeO with solid carbon and CO can occur at temperatures above approximately 710 °C. FeO can also be reduced to Fe^0 with solid carbon at the afore-mentioned temperature. However, the reduction of Cr_2O_3 with solid carbon only occurs at temperatures higher than 1250 °C. The reduction of Fe_2O_3 to Fe_3O_4 with CO can occur over the entire calculated temperature range, but due to kinetic limitations, reduction of Fe_3O_4 to FeO only occurs above 710 °C. Kleynhans (2016b) stated that a high CO/CO_2 ratio would be required for such reduction to take place. Lastly, the diagram indicates that the reduction of Cr_2O_3 and Cr_2FeO_4 is not possible with CO alone.

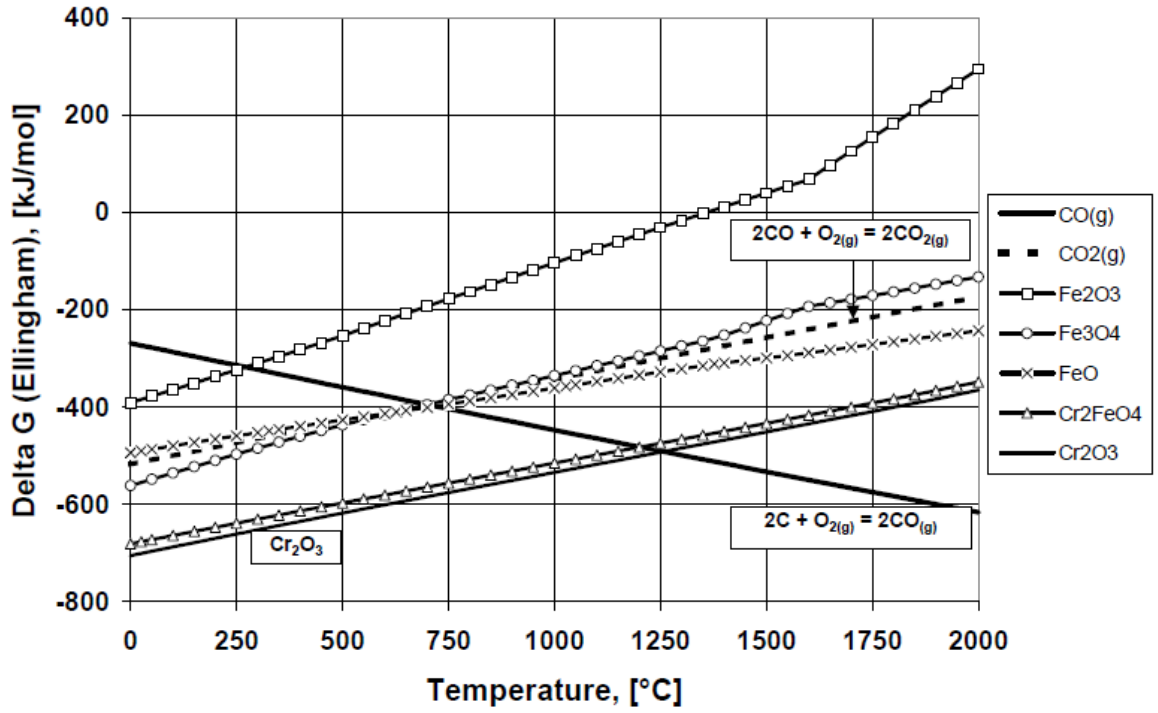

Figure 2.8: Standard free energies of metal reduction with carbon and CO (Niemelä *et al.*, 2004).

For chromite pre-reduction, a stoichiometric ionic diffuse reduction model was proposed by Soykan et al. (1991a; 1991b). This model involves complex reactions among the altered chromite spinel phases, the solid carbon reductant, and various ionic species. It was also postulated that site exchange between Fe^{2-} and Cr^{3+} ions occur, with the Cr^{3+} being placed in octahedral sites due to its very high affinity for octahedral coordination. An exchange between the Cr^{2+} and the Fe^{2+} ions of the unit cell just below the surface was also suggested.

The authors (Soykan *et al*., 1991a; 1991b) also observed that localisation in partially reduced chromite occurs and that as Fe and Cr are reduced, all the oxygen is removed from the surface as well as the inner cores being rich in Fe, while the outer surface was depleted of Fe. These results were later augmented by findings from Ding and Warner (1997) who proposed a graphic representation of so-called shrinking core mechanism for chromite reduction. This graphical representation is presented in Figure 2.9. In the "Reduced area" in Figure 2.9, Fe^{2+} and Cr^{3+} ions diffuse outward and Cr^{2+}, Al^{3+} and Mg^{2+} ions diffuse inward. Initially, Fe^{2+} and Fe^{3+} ions at "Interface 1" (surface of chromite particles) are reduced to the metal state, which is immediately followed by the reduction of Cr^{3+} to Cr^{2+}. Fe^{3+} ions in the spinel under the surface are then reduced to Fe^{2+} by Cr^{2+} ions in the "Reduced area". Fe^{2+} ions diffusing outward are then reduced to Fe^0 and after complete reduction of Fe, Cr^{3+} and remaining Cr^{2+} are reduced to the metal state. Eventually this can result in a Fe and Cr free spinel ($MgAl_2O_4$).

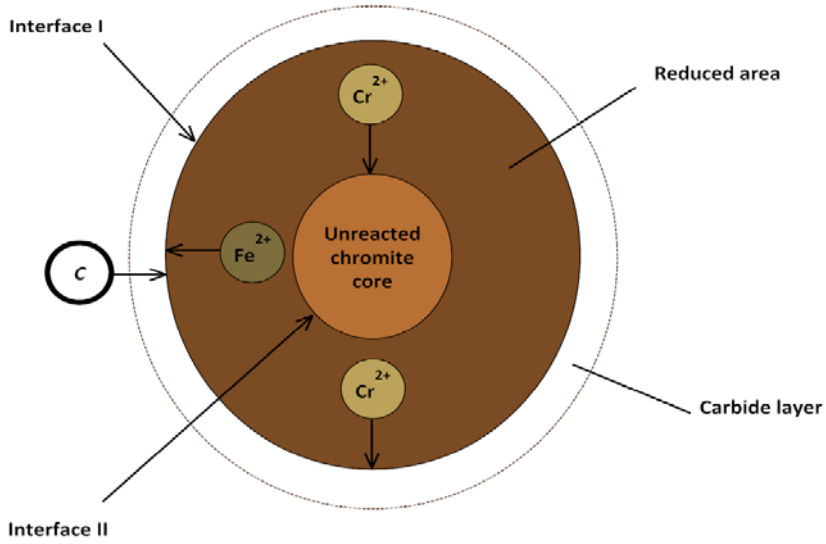

Figure 2.9: A graphical representation of the reduction mechanism of chromite (Ding and Warner, 1997, as redrawn by Kleynhans, 2016b).

2.3.2 History of pre-reduction

Investigations such as selective iron reduction in shaft kilns in the 1960s and pre-reduction of chromite ore in a fluidised bed reactor using methane and hot reduction gasses opened the way for the development of chromite pre-reduction processes. The agglomeration and pre-reduction in a rotary kiln was successfully demonstrated by Outokumpu in the 1970's.(Basson and Daavittila, 2013). In the 1980's Krupp Industrietechnik successfully

preformed pre-reduction of non-agglomerated chromite in a rotary kiln. This Chrome Direct Reduction (CDR) process, was commercialised in South Africa in the late 1980's. However, due to operational difficulties the process was abandoned fairly quickly (Basson and Daavittila, 2013; McCullough *et al*., 2010).

By far the most successful commercial application of chromite pre-reduction has been the Showa Denko Solid-State-Reduction of chromite ore (SRC) process (and processes developed from it). It was developed in the 1970's and was the first successful pre-reduction process implemented commercially. Figure 2.10 presents a diagram of this process. In this process the ore undergoes pre-reduction in a rotary kiln after pelletisation. The hot pellets with about 60% reduction are directly charged into the submerged arc furnace. The power consumption of this process was reported to be in the range of 2000-2500 kWh/ton alloy (Goel, 1997). The SRC process was implemented successfully at two plants, i.e. the Showa Denko operations in Japan and the Consolidated Metallurgical Industries (CMI) operations in Mpumalanga, South Africa. At that time, these two plants were considered to be the most energy efficient FeCr production units in the world (Naiker, 2007). The Premus process, which was based on the SRC process was developed by Xstrata Alloys (now Glencore Alloys) and patented in 2006 (Naiker, 2007). The major differences of the Premus process to the original SRC process are i) the use of fine anthracite, instead of coke as a composite pellet reductant, and ii) the maximisation of total energy contribution (which is the combined effect of pre-reduction and hot pellet feed) to the smelting furnaces, instead of just maximising pre-reduction.

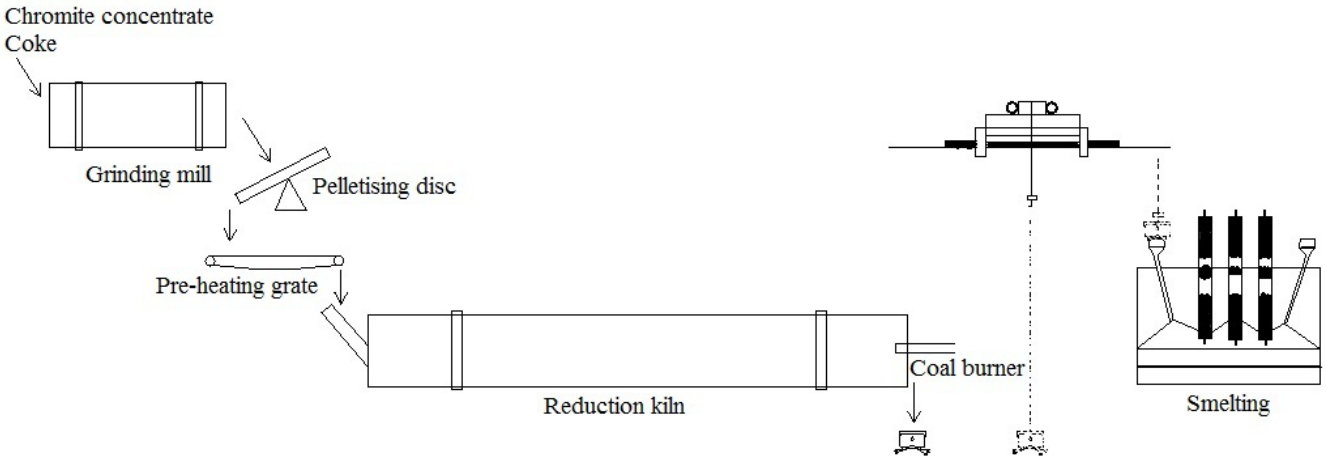

Figure 2.10: Showa Denko Process –The pre-reduction of pellets and the smelting process. Adapted from Goel (1997).

2.3.3 Pre-reduction process and challenges associated with it

As mentioned in Section 2.3.1, the Premus process is based on the SRC process. Although a brief overview of the process was presented in Section 2.2.3.2, a more detailed description is presented here, since this process was the focus of this study. Figure 2.11 presents a flow diagram of the preparation of the pelletised feed. In this part of the process, fine chromite ore, a fine reductant (anthracite, coke or char, depending on availability and cost) and an unrefined clay binder (usually bentonite or attapulgite) are fed into a rotary dryer to remove excess moisture. The materials are then dry milled together, which ensures complete mixing and also intimate particle contact (which enhance pre-reduction). The particle specification for milling is 90% of the particles smaller than 75 µm (i.e. d_{90} of 75 µm) (Kleynhans *et al*., 2012). A large quantity of milled material is stored in a surge bin, to ensure further operation, even if milling does not take place for a considerable time. Dry milled material is withdrawn from this surge bin and pre-wetted with water, where after pre-wetted material is stored in a second much smaller surge bin. This storage allows some maturing of the binder. However, it cannot be too large, since it is relatively difficult to withdraw this very fine moist material that contains clay, at a controlled feed rate. The pre-wetted material is then fed to disc pelletisers to produce pellets of between 15 and 30mm. A disk pelletiser, instead of a

pelletising drum is preferred in this process, since it auto size the pellets to a certain degree, therefore preventing re-circulating feed of over and under size green pellets, as is the case with the Outotec pelletising system. However, the green pellets are not perfectly sized. Green pellets that are too large are prone to disintegration, later during the heat treatment. In contrast, green pellets that are too small might have a substantial fraction of oxidised mass after pre-reduction, since the pre-reduced pellets typically have an outer crust that is oxidised (Kleynhans *et al*., 2012). After pelletisation, the green pellets are dried and pre-heated in a traveling grade and then fed into a counter current rotary kiln fired by pulverised fuel (PF) coal, in addition to CO rich off-gas from the closed submerged arch furnace and/or heavy crude oil (Naiker, 2007).

The material temperature inside the kiln rarely exceeds 1300 °C, although the gas temperature can be higher. However, effective heat transfer prevent the gas and material temperatures from being closer to one another. The partial positive CO pressure inside the pellet prevents oxygen from entering the pellets, causing a reducing atmosphere inside the core of the pellets (and to a certain degree between pellets in the pellet bed). However, a partially oxidising environment needs to be maintained inside the kiln itself, to ensure combustion of the PF, as well as combustion of the CO gas emitted by the pellets. This mixed atmosphere results in pre-reduced pellets, which typically have pre-reduced cores and a thin outer crust that is partially oxidised (Kleynhans *et al*., 2012). The Cr and Fe present in the chromite spinel are partially reduced to form carbides and/or metal, with the degree of pre-reduction depending on kiln temperature, pellet retention time in the kiln, % C present in pellets, pellet size, etc. (Riekkola-Vanhanen, 1999). One of the most significant disadvantages of the SRC/Premus process is the relatively difficult metallurgical control of the submerged arch furnaces that smelt the pre-reduced feed material. This stems from the varying level of pre-reduction, as well as fluctuating C remaining in the pre-reduced pellets. Both these effect that lumpy carbon balance of the furnaces significantly. In order to maintain efficient metallurgical control, pellet pre-reduction level and C-content has to be determined at least on an 8-hour shift basis and the metallurgical recipe adjusted accordingly to prevent over, or under carbon furnace conditions.

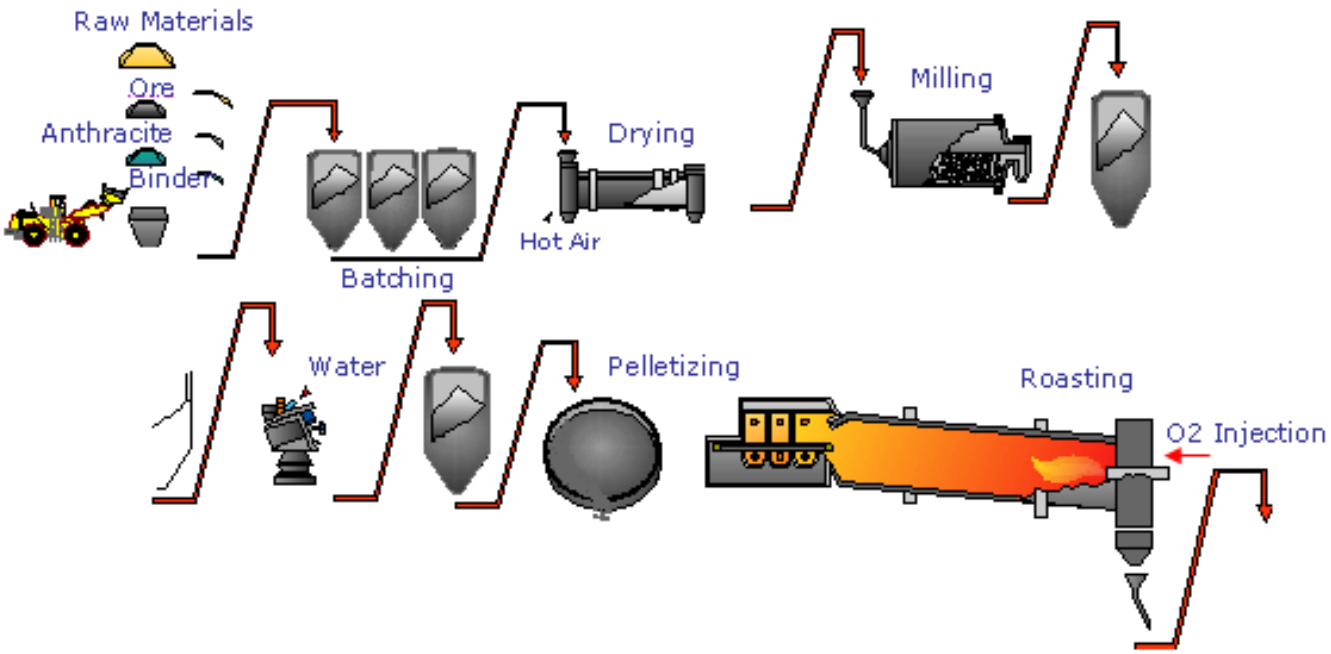

Figure 2.11: Premus process-flow diagram of the pelletising and pre-reduction sections (Naiker, 2007).

Figure 2.12 presents a flow diagram of the smelting section associated with the Premus process. After the pellets are pre-reduced in the rotary kiln, the hot pre-reduced pellets are fed into closed submerged arc furnaces. The furnace is closed to ensure a reducing environment and also to limit the production of Cr(VI), which is carcinogenic (at least some Cr(VI) compounds are). A water venturi scrubbing system cleans the CO rich off-gas, which is used as a source of energy in the plant (material drying, tapping runner heating, ladle heating, etc.), which is also a great advantage of this process (Naiker, 2007).

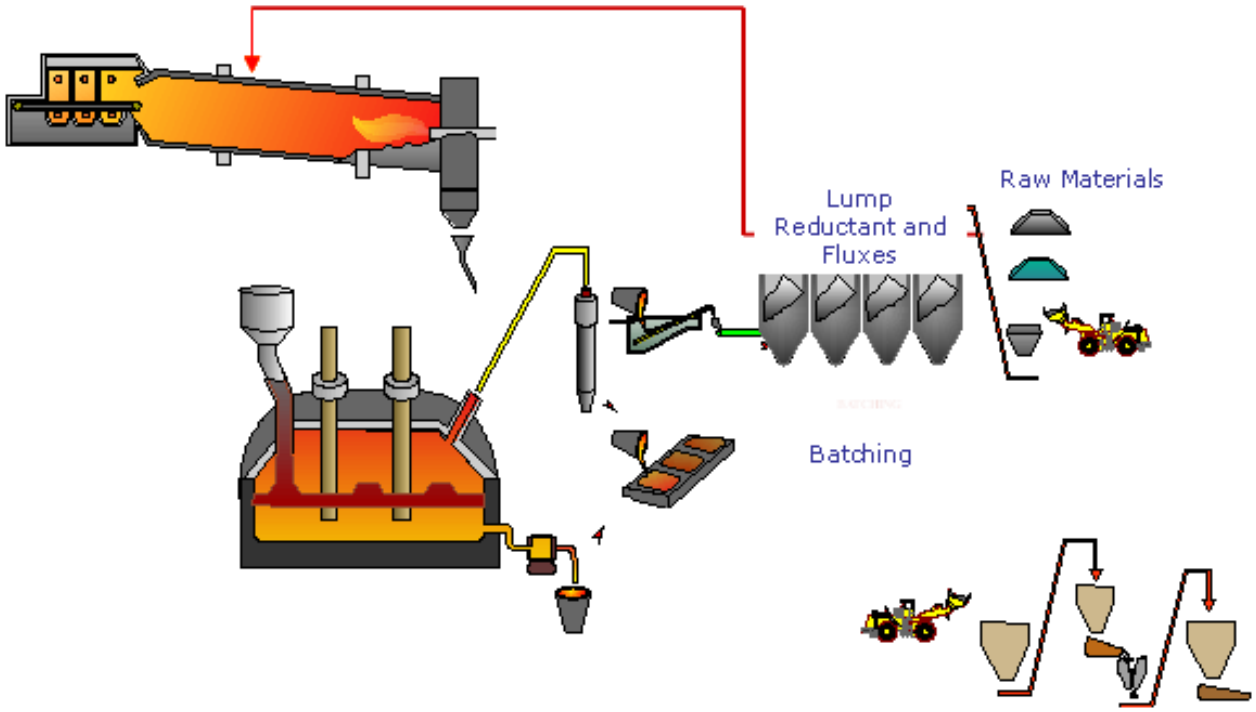

Figure 2.12: Flow diagram of smelting section associated with Premus process.

2.3.4 Research relevant to chromite pre-reduction

Most of the research done to develop the SRC process is confined in aged Showa Denko company literature. A so-called Showa Denko manual was developed for the Lydenburg operations that applied this process. Xstrata Alloys that took over these operations, which was later taken over by Glencore Alloys, still have access to this literature. However, this information is not available in the peer reviewed public domain. In fact very little research has been done specifically for the Premus process (which is based on the SRC process). As far as the candidate could asses, only the Chromium Technology group of the North-West University (NWU) have published research over the last decade that focussed on specific aspects of the Premus process. Kleynhans *et al*. (2012) investigated the influence of using different clay binders in the pre-reduced pellets. These authors proved that binder selection had a significant effect on pellet strength as expected, but unexpectedly it also affected pre-reduction level significantly. Neizel *et al*. (2013) investigated the influence of $CaCO_3$ as an additive to the composite pre-reduction pellets. Although pre-reduction levels increased due to this addition, pellet strength deteriorated so significantly that this would not be a feasible option. Kleynhans *et al*. (2016a) proved that pre-oxidation of the as-received fine chromite ore, prior to the ore being processed with the current process route (as presented in Figures

2.9 and 2.10) significantly increased the level of pre-reduction, which relate to approximately 8.5% lower SEC and 14% lower lumpy carbonaceous reductant requirement, during the smelting of the pre-reduced pellet feed. Subsequently, Kleynhans *et al*. (2017) also proved that this process modification would be financially viable, by conducting a techno-economic study (Kleynhans *et al*., 2017). Kleynhans *et al*. (2017b) also investigated the optimised selection of reductants to include in the composite green pellets, prior to pre-reduction. This study proved that the current maximum volatile matter content, used as a selection criteria by FeCr producers applying this process, is correct, since it ensured pellet strength. However, in addition, reductant ash composition and reductant H-content (as determined with ultimate analysis) needs to be included in reductant selection. The ash composition could have a catalysing or inhibiting effect, while higher H-content resulted in *in situ* H_2 gas formation during pre-reduction, which significantly improved pre-reduction levels. Lastly, Mohale *et al*. (2017) presented how scanning electron microscopy (SEM) in conjunction with image processing can be used to assess the level of pre-reduction, as a quicker alternative to the chemical analysis that is currently conducted at the laboratories associated with FeCr producers.

Some older literature specifically related to the SRC/Premus process, as well as literature that is not specific for the afore-mentioned process, but related to chromite pre-reduction in general are also briefly discussed. Chakraborty *et al*. (2007) studied the influence of temperature and particle size on the reduction of chromite. The author found that the nature of the reducing agent had a very significant influence on the rate of reduction. It was also found that increasing the size of the reducing agent, initially increased the rate of reduction, until a certain size was reached, whereafter reduction decreased. However the authors also concluded that increasing the ore particle size, initially decreased the rate of reduction, while beyond a certain size it increased again. Therefore optimum particle size is an important factor in maximising the degree of pre-reduction. The pre-reduction and smelting characteristics of UG2 ore were studied by Barnes (1983) and compared with other chromite ores. UG2 ore proved to be more reducible than metallurgical grade ores and very significant pre-reduction was obtained. The authors also postulated that using UG2 ores would result in significant savings in SEC.

Xiao *et al*. (2007) found chromite reduction proceeded faster in the outer part of the sample than in the centre and also that reduction of lumpy ore was slower than that of a pellet. The authors concluded that the reduction of chromite with CO is possible, but the presence of solid carbon is required to convert the formed CO_2 gas back to CO through the Boudouard reaction.

Takano *et al*. (2007) concluded that significantly better reduction behaviour was found in pellets in which a liquid slag phase was formed at high temperatures, as opposed to when the liquid slag phase was formed at low temperatures. The reduction of chromite in the presence of many different additives/fluxes have been investigated, as recently summarised by Kleynhans (2017b). Sundar Murti *et al.* (1983) studied the effect of CaO, with graphite as a reductant and found that the additive enhanced reduction. They attributed this to CaO diffusing into the spinel and releasing FeO. Katayama *et al.* (1986) proved that addition of $Na_2B_4O_7$, NaF, NaCl, CaB_4O_7, B_2O_3 and CaF_2 improved chromite reduction, while $CaCl_2$ addition inhibited it. The addition of CaF_2 as a flux, as well as the eutectic mixture NaF-CaF_2 was investigated by Dawson and Edwards (1986). A moderate addition of CaF_2 was found to be beneficial, but the addition of the eutectic mixture was much more effective in promoting reduction. Van Deventer (1988) studied the effect of addition of K_2CO_3, Na_2O_2, CaO, SiO_2, Fe^0, Cr^0, Al_2O_3 and MgO, using graphite as a reductant. It was found that K_2CO_3, Na_2O_2, CaO, SiO_2, Fe^0 enhance the rate of reduction, while Al_2O_3 and MgO inhibited it, and Cr^0 had little effect. Nunnington and Barcza (1989) found that granite and fluorspar addition acted as fluxes and improved reduction rates. Weber and Eric (Weber and Eric, 1992; Weber and Eric, 1993; Weber and Eric, 2006) investigated the reduction of chromite in the presence of silica flux and found that reduction was enhanced at and above 1400 °C. Ding and Warner (1997) investigated the catalytic effects of both lime and SiO_2 additions and found that SiO_2 enhanced reduction rates at and above 1380 °C, but only at reduction levels > 40%, when liquid slag formed. Reduction rate and the extent thereof were found to increase with increasing reduction temperature and lime addition. Wang *et al.* (2015) studied the isothermal reductions at 1400 °C of synthetic chromite, with the additions of CaO, MgO, Al_2O_3 and SiO_2. The rate and degree of reduction was improved by CaO and Al_2O_3 additions, which was attributed to CaO and Al_2O_3 improving Cr^{3+} diffusion in the solid phase. MgO inhibited the reduction, due to the formation of $MgCr_2O_4$. SiO_2 additions did not influence the degree of reduction.

Kekkonen (1995) conducted a thermo-gravimetric analysis (TGA) in the temperature range of 1420 – 1595 °C to study the kinetic mechanisms of solid state carbothermic and CO reduction of chromium pellets. The authors found that the extent of reduction of the chromite particles was more in the outer parts than that of the inner parts of the pellet. CO_2 diffusion was found to be the rate controlling step. The investigation was conducted under an Argon (Ar) atmosphere. Khan (2013) also conducted thermo-gravimetric (TGA) analysis of a single chromite pellet. The author concluded that the single pellet showed similar behaviour than multiple pellets treated in a muffle furnace at 1500 °C. Neuschütz (1992) determined reduction rates from 1200 °C to 1550 °C using TGA and found that additions of silica accelerated the reduction.

2.4 Damring formation in chromite pre-reduction rotary kilns

Damring formation in pre-reduction rotary kilns are one of the challenges FeCr producers utilising the pelletised pre-reduction process are facing. This aspect is of particular interest in this study. As indicated in Section 1.1, damrings (material build-up) are formed in the kiln during chromite pre-reduction (Figure 1.1). The formation of excessive damrings, or damrings in unwanted areas of the kiln can reduce the operational life between kilns shutdowns (to remove damrings) significantly. Mechanical damring removal also damages the kiln refractories.. Even though damring formation is a significant problem in the SRC/Premus process (Section 2.3.3), no peer reviewed literature could be found in the public domain that addressed this issue specifically. The hypothesis stated in Section 1.1 was that damring formation is most likely a result of either PF coal ash softening, or pellet/pellet fragment softening, or a combination of the two. Considering this, PF coal ash fusion temperature (AFT) tests will be a relevant investigation method. AFT analysis was developed to give an indication of clinker forming characteristics of ash from lump coal in stoker-fired furnaces (Reifenstein *et al*., 1999). Currently the one main application of AFT is as an indication of slagging properties of carbonaceous ash in coal combustion or gasification furnaces (Van Dyk *et al*., 2009).

In addition to experimentally determining AFTs, various thermodynamic and mathematical models have also been developed to predict AFTs (Seggiani, 1999; Winegartner and Rhodes; 1975; Van Dyk and Waanders, 2007; Özbayoğlu and Özbayoğlu, 2006). Since thermodynamic modelling was not considered in this particular study, only the mathematical

models are discussed further. Seggiani (1999), as well as Winegartner and Rhodes (1975) used regression analysis to calculate AFTs under reducing conditions using ash chemical composition. The developed equations had a standard deviation of about 45 to 80 °C and 50 °C, respectively. The equations proposed by the authors were complex and included a large number of parameters, including for instance dolomite ratio, as well as acidity and base characteristics, which are not standard analyses. Özbayoğlu and Özbayoğlu (2006) on the other hand used non-linear correlations to relate ash composition to AFT. In terms of regression coefficient and variance, the authors concluded that non-linear regression proved more accurate than linear regression when considering ash composition. These authors also used various parameters to derive their equations that are not considered as standard analysis in FeCr industry. Mathematical modelling has many limitations. For instance, many interactions between species are not taken into consideration. But even with these constraints, valuable information can still be gained (Gibbs *et al*., 2004). The conclusions from the above-mentioned research are that previously postulated equations for predicting AFTs are not specific for the chromite pre-reduction process, and these equations are complex, with some including more than 40 variables. Therefore, there is a need for simpler mathematical model equations, using variables that would be readily available.

As an alternative to AFT determinations, the sessile drop test could be considered. Sessile drop tests are widely used to measure interface and surface energies by determining the wettability angle of a liquid droplet on a surface. Ciftja *et al*. (2010) studied the wetting properties of molten silicon with several graphite materials. Brynjulfsen *et al*. (2010) used wetting experiments to investigate the influence of oxidation on the wetting behaviour of liquid silicon on coated substrates and Bao *et al*. (2011) studied the wettability of molten aluminium on solid alumina. Even though wettability tests are the more common application of sessile drop tests, it can also be used to retrieve other valuable information. Sessile drop tests can also be used to observe the melting point of substances and investigate the reactivity between different materials in different atmospheres. Ringdalen *et al* (2010) used this method to investigate ore melting and reduction in silicomanganese production. Safarian *et al*. (2009) also studied the carbothermic reduction of ferromanganese slag by using the sessile drop test method.

The conditions under which the sessile drop experiments were conducted (i.e. high temperatures and CO gas environment) would provide a feasible environment for studying the thermal behaviour of chromite ores, relevant to pelletised chromite pre-reduction. The melting behaviour of the samples could be observed in order to find the temperature at which deformation starts taking place. Therefore this technique would provide valuable information in this study.

2.5 Conclusions

It was evident from the literature review that there are many research questions, relevant to pelletised chromite pre-reduction (SRC/Premus process), that remain. No literature that specifically considering damring formation in the pre-reduction rotary kiln could be found. The literature study therefore confirmed the importance of investigating damring formation, as stated in Section 1.2, Objectives 1 and 2. Methods that could be used to investigate the afore-mentioned damring formation, e.g. AFT determinations, multi-variant deduction of equations to estimate/predict AFTs, thermodynamic modelling and the sessile drop test method, were identified from literature.

It was also evident from the literature survey that TGA is a commonly used method to follow chromite pre-reduction. However, no evidence could be found that thermo-dimensional changes have been related to chromite pre-reduction. This reinforced that the possible use of TMA to investigated pre-reduction (as stated in Objective 3, Section 1.2), could be a significant new scientific contribution.

Chapter 3

Experimental methods

In this chapter, a description of the different materials used is provided in Section 3.1. The methods of material characterisation (Section 3.2.1) is presented, as well as the computational methods applied (Section 3.2.2). The sessile drop test method used to observe the high temperature behaviour of composite chromite pellets and pellet components is described is Section 3.3.3. Thereafter, detailed descriptions are given of the methods and conditions used in the thermo-gravimetrical (TGA) and – mechanical (TMA) analyses of the composite chromite pellets and pellet components (Section 3.3.4 and 3.3.5).

3.1. Materials

3.1.1 Carbonaceous materials

In the pelletised chromite pre-reduction process, coal is mainly used as pulverised fuel (PF) to fire the rotary kilns. Coal is used because it is a less expensive material than for instance coke and anthracite. Coal usually also has a higher volatile matter content, which makes it easier to ignite than the afore-mentioned carbonaceous materials. Even though coal is currently the material used for this purpose, a wider selection of materials was included in this study to for two reasons, i.e.:

i) Only three different coals used as PF could be obtained from FeCr producers applying the pelletised chromite pre-reduction process. Three samples would be too few to make any significant deduction regarding trends. Therefore, other carbonaceous materials were also included in the assessment.

ii) Including other carbonaceous materials (i.e. coke, char and anthracite) in the assessment would also make it possible to test the developed method and/or identify trend(s) that would be applicable for a wider selection of carbonaceous materials and a wider chemical composition range. This would give FeCr producers confidence in applying the results, even if materials or material compositions changed in future.

A total of twenty anthracites (An-1 to An-10), chars (Ch-1 and Ch-2), cokes (Co-1 to Co-5) and coals (Coal-1 to Coal-3) were obtained as sample materials. At the time when this research was initiated the afore-mentioned carbonaceous materials were either used as PF to fire chromite pre-reduction rotary kilns, or as reductants in the composite pre-reduced pellets at FeCr producers applying the pelletised chromite pre-reduction process.

3.1.2 Chromite ores and typical chromite composite pellet components

Seven typical fine South African chromite ores used as feed material for the production of chromite pellets (either pre-reduced or oxidative sintered pellets) were obtained from FeCr producers. Six of these were metallurgical grade ores and one was an Upper Group 2 (UG2) ore (see Section 2.1.4). The producers that provided the ore samples requested anonymity, therefore the mines of origin of these ores were omitted and the ores were merely indicated as Met grade 1 to 6, and UG2, in further discussions. Since more than a quarter of chromite consumed by the international FeCr industry (excluding South Africa) originate from South Africa (Kleynhans *et al.*, 2016a), results obtained from these ores will also be of international relevance.

Chromite composite pellets used in the pre-reduction process contain reductant and a clay binder. Anthracite breeze from Nkomati Anthracite (Pty) Ltd in the Mpumalanga province (Sentula mining, 2017) was obtained and used as the reductant included in the pellet mixtures. Bentonite clay, which is commonly used as a binder, was obtained from Koppies Bentonite mine in the Free State province (G&W Base (Pty) Ltd., 2011). Both these materials were utilised at FeCr producers applying the pelletised chromite pre-reduction process at the time this study was initiated. Both these materials were also previously characterised and used in a non-related chromite pre-reduction study conducted in the Chromium Technology group at the North-West University (NWU) (Kleynhans *et al*., 2012).

3.1.3 Damrings from a pre-reduction kiln

Actual damrings formed in an industrial chromite pre-reduction rotary kiln (Figure 1.1, Section 1.1) were obtained from a FeCr producer applying this process, after damrings were broken out during a routine shutdown.

3.2. Methods

3.2.1 Material characterisation

3.2.1.1 Proximate and ultimate analysis of carbonaceous materials

During the proximate analysis (air dried basis) the inherent moisture content (MC) was determined according to SABS ISO 11722:1999 and was done by placing a 1 g sample in a glass dish with a cover that has a known mass (m_1). The initial mass was determined (m_2). The sample was then heated uncovered in an air-oven at 105 °C for 1 hour until the mass remained constant. The cover was replaced on the glass dish containing the sample and it was allowed to cool on a metal plate for 10 min. The sample (in the glass dish) was then transferred to a desiccator and allowed to cool for another 10 min after which the mass was determined again (m_3). The MC was then calculated by $MC= (m_2-m_3)/m_2-m_1) \times 100$.

The ash content was determined according to SABS ISO 1171:2010 and it entailed heating 1 g of sample that was spread evenly on a silica dish, to 815 °C ±10 °C for at least 1.5 hours. The dish was removed from the furnace and allowed to cool for 10 min and thereafter cooling was continued to room temperature in a closed container. The mass of the ash was then determined.

The volatile matter (VM) content was determined according to SABS ISO 562:2010. In this method the sample is heated in inert atmosphere at 900 ° C ± 10 °C for 7 min. The % mass fraction of VM is calculated from the loss in mass after deducting the loss of mass due to moisture. The fixed carbon (FC) content was calculated by deducting the MC, ash content and VM from the total weight.

The specifications for the type of furnace that should be used during the above-mentioned procedure are stipulated in the relevant standard referenced. All of the above analyses are reported to the nearest 0.1 % mass fraction.

The ultimate analysis was undertaken according to SABS ISO 29541:2010 in which the C, hydrogen (H), nitrogen (N) and oxygen (O) contents were determined. The C and H contents were determined by heating the sample in a stream of O_2 at 1350 °C and converting C and H into their corresponding gases, i.e. carbon dioxide and water. Anhydrous magnesium perchlorate (< 1.2 mm in size) was used to absorb the water and coarse grained (between 1.5 and 3 mm) sodium hydroxide to absorb the carbon dioxide, which was then determined

gravimetrically according to the above mentioned standard. For the determination of N, the sample was heated with 4 ml concentrated sulphuric acid (98 %) in the presence of 2 g mixed catalyst (consisting of anhydrous potassium sulphate, selenium powder and vanadium pentoxide in a ratio of 90:2:5, respectively) to convert N into ammonium sulphate. The ammonia in the solution is then released using steam distillation after which it was absorbed in boric acid solution. The boric acid solution was made by dissolving 60 g boric acid in 1 L hot water that was allowed to stand for 3 days after which it was decanted. The N was then determined by titration with a 0.005mol/L sulphuric acid solution. The sum of these elements, i.e. C, H and N, together with the ash, MC and total sulphur (S) content, expressed as mass percentage, were used to calculate the O content (adding up to a total of 100). All of the chemicals used during the ultimate analysis was obtained from Radchem.

3.2.1.2 Total sulphur, calorific value and ash composition of carbonaceous materials

The determination of the total S content was done according to SABS ISO 19579:2006 using a LECO CS 244 Sulphur analyser. A sample of 0.2 g was combusted at 1350 °C in a stream of oxygen. Thereafter, particulates and water vapour are removed from the gas stream. The gas stream then passes through a cell in which sulphur dioxide is measured by an infrared absorption detector. The S in the sample is then calculated from the results. For the accelerator flux, a 1:1 mixture of tungsten and iron chips was used.

The gross CV was determined (according to SABS ISO 1928:2009) by burning a sample of solid fuel in high-pressure oxygen in a bomb calorimeter. The sample was burnt in a closed vessel under an oxygen pressure high enough to fill the bomb to 3 MPa. The gross CV is calculated from the corrected temperature rise and the effective heat capacity of the calorimeter.

The ash composition of carbonaceous samples was determined by fusion bead X-ray fluorescence (XRF) as specified in ASTM D4326. The samples containing a high Cr content was analysed using ICP-MS, according to ASTM D6357-11. For the afore-mentioned analysis only contents above the detection limit of the various ash components were retained. The chemical used in the above methods were obtained from De Bruyn Spectroscopic.

3.2.1.3 Reducing and oxidising carbonaceous material ash fusion temperatures

The samples used in the ash fusion temperature (AFT) determination were sized to < 0.075 mm using an agate mortar and pestle. The sample was ashed according to the method described earlier, using SABS ISO 1171:2010. AFT tests were performed according to the SABS ISO 540:2008. The sample was moistened with a sufficient quantity of demineralized water and made into a paste. The paste was placed into a cone mould and allowed to dry. The sample (which is now in the shape of a cone) was removed and mounted onto a support made of sintered alumina. The test piece (sample mounted on support) was heated slowly up to 815 °C to remove any organic matter. The test piece was then placed in the furnace of which the detail is specified in the above-mentioned standard. The temperature was raised to a temperature that is close to the expected deformation temperature of the sample after which the temperature was raised at a rate of 3 °C /min. . Four different temperatures are then recorded according to the specific shape of the ash cone, i.e. the initial deformation temperature (T_{indef}) when the corners of the cone first become rounded; softening temperature (T_{soft}) when the top of the cone first become rounded; hemispherical temperature (T_{hem}) when the entire cone took on a hemispherical shape; and the fluid temperature (T_{fluid}) when the cone collapsed to a flattened button on the furnace floor (Nel *et al*., 2014). According to SABS ISO 540:2008, the standard deviation of AFTs measured in this manner is typically ±30 °C.

AFT tests were conducted in both oxidising (normal air) and reducing atmospheres (CO/CO_2). The reducing atmosphere was obtained by introducing a mixture of 55 vol% CO and 45 vol% CO_2 into the furnace.

Both oxidising and reducing atmospheres were conducted since both atmospheres are relevant to chromite pre-reduction kilns (Kleynhans *et al*., 2012). The atmosphere inside the kiln is partially oxidising to allow PF combustion, while the high carbon content inside the pellets causes a partial positive CO pressure inside the pellets themselves, preventing oxygen from entering the pellets (therefore a reducing environment inside the pellets and surrounding pellet bed) (Kleynhans *et al*., 2012).

3.2.1.4 Chemical analysis of ores and ore components

All the chemicals used were analytical grade (AR) reagents, obtained from the different suppliers and used without any further purification. Ultra-pure water (resistivity 18.2 MΩ cm^{-1}), produced by a Milli-Q water purification system, was used for all procedures requiring water. Instrument grade synthetic air and nitrogen gas were supplied by Afrox.

Inductively Coupled Plasma optical emission spectrometry (ICP-OES) was performed on the ore samples and on the Nkomati anthracite reductant using a Spectro Ciros Vision ICP-OES Spectrometer. The major elements in the anthracite was determined by placing 1 g of sample and 1 g of SARM 18 (used as reference), supplied by Industrial analytical (Pty) Ltd, on silica dishes and exposing them to 815 °C for 90 min using a muffle furnace. The ash residues were then separately transferred into zirconium crucibles containing 2 g sodium peroxide and 0.5 g sodium carbonate as fluxes and mixed using a spatula. The mixtures were fused over a Bunsen flame until melted. After cooling, the fused materials were tapped loose and transferred to 500 ml beakers. The remaining residue was washed out of the crucible with water. 20 ml 1:1 nitric acid was added to the beakers and the crucibles were rinsed with 10 ml 1:1 nitric acid and also added to the beaker. The solutions were heated until dissolved. The solutions were transferred to 200 ml volumetric flasks and 10 ml of a previously prepared yttrium solution was added to each solution. The solutions were diluted and ICP analysis was performed. 0.635 g yttrium oxide was dissolved in 50 ml 1:1 water:nitric acid to make the yttrium solution. The chemical analysis of bentonite clay was determined using a Perkin Elmer ICP-OES according to ISO 172025 standard.

X-ray diffraction (XRD) of bentonite clay was performed using a Phillips X-ray diffractometer (PW 3040/60 X'Pert Pro) with Cu-Kα radiation. X'Pert Highscore plus software was used to identify the phases.

3.2.1.5 Surface analysis of damring samples and ores

The damrings were polished using a SS20 Spectrum System Grinder polisher. It operates at an average speed of 300 r/min for grinding and 150 r/min for polishing. 250 mm platinum 2 green cameo (comparable to a 220-280 grit) and 250 mm platinum 4 red cameo magnetic discs (comparable to a 600 grit) were used. Thereafter 9, 3, and 1 µm Cameo Disk diamond paste polishing cloths were used. Continuous water flow was used as cleaner and lubricant

for the two rough grits, whereas diamond paste suspension poly lubricant supplied by Proscience Laboratory Solutions was applied on the diamond paste cloths to obtain a smooth polished surface. Surface analysis of the polished sample was conducted with a FEI Quanta 200 scanning electron microscope (SEM) with an integrated Oxford Instruments INCA 200 energy dispersive x-ray spectroscopy (EDS) microanalysis system. Since the sample was not set in resin, no surface coating was required to improve the conductivity thereof.

Additionally two ore samples (Met grade 6 and UG2) were set in Technoresin LR151 B:7 resin and polished as indicated above, where after surface analysis were conducted. However, since the samples were set in resin, carbon coating using an Emscope TB 500 carbon coater, was required prior to SEM analysis, using the above mentioned instrument.

Care was taken when comparing chemical analysis, during which the entire sample was digested, and surface analysis, which only reflect the chemical composition of the surface (e.g. surfaces and less than approximately 10 nm depth). Such comparisons were only done to give an indication (not absolute) of the possible origin of phases observed during surface analysis.

3.2.2 Computational methods

In this study it was proposed that the AFT at which PF coal ash and reductant ash would most likely start contributing to damring formation was the T_{soft}. As indicated in Section 3.2.1.5, T_{soft} can be determined experimentally. However, AFTs are not routinely measured by FeCr producers, nor are AFTs supplied by the raw materials suppliers. Therefore, this study could assist FeCr producers to select PF coal and reductants more optimally, if specifically T_{soft} could be calculated/predicted based on more commonly measured parameters. Considering this goal, a multi-variant method, i.e. multiple-linear regression (MLR) analysis was applied, as indicated below.

A simple linear regression model includes a constant (c), an independent variable (x) and a dependent variable (y). The objective is then to establish the relationship between the independent (x) and the dependent (y) variables by fitting a linear equation to the data. In MLR, there is more than one independent variable (x) and the relationship between the dependent variable (y) and the independent variables (x) is given by the following equation (Du Preez *et al*., 2015).

$$y = c_0 + c_1x_1 + c_2x_2 + \ldots\ldots c_px_p \quad [3.1]$$

In this study T_{soft} for oxidising and reducing environments were considered as the dependent variable, while the proximate, ultimate, total S, CV and the ash composition data as independent variables. To measure the difference between predicted values (e.g. calculated by MLR model) and observed/experimental values the root mean squared error (RMSE) was calculated. It basically measures the quality of the fit between actual data and predicted values (Salkind, 2010), as applied in numerous previous studies (Du Preez *et al.*, 2015; Venter *et al.*, 2015; Awang *et al.*, 2015). RMSE is calculated using the following equation:

$$\text{RMSE} = \sqrt{\frac{\sum_{i=1}^{n}(Y_{calc,i} - Y_{exp},i)^2}{n}} \quad [3.2]$$

Where

Y_{calc} is the predicted/calculated value using a specific model

Y_{exp} is the experimental/observed values from the actual data

n being the number of observations

Data from sixteen of the twenty carbonaceous samples were used to construct the MLR equation, while the remaining four samples were used to assess how well the method performed. This was done by using the constructed equations to calculate the values of the T_{soft} and comparing it to the actual data.

SPSS programming software (https://www.ibm.com/analytics/data-science/predictive-analytics/spss-statistical-software, Date of access: 20 October, 2017) was used to calculate parameters that could be used to interpret the MLR results and to determine the contributions of the different independent variables to the calculated T_{soft} values.

3.2.3 Sessile drop analysis of chromite ore, composite pellet mixtures and pellet components

The maximum temperature of the AFT test instrument (Section 3.2.1.5) was 1550 °C. Due to the spinel crystalline structure of chromite, the melting temperature thereof is higher than the afore-mentioned temperature. Therefore in order to determine the temperatures at which

softening of the ores and composite chromite pellet mixtures took place, an alternative method, i.e. sessile drop, was used. The sessile drop furnace has a maximum operating temperature of 2400°C and could therefore be used for this purpose (Gaal *et al*., 2007; Safarian *et al*., 2009; Ringdalen *et al*., 2010).

The seven sample ores (Section 3.1.2) were individually mixed with a carbonaceous reductant and a clay binder to form pellet mixtures. Mass ratios used for the pellet mixtures were 3 wt% clay and 20 wt % (relating to 15 wt % FC) reductant with the remainder of the mixtures made up with the ore. These mass ratios are similar to what is industrially applied (Kleynhans *et al*., 2012). The softening temperatures of the anthracite breeze (Section 3.1.2) and the bentonite clay (Section 3.1.2) were also investigated individually, using the sessile drop test method.

The chromite ore samples were dry milled to the particle size applied in the pre-reduction process, i.e. 90% smaller than 75μm (d_{90} = 75μm). A laboratory disc mill (Siebtechnik) with a tungsten carbide grinding chamber was used, to avoid possible iron (Fe) contamination. This was done since the presence of additional metal Fe would influence the level of pre-reduction/metallisation of the composite pellets, which could have an influence on T_{soft}. The particle size distribution was determined using a Malvern Mastersizer 2000 as described by Glastonbury *et al*. (2015). Each pellet mixture consisted of 3 weight % clay, ~20 weight % anthracite (to ensure 15 weight % FC content) and the remainder was made up with chromite ore. These pellet mixtures were also dry-milled to the same particle size as indicated for the ores (d_{90} = 75μm).

The above-mentioned milled samples were pressed into small pellets of approximately 3 mm in diameter and height. An investigated pellet was placed on a graphite substrate disk (diameter of 10 mm and height of 3 mm), which was then placed in the sample holder in the sessile drop furnace. In Figure 3.1 an image of the sample holder with a pellet placed on the graphite substrate can be seen. These small pellets must not be confused with the larger composite pellets that were made for the Thermo-gravimetric (TGA) and Thermo-mechanical (TMA) analyses. These larger pellet were produced (Section 3.2.4 indicating how) to simulate industrially produced composite chromite pellets that are pre-reduced.

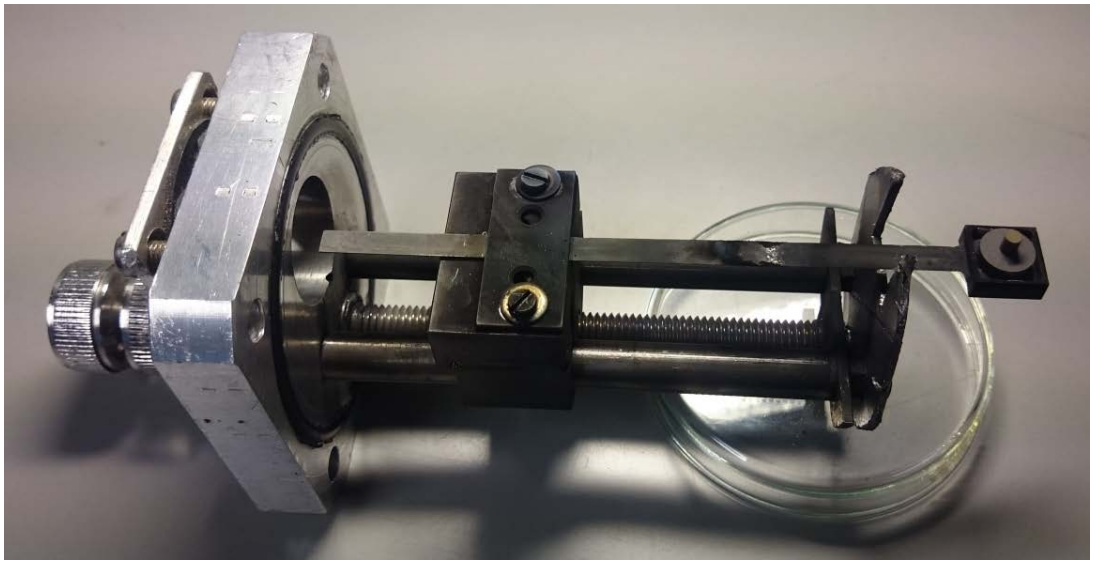

Figure 3.1: Sample holder of the sessile drop furnace with a pellet placed on the graphite substrate.

The sessile drop furnace was heated at 300°C/min up to 900°C and then at 10°C/min up to 1950°C. The furnace was continuously purged with 0.5 Nl/min of carbon monoxide for the entire duration of the experiment. A firewire digital video camera with a telocentric lens was used to record images at a resolution of 1280 x 960 pixels, to determine the different stages of melting. The telocentric lens has a 12x zoom, enhancing the images in such a way that the melting stages can be viewed clearly. The instrument was calibrated using pure iron on a pure alumina substrate in an argon atmosphere. In Figure 3.2a the actual image of the sessile drop test unit can be seen. Figure 3.2b shows an enlarged image of the furnace part of the sessile drop unit.

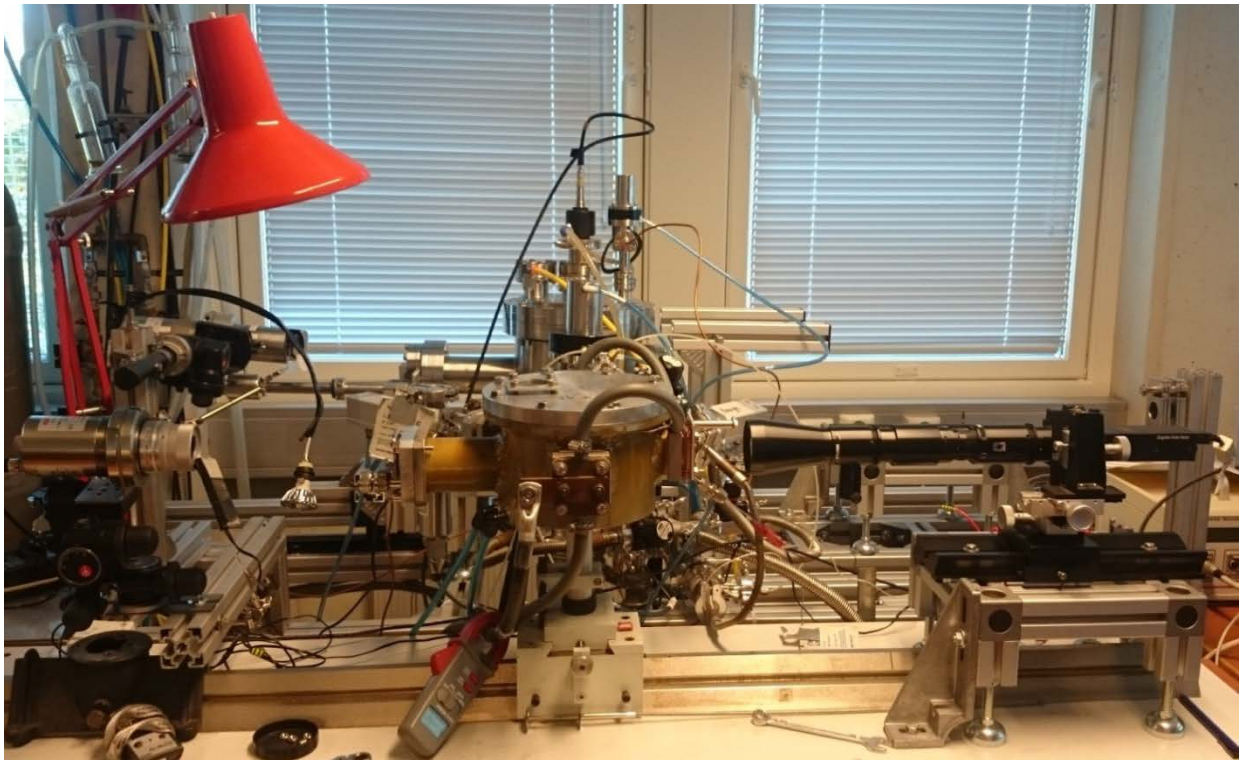

(a)

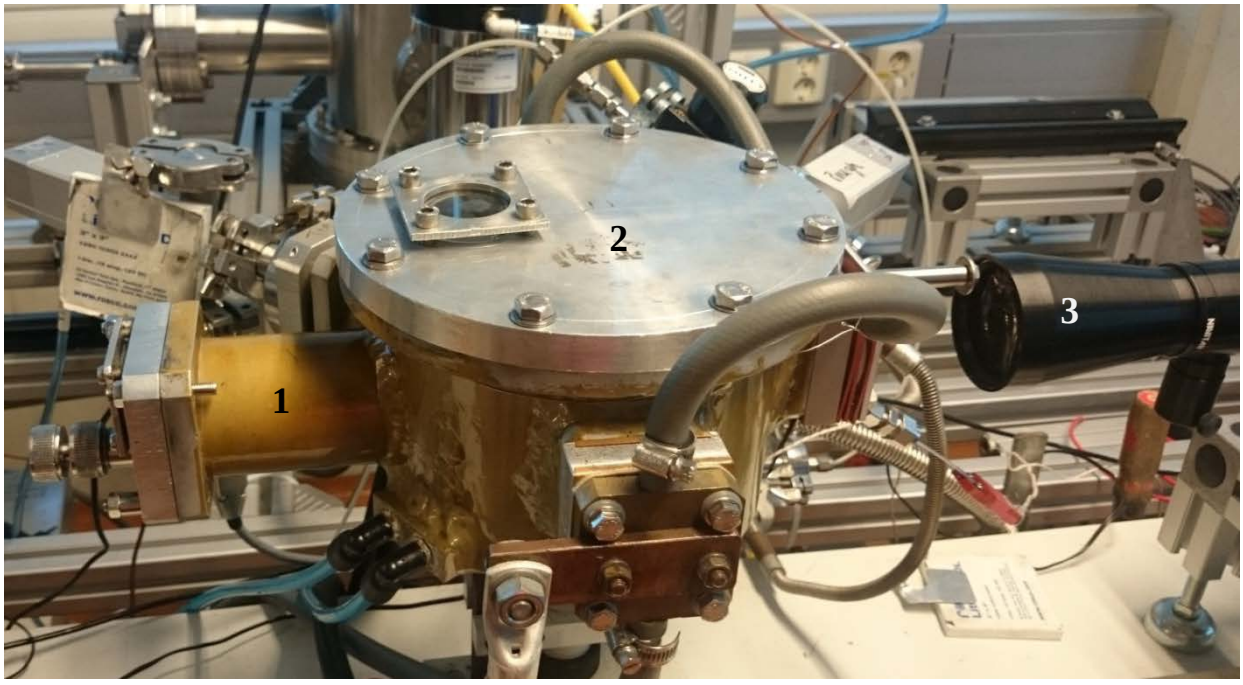

(b)

Figure 3.2: Sessile drop furnace setup (a) and an enlarged image of the furnace only (b). The section marked “1” is the furnace. The section marked “2” is the furnace chamber and the “3” is the camera.

3.2.4 Thermo-gravimetrical analysis

Thermo-gravimetric analysis (TGA) provides the change in mass as a function of temperature or time. This data can be converted to derivative mass loss (DTG), which indicates the rate of mass loss and is defined by Equation 3.3

$$\frac{m_i - m_0}{t_i - t_0} \qquad [3.3]$$

where

mi is the mass loss (mg or %) at time interval i and m_0 is the mass loss at time interval 0

t_i is the time (min) at point i and t_0 is time at point 0.

TGA (together with DTG) can be used to investigate physical transitions and chemical reactions influencing the thermal behaviour of a sample. In this study it was used to investigate the thermal behaviour (and more specifically reduction) of composite chromite pellets, to understand the process inside the pre-reduction rotary kiln better. A large mass TGA, which was specifically designed for this purpose, was used. It worked on the same principle as a commercial TGA, but could analyse a sample with a maximum mass of approximately 100 g instead of 50 mg.. As the development of this large mass TGA formed part of the results of this study, it is described in Chapter 6, Section 6.2.

The same pellet mixtures and pellet components that were used in the sessile drop analysis were also used during TGA analysis. These samples were milled and mixed as described in Section 3.2.3. Met grade 1 was selected for the investigation of thermal behaviour of pellets. As previously stated, the size of the pellets used for TGA were selected to be as close as possible to industrial size pellets, while still being small enough to fit into the thermo-mechanical analyser (TMA) used in Section 3.2.5. The composite pellet mixtures (reductant and clay) were pressed into cylindrical pellets using LRXplus strength tester from Ametek Lloyd Instruments with a 5kN load cell. Figure 3.3a presents an image of the LRXplus and Figure 3.3b an image of the die set. The samples mixtures that were to be pelletised were placed in a Specac PT No. 3000 10 mm die set with a drop of water (to bind the mixture together) and compressed at a rate of 10mm/min with a force of 1500 N for 10 seconds. Using this pelletising method ensured consistency of pellet sizes and densities. Pellets of individual pellet component, i.e. ore, reductant or clay, were also produced, to investigate separately with TGA.

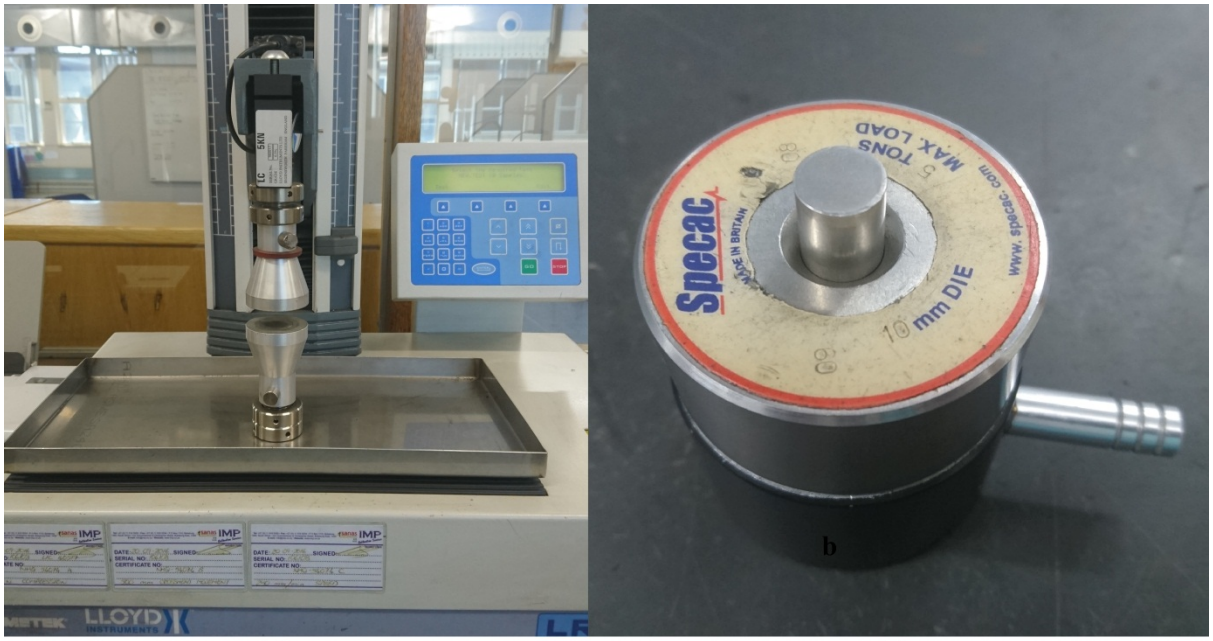

(a) (b)

Figure 3.3: An image of the LRXplus strength tester (a) and a Specac die set (b).

As mentioned in Section 3.1, the atmosphere inside the kiln is partially oxidising allowing for PF combustion, but also partially reducing because of the high carbon content inside the pellets that causes a partial positive CO pressure inside the pellets themselves, preventing oxygen from entering the pellets. To imitate the conditions inside a pre-reduction rotary kiln, 15 to 20 pellets (about 20 g) were placed in an alumina crucible with a lid on it (supplied by Ceradvance engineering ceramics), in an attempt to recreate a pellet bed that forms a reducing (CO) environment. It is generally accepted that the pre-reduction temperature that the pellets achieve during the industrial process is approximately 1300 °C. Therefore the TGA analyses were mostly done for a temperature of up to 1450 °C. The furnace was heated at a rate of 5 °C/min. up to 500 °C and held at that temperature for 30 min. Thereafter it was heated at a rate of 10 °C/min up to 1450 °C (50 °C below the maximum furnace temperature) and held there for 20 min to make sure it reaches the correct temperature.

The TGA analyses were conducted in inert atmosphere by keeping an N_2 flow-rate of 1 NL/min throughout the experiment. The inert atmosphere was utilised to avoid pre-reduction or oxidation, due to the presence of external gas (Kleynhans *et al*., 2012). Although it is common to use argon (Ar) during TGA analyses, N_2 was used in this study. This was done to more accurately recreate a realistic situation, i.e. > 78% of the atmosphere consist of N_2. This N_2 is blown with the combustion air into pre-reduction rotary kilns. Du Preez *et al*. (2018)

proved that nitrites, which can influence the pre-reduction of chromite, form at temperatures relevant to chromite pre-reduction. Therefore, the presence of N_2, instead of Ar, is a better simulation of actual conditions. However, the atmosphere in a pre-reduction rotary kiln is complex and varies. For instance at the firing end (discharge end) more oxygen (O_2) needs to be present to ensure PF combustion, while in the feed end (connected to the travel grate that pre-heat the pellets) a CO/CO_2 environment dominate (CO concentrations typically < 10%) with a much lower partial O_2 pressure. Therefore, it would also be relevant to use a CO/CO_2 environment; however, the high temperature laboratory available to the candidate at the NWU was not equipped with the necessary safeguards required for CO gas use. Considering all the afore-mentioned, a N_2 atmosphere was the best option for this specific study, while the simulated pellet bed recreated in the crucible was allowed to form a reducing CO gas environment.

The accuracy of the large mass TGA built as part of this study (Section 6.2) was evaluated by comparing the results thereof, with that of a commercial TGA, using the same sample material. The commercial TGA used was a Netzsch STA 449F3 using an Al_2O_3 crucible. The commercial TGA was heated at 35 °C/min from ambient temperature to 1450 °C, in a N_2 gas environment.

3.2.5 Thermo-mechanical analysis

A TMA instrument measures dimensional changes of a sample as a function of temperature or time. The differential dimensional change (DTMA) was also obtained for the TMA instrument, which indicated the rate of dimensional change. The thermal expansion/contraction of a pre-reduction pellet, as well as individual pellet components, were investigated using a Seiko Instruments Inc. TMA/ss 6100 thermo-mechanical analyser interfaced with S11 EXSTAR 6000. An image of the TMA instrument that was used is presented in Figure 3.4.

Figure 3.4: Image of the TMA instrument used with the section marked "1" being the furnace and "2" being the chamber.

As discussed in Section 3.2.4, similar pellets that were used in the TGA measurements were also used for TMA measurements. The pellet mixtures and pellet components were milled and mixed in the same way as described in Section 3.3 and the pellets were pressed as discussed in Section 3.2.4. Prior to an analysis, the TMA furnace was purged with N_2 for 30 min. A gas flow of 1.67 Nl/h N_2 was maintained through the entire experiment and during cooling, to ensure comparability to TGA results and to avoid oxidative corrosion of the instrument. The sample pellet was placed in the furnace in the sample container presented in Figure 3.5, and heated at a rate of 5 °C/min up to 500 °C and then 10 °C/min up to 1450 °C (the same heating rate used for the large mass TGA). In accordance with the operational manual of the TMA instrument, an alumina correction coefficient was applied to the data, since the probe used to measure the dimensional changes was made of alumina.

Figure 3.5: Image of the sample container of the TMA with the TMA furnace below it.

Chapter 4

Results and discussion

Pulverised fuel coal ash contribution to damring formation in chromite pre-reduction rotary kilns and material selection to minimise it

In this chapter, high temperature softening of pulverised fuel coal ash was investigated and considered as a contributor to damring formation in chromite pre-reduction rotary kilns. Twenty carbonaceous materials were characterised (Section 4.1), where after multiple-linear regression analyses (Section 4.2) were conducted to determine optimum equations to calculate ash softening temperatures of the afore-mentioned materials (Section 4.2.1). The accuracy of softening temperatures calculated with these equations were then determined (Section 4.2.2). Thereafter the chemical information that could be derived from these equations was explored (Section 4.2.3). Finally, conclusions derived from the results were presented (Section 4.3).

4.1 Carbonaceous material characterisations

To facilitate investigating the contribution of pulverised fuel (PF) coal ash to damring formation in chromite pre-reduction rotary kilns, the twenty carbonaceous materials considered in this study (introduced in Section 3.1) were characterised in detail. As previously stated, less expensive coal (if for instance compared with metallurgical coke) is usually used as PF in the afore-mentioned process. However, only three different PF coals samples were obtained from ferrochrome (FeCr) smelters applying the pelletised chromite pre-reduction process. Since this study attempted to find systematic trends in explaining the formation of damrings, other carbonaceous materials (e.g. metallurgical coke, char and anthracite) commonly used in pyro-metallurgical applications (e.g. smelting, pellet sintering or pre-reduction) were also included as study materials. The inclusion of these additional carbonaceous sample materials had two advantages, i.e.:

i) This larger sample size made it more likely to identify trends, which would be highly unlikely if only the three PF coal samples obtained from industry were considered.

ii) If trends that are valid across carbonaceous material types could be identified, it would give confidence that these trends would be valid, even if material composition or type varied.

Table 4.1 presents the proximate- and ultimate analyses, total S contents, CVs, ash compositions, as well as the reducing and oxidising ash fusion temperatures (AFTs) of all the carbonaceous materials considered. The carbonaceous materials consisted of anthracites (An-1 to An-10), chars (Ch-1 and Ch-2), cokes (Co-1 to Co-5) and coals (Coal-1 to Coal-3). Obviously, elements occurring in the ash could occur in a different phase than what is presented in the ash compositions in Table 4.1, however, the reported species are standard for this type of analysis. For example, iron occurring in carbonaceous materials such as coal is usually reported as iron(III)oxide or hematite (Fe_2O_3). This standard reporting format is used, since Fe_2O_3 is the most common natural oxide of iron. However, naturally occurring iron(II)oxide (FeO), which is much more rare, and iron(II,III)oxide (Fe_3O_4), which occurs naturally as magnetite, could also have been incorporated into the coal during formation. Therefore, by presenting the ash compositions in the standard format, the candidate by no means implied that the elements occurred exclusively as these species.

Of all the carbonaceous material characteristics presented in Table 4.1, the most obvious that could be used directly to assess the contribution to damring formation are the AFTs. It stands to reason, that in general lower AFTs would result in softening of the PF coal ash at lower temperatures, which would promote damring formation. From the AFT results (Table 4.1), it is clear that some carbonaceous materials would more likely contribute to damring formation than others. Even though both the oxidising and reducing atmosphere ash fusion fluid temperatures (T_{fluid}) of all the carbonaceous materials were above the temperature that would typically be found inside the kiln (usually fired at approximately 1300 °C), many of the samples will start softening (T_{soft}) at or even below the afore-mentioned temperature.

Table 4.1: Proximate and ultimate analysis, total S, gross CV, ash composition and reducing and oxidising AFT of materials considered.

		An-1	An-2	An-3	An-4	An-5*	An-6	An-7	An-8	An-9*	An-10	Ch-1	Ch-2	Co-1*	Co-2	Co-3	Co-4	Co-5	Coal-1	Coal-2	Coal-3*
Proximate analysis (air-dried) (%)	MC	3.8	1.9	2.9	2.1	1.4	1.3	3.2	1.2	1.6	3.2	4.4	5.6	1.2	0.2	0.6	0.4	0.4	4.0	2.3	2.8
	Ash content	15.7	20.3	11.8	12.1	15.5	15.9	15.0	16.0	11.7	16.3	34.9	22.1	20.4	7.7	16.5	9.8	12.4	10.7	10.3	13.1
	VM	5.0	9.7	4.9	4.5	6.5	8.6	4.0	7.6	5.1	5.0	8.4	4.7	1.6	0.6	0.8	0.8	0.9	30.9	35.5	32.2
	FC	75.5	68.1	80.4	81.3	76.6	74.2	77.8	75.2	81.6	75.5	52.3	67.6	76.8	91.5	82.1	89.0	86.3	54.4	51.8	51.9
Ultimate analysis (air-dried) (%)	C	74.1	70.6	78.3	79.9	76.1	75.3	76.2	75.8	80.1	73.6	54.7	67.3	75.5	89.1	81.0	87.5	84.7	69.4	71.8	68.6
	H	1.6	2.6	2.1	2.0	2.5	3.1	1.5	3.0	2.3	1.7	1.0	0.5	0.2	0.0	0.0	0.1	0.0	4.7	5.2	4.6
	N	1.6	1.7	1.8	1.4	1.6	1.6	1.6	1.6	1.5	1.6	1.1	1.1	0.9	1.3	0.7	1.0	1.2	1.9	1.6	1.6
	O	2.0	2.1	2.1	1.8	2.2	2.0	1.8	1.9	2.1	2.1	3.6	3.1	1.0	0.8	0.4	0.7	0.5	8.9	7.6	9.0
Total S (air-dried) (%)		1.1	0.7	1.1	0.7	0.8	0.8	0.7	0.6	0.7	1.4	0.4	0.3	0.8	0.8	0.8	0.5	0.8	0.5	1.1	0.5
Gross CV (air-dried) (MJ/kg)		27.2	27.2	29.5	29.5	29.4	29.6	28.1	29.7	30.5	27.4	19.5	23.5	23.3	29.3	22.8	27.8	27.0	27.9	29.3	27.7

* These samples were excluded from the MLR calculations, but were used to verify the accuracy of the MLR calculations.

Table 4.1 continued...

		An-1	An-2	An-3	An-4	An-5*	An-6	An-7	An-8	An-9*	An-10	Ch-1	Ch-2	Co-1*	Co-2	Co-3	Co-4	Co-5	Coal-1	Coal-2	Coal-3*
Ash composition (%)	Al_2O_3	22.70	19.70	28.59	28.85	17.97	19.25	25.35	21.03	28.58	25.92	19.80	28.77	17.41	24.88	19.77	24.89	22.39	24.39	19.23	23.59
	CaO	1.22	4.99	2.35	3.08	4.18	1.82	6.29	2.07	2.88	0.97	2.65	2.66	1.69	1.78	1.55	5.32	3.74	3.52	0.99	2.28
	Cr_2O_3	6.79	16.40	0.38	0.08	1.45	0.06	0.09	0.04	0.09	3.14	26.20	6.53	5.64	1.79	0.88	2.20	4.57	0.44	0.44	0.13
	Fe_2O_3	21.03	16.20	10.44	4.90	7.28	5.90	5.36	4.15	4.05	13.61	17.50	6.94	12.16	17.00	9.01	15.09	14.87	3.75	5.66	2.77
	K_2O	1.33	1.00	2.42	2.03	1.69	1.77	1.79	1.64	1.57	1.49	0.33	0.45	0.95	1.95	1.16	1.72	2.25	1.08	1.03	1.19
	MgO	3.31	5.28	1.30	1.43	1.33	0.87	1.59	0.86	1.29	2.39	6.25	3.52	1.93	1.09	0.78	3.03	2.30	1.51	0.55	1.03
	MnO	0.11	0.14	0.10	0.07	0.11	0.07	0.10	0.07	0.06	0.07	0.17	0.09	0.16	0.12	0.12	0.20	0.13	0.02	0.08	0.01
	Na_2O	1.27	1.14	2.37	1.52	0.36	0.70	3.13	1.19	1.11	1.49	0.08	0.04	0.09	0.92	0.11	1.37	1.25	0.27	0.22	0.16
	P_2O_5	0.08	0.11	0.15	0.08	0.19	0.21	1.83	0.31	0.08	0.08	0.08	0.07	0.17	0.33	0.21	1.11	0.29	0.27	0.11	0.09
	SiO_2	40.57	29.00	48.52	54.13	61.78	67.04	50.17	67.36	55.60	49.36	23.70	48.94	57.45	48.34	63.35	40.21	46.15	59.43	68.66	65.97
	TiO_2	1.41	1.09	1.76	1.24	0.96	0.94	1.31	0.84	1.14	1.25	0.86	1.25	1.43	1.25	1.69	1.00	0.93	1.28	1.76	1.00
	V_2O_5	0.13	0.18	0.15	0.06	0.08	0.06	0.04	0.05	0.06	0.07	0.21	0.10	0.16	0.11	0.14	0.10	0.11	0.05	0.12	0.03
	ZrO_2	0.07	0.04	0.12	0.07	0.05	0.05	0.06	0.03	0.06	0.06	0.03	0.05	0.14	0.04	0.17	0.04	0.04	0.11	0.18	0.08
	Ba	0.20	0.16	0.12	0.11	0.14	0.13	0.16	0.13	0.09	0.23	0.04	0.07	0.08	0.12	0.12	0.31	0.19	0.08	0.08	0.05
	Sr	0.15	0.18	0.33	0.32	0.08	0.07	0.31	0.08	0.29	0.13	0.05	0.05	0.04	0.11	0.06	0.19	0.11	0.11	0.05	0.04
	SO_3	0.72	4.32	1.77	2.85	3.18	1.50	2.33	1.32	3.89	0.86	2.31	1.20	1.02	0.68	0.90	2.72	1.32	3.20	0.76	1.36
AFT (Red. atmos.) (°C)	T_{indef}	1318	1308	1226	1417	1244	1323	1228	1392	1470	1206	1242	1444	1274	1190	1334	1225	1136	1378	1446	1454
	T_{soft}	1329	1325	1258	1438	1261	1346	1237	1406	1516	1254	1292	1456	1320	1218	1369	1244	1142	1408	1466	1512
	T_{hem}	1298	1300	1244	1430	1247	1338	1210	1398	>1550	1326	1290	1458	1302	1227	1366	1288	1156	1389	1448	1496
	T_{fluid}	1389	1470	1426	1500	1384	1443	1308	1477	>1550	1438	1484	1484	1456	1398	1456	1475	1454	1462	1502	>1550
AFT (Oxid. atmos.) (°C)	T_{indef}	1324	1318	1344	1466	1270	1366	1252	1402	>1550	1392	1309	1456	1348	1365	1379	1266	1232	1463	1485	1508
	T_{soft}	1338	1330	1398	1496	1288	1386	1265	1433	>1550	1424	1322	1464	1372	1378	1397	1288	1268	1495	1504	1544
	T_{hem}	1359	1344	1421	1508	1314	1412	1283	1451	>1550	1439	1344	1498	1381	1394	1430	1378	1308	1519	1525	>1550
	T_{fluid}	1486	1522	1490	1546	1432	1512	1360	1530	>1550	1486	1530	1544	1520	1458	1504	1522	1514	1549	1550	>1550

* These samples were excluded from the MLR calculations, but were used to verify the accuracy of the MLR calculations.

As expected, the coal samples had the lowest fixed carbon (FC) and highest volatile matter (VM) contents, while the char samples had the highest ash contents. The coke samples had relatively high FC and the lowest VM contents. There are many factors influencing the melting point of carbonaceous materials, hence it is difficult to relate the measured parameters reported in Table 4.1 directly to AFTs. However, some authors have made general observations. Van Dyk and Keyser (2005) found that low ash melting temperatures were generally accompanied by high CaO and high Fe_2O_3 contents. Also, Van Dyk (2006) investigated the influence of acidic components (Si, Al and Ti) on AFTs and found that increases of these components all resulted in increased AFTs. The effect of different mineral species on AFTs has also been investigated by Van Dyk *et al.* (2005). It was found that certain combinations of species has a statistical significant effect on AFT, but it is also stressed that ash composition alone does not accurately explain AFT behaviour. Song *et al*. (2009) also investigated the effect of coal ash composition on AFTs. According to these authors AFTs decrease with increasing CaO, Fe_2O_3 and MgO contents, and then increases again after reaching a minimum value. In the results presented (Table 4.1) An-4, An-8, An-9, Ch-2, Coal-1 and Coal-2 generally had the highest AFTs and these samples also had very low Fe_2O_3 ash contents in comparison to the other samples. Also, Co-5 had the lowest deformation temperatures (T_{indef}) and T_{soft} and contained 14.87 % Fe_2O_3, which is fairly high in comparison to the other samples. Additionally, SiO_2 seemed higher in the samples with higher AFTs. However, the afore-mentioned deductions from the experimental results (Table 4.1) are made by general observations of trends and can therefore not be used on its own as the basis for selecting carbonaceous PF to reduce damring formation during chromite pre-reduction. A more systematic approach is required, as there are too many variables and interactions between the variables that need to be taken into consideration. Therefore multiple-linear regression (MLR) analysis was used to establish mathematical relationships between the different factors.

4.2 Multiple-linear regression analysis to calculate AFTs of carbonaceous materials

4.2.1 Determination of optimum multiple-linear regression equations

In this study T_{soft} was considered as the temperature at which PF coal ash will start contributing to damring formation in the chromite pre-reduction kiln. Therefore, oxidising T_{soft} and reducing T_{soft} were considered as the dependent variables while the other parameters

presented in Table 4.1 (excluding the AFTs) were considered as independent parameters in MLR calculations. As mentioned in Section 3.1, both oxidising and reducing atmosphere AFTs were considered in this study, since both atmospheres are relevant to chromite pre-reduction kilns (Kleynhans *et al.*, 2012). The atmosphere inside the pre-reduction kiln is partially oxidising to allow PF combustion, while the relatively high carbon content inside the chromite composite pellets (typically 10 to 15 weight.% FC) causes a partial positive CO pressure inside the pellets themselves, preventing oxygen from entering the pellets (therefore a reducing environment inside the pellets) (Kleynhans *et al.*, 2012).

The relationship between the number of independent variables included in the optimum MLR solutions and the root mean squared error (RMSE) between the calculated T_{soft} values and the experimental values (Table 4.1) are presented in Figures 4.1a and 4.1b, for the reducing T_{soft} and the oxidising T_{soft}, respectively. As indicated in Section 3.2, RMSE was used in this study as a measure to quantify the differences between the calculated and experimental values. The use of RMSE in this manner is relatively common scientific practice (e.g. Pham *et al.*, 2018; Khaosravi *et al.*, 2018; Hong *et al.*, 2016). As is evident from the results for the reducing T_{soft} (Figure 4.1a) the RMSE for the optimum MLR equation containing one independent variable was approximately 75 °C. This could be reduced to approximately 55 °C, if an optimum MLR equation containing two independent variables was calculated. This equation implies that the combined effect, not the individual effects, of the afore-mentioned two independent variables resulted in the lower RMSE. In this manner, MLR accounts better for combined effects than simple linear regression analysis. In a similar manner, the inclusion of more independent variables in the optimum MLR solution further reduced the RMSE. Additional independent variables were included until the relative improvement (RMSE for equation with x-1 independent variable – RMSE for equation with x independent variables)/(RMSE for equation with 1 independent variable – RMSE for equation with infinite independent variables) in RMSE, was less than 1 %. The latter term, i.e. relative improvement in RMSE, was defined since it is important to quantify when an insignificant improvement in RMSE would be achieved. Similar terms to quantify RMSE improvement during MLR calculations have been proposed by previous authors (e.g. Carter and Liang, 2018; Germec *et al.*, 2018; Zaouche *et al.*, 2017; Dennison and Roberts, 2003). Applying the afore-mentioned for the reducing T_{soft} (Figure 4.1a) an optimum MLR equation containing 10 independent variables for which the RMSE was approximately 1.7 °C was obtained. In a similar manner the optimum MLR solution for oxidising T_{soft} (Figure 4.2b),

which had a relative improvement in RMSE of less than 1 % (correlating to approximately 0.5 °C), was found to contain 11 independent variables.

Considering that the uncertainty associated with AFT measurements is 30 °C (SABS ISO 540:2008) the above-mentioned RMSE differences between calculated T_{soft} values and the experimental values (1.7 and 0.5 °C, respectively) could be considered as over-fitting of the data. However, if a 30 °C RMSE limitation was applied, instead of the relative improvement in RMSE of less than 1 %, only 5 independent variables would be included for the reducing T_{soft} equation and 4 independent variables for the oxidising T_{soft} equation. The absolute differences in the MLR calculated T_{soft} between the applied rule (1 % relative improvement in RMSE) and if a 30 °C RMSE limitation were found to be in the range of 50 to 100 °C. Within the context of industrial application and optimum selection of PF coal, 50 to 100 °C lower/higher T_{soft} can have a significant effect on damring formation. Therefore, it was decided to rather implement a relative improvement in RMSE as described, which is quantifiable (is associated with a rule) and gave more accurate calculated T_{soft} values.

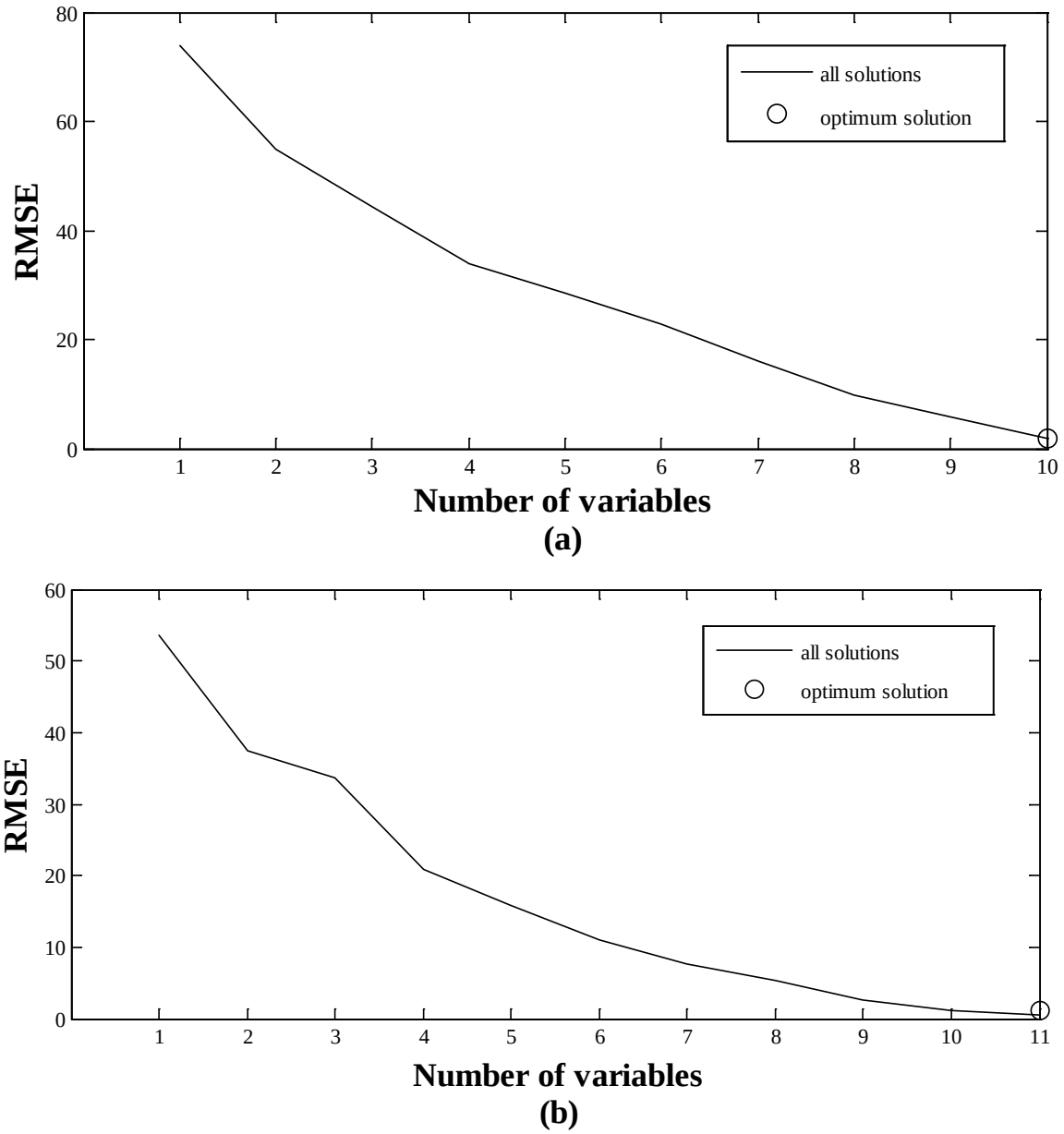

Figure 4.1: RMSE between the calculated and experimental T_{soft} for reducing (a) and oxidising (b) atmospheres, as a function number of independent variables included in the optimum MLR equation.

Considering the method applied, the optimal MLR equations that were derived for calculating reducing T_{soft} and oxidising T_{soft}, are presented in Equations 4.1 and 4.2, respectively.

$T_{soft\ (reducing)}^{*}$ = -1.4286E4 + (1.7570E2 x MC) + (1.5738E2 x Ash) + (1.6621E2 x C) + (2.5337E2 x H) + (1.3008E2 x O) + (-1.8626E2 x K_2O) + (-1.1178E2 x P_2O_5) + (-5.0067E2 x V_2O_5) + (7.1129E2 x Sr) + (-3.5258E1 x SO_3) [4.1]

$T_{soft\ (oxidising)}^{*}$ = 2.1568E3 + (-2.4588E1 x MC) + (-5.1311E0 x FC) + (-3.4287E0 x H) + (1.2248E1 x Al_2O_3) + (-1.4721E2 x K_2O) + (-6.4158E1 x MgO) + (1.5306E2 x MnO) + (-1.2579E2 x P_2O_5) + (-6.9090E2 x ZrO_2) +(1.8523E2 x Ba) + (4.8366E2 x Sr) [4.2]

*The temperature calculated using Equation 2 and 3 is given in Kelvin.

Detailed ash compositional analyses, which include trace compositions as considered thus far, are not always available to FeCr producers. Therefore, alternative MLR analyses were also conducted by only considering parameters/species obtained from the most common analyses (i.e. proximately and ultimate analyses, CV, as well as S and P contents) as independent parameters. Such optimized MLR equations are indicated in Equations 4.3 and 4.4.

$T_{soft\ (reducing)}$ = 5.1644E4 + (-4.4774E2 x MC) + (-5.0252E2 x Ash) + (-5.7204E2 x S) + (-4.9658E2 x C) + (-3.8675E2 x H) + (-8.2477E2 x N) + (-5.2977E2 x O) [4.3]

$T_{soft\ (oxidizing)}$ = 4.9162E4 + (-4.7869E2 x MC) + (-4.7767E2 x Ash) + (-4.0485E2 x VM) + (-3.7872E2 x FC) + (8.1854E0 x CV) + (-9.6356E1 x C) + (-4.1131E2 x N) [4.4]

The above-mentioned optimized MLR equations had RMSE differences between the calculated and experimental reducing and oxidizing T_{soft} of 39.3 and 41.4 K, respectively. Therefore, these values are less accurate than those calculated with Equations 4.1 and 4.2, however, they are still useful as coarse-grained estimates of reducing and oxidizing T_{soft}. Since this is a less accurate alternative method of calculation AFT, the preferred method

would be to use Equations 4.1 and 4.2. Therefore the following sections only focussed on discussing Equations 4.1 and 4.2.

4.2.2 Accuracy of calculated ash fusion temperatures

In order to assess the accuracy of the AFTs that can be calculated with Equations 4.1 and 4.2, calculated reducing and oxidising T_{soft} values were plotted against the experimentally determined values, as indicated in Figures 4.2a and b, respectively. As is evident, the calculated reducing and oxidising T_{soft} values of the samples that were used in determining the optimum MLR equations correlated well with the experimentally determined values. In addition, as mentioned in Section 3.2, four samples were not included in the computation of the optimum MLR equations, since it is scientifically better to verify accuracy with samples that were not included in these calculations. The T_{soft} values for these four samples were calculated using the optimum MLR equations obtained. The measured, as well as the calculated T_{soft} values (using Equations 4.1 and 4.2) of these samples are additionally indicated in Figures 4.2a and b. An-9 was not included in the determination of the optimum MLR equations because its oxidising T_{soft} was above the AFT test limitation of 1550 °C. However, its reducing T_{soft} value was within the limit and could still be used as an assessment of the accuracy of Equation 4.1. The other three samples that were left out from the MLR calculations (i.e. An-5, Co-1 and Coal-3) were selected randomly to assess the accuracy of both Equations 4.1 and 4.23.

As is evident from Figure 4.2a, the reducing T_{soft} of the four additional samples (An-9, An-5, Co-1 and Coal-3) compared relatively well with the linear relationship derived from the optimised MLR equation, although two of the values (An-9 and Coal-3) differed by just more than the 30 °C standard deviation associated with AFTs (Nel *et al.*, 2014). However, within the context of the absolute values of reducing T_{soft}, which ranged between 1136 and 1550 °C (Table 4.1), the calculated T_{soft} of even these samples that did not fit perfectly on the predicted line would still be useful for selecting PF coal better (to reduce damring formation). For the oxidising T_{soft} (Figure 4.2b) the values of two of the three additional samples (Co-1 and Coal-3) correlated very well with the linear relationship derived from the MLR calculations, while An-5 was still a good fit if the 30 °C standard deviation (Nel et al., 2014) is taken into account. The calculated oxidising T_{soft} of An-9 (using Equation 4.2) was also added to the figure, even though the experimental value could not be determined.

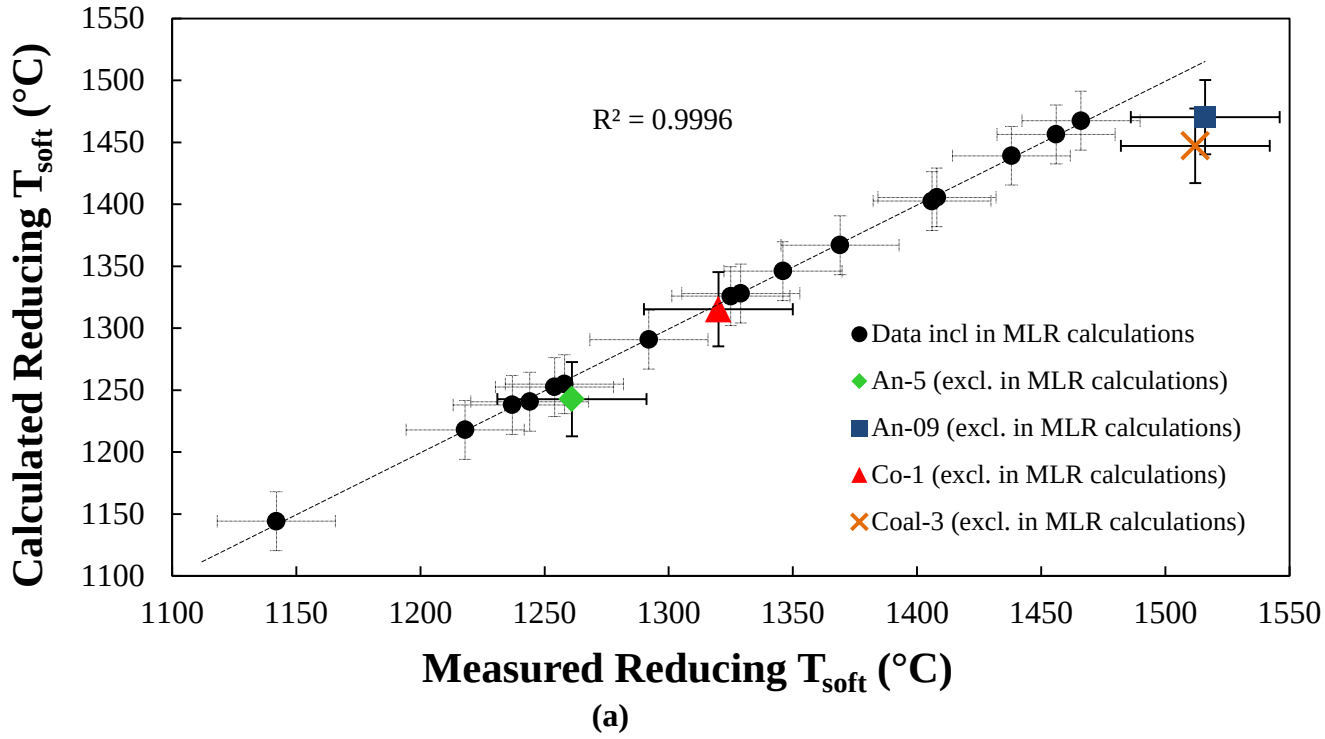

(a)

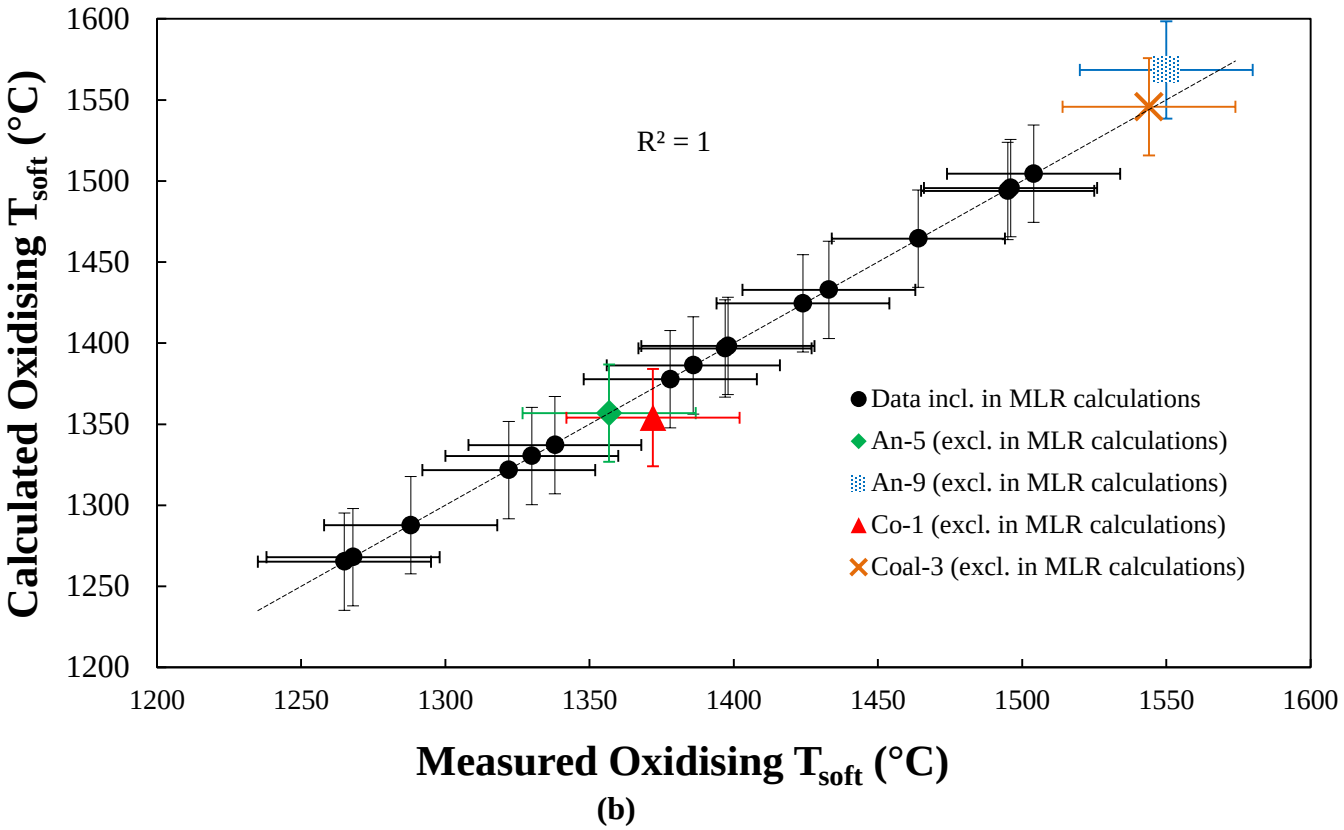

(b)

Figure 4.2: Calculated (Equations 4.1 and 4.23) and experimental (Table 4.1) T_{soft} values and R^2 using a bivariate correlation method (Thirumalai *et al.*, 2011) for the reducing (a) and oxidising (b) environments. The error bars indicate the 30 °C standard deviation that is common for AFT measurements.

It is also important to consider the two optimum MLR equations (Equations 4.1 and 4.2) in context of similar work done previously. Chen and Jiang introduced equations cited by Liu *et al*. (2007) that differ from those determined during this study, for predicting oxidising AFTs of Chinese coal. The method that is suggested in Liu *et al*. (2007) consists of four different equations, with the one that has to be applied selected based on the compositional content of the sample. As a comparison this method was applied to calculate the oxidising T_{soft} of the samples that was left out of the MLR calculations (i.e. An-5, An-9, Co-1 and Coal-3). Since the equations given by Liu *et al*. (2007) were only for oxidising T_{soft}, Equation 4.2 was used to calculate the T_{soft} so that the two methods can be compared. The experimental value of the oxidising T_{soft} for An-9 is given as >1550 °C. Using the equation proposed Chen and Jiang as cited by Liu *et al*. (2007), the oxidising T_{soft} was calculated as 1437 °C, which is too low. An-5 had an experimental value of 1288 ° C and with the equation in Liu *et al*. (2007) it was calculated as 1303 °C, which is fairly accurate. Co-1 and Coal-3 had experimental values of 1372 °C and 1544 °C, which were calculated with the Liu *et al*. (2007) equations as 1315 °C and 1447 °C, respectively. Even though the calculated values in some cases seem to be reasonable, the average error using the equation by Liu *et al*. (2007) is more than 3 %. Therefore, the equations proposed in this paper seem to enable similar or even better accuracy, to calculate T_{soft} than what has been proposed before. The higher accuracy might be due to the inclusion of more independent variables during the determination of the optimum mathematical solution. Our method also only has one equation for calculating oxidising T_{soft}, which is much simpler than the four equation method proposed by the afore-mentioned authors (Liu *et al*., 2007). Additionally, the equations proposed in the current study enables calculation of reducing T_{soft}, which has been proven to be important within the application of chromite pre-reduction in rotary kilns (Kleynhans *et al*., 2012).

4.2.3 Chemical interpretation of the optimum multiple-linear regression equations

Apart from being able to relatively accurately calculate AFTs (as indicated In Section 4.2.2) and considering this as a pure mathematical solution, it would be advantageous to chemically understand the system better. Several authors (Lorenzo-Seva *et al*., 2010; Kraha *et al*., 2012; Nathans *et al*., 2012) have proposed statistical techniques to calculate parameters that can be used in the interpretation of regression results and to determine the contributions of the different independent variables (which correlate with chemical species or parameters

presented in Table 4.1). For instance, beta weights (β) are applied to standardised variable scores in the MLR equation and can be used to interpret independent variable contribution to the regression effect. However, studies from Kraha *et al.* (2012) and Nathans *et al.* (2012) showed that considering β weight in isolation is at least partially problematic. Covariance, i.e. the measure of strength of the correlation between two or more independent variables, has a large effect on β weights because all relationships among variables are accounted for. Therefore, β weights do not have the ability to detect and interpret suppression, as it can be influenced by relationships between variables. In this study 26 independent variables were considered in the determination of the optimum MLR equations for the reducing and oxidising T_{soft}. Therefore, interactions between these variables would not be described by using β weights. Structure coefficients (r_s) are another method that was examined by Kraha *et al.* (2012). Structure coefficients are Pearson correlations between the calculated/predicted value given by the regression equation and each independent variable. A squared structure coefficient (r_s^2) gives an indication of the contribution of each independent variable to the variance given by the structure coefficient. Negative r_s values show that there are an inversely proportional correlation between the independent variable and the calculated/predicted value. Commonality coefficients can also be calculated using the SPSS programming software (Nathans *et al.*, 2012). Two types of commonality coefficients exist, namely unique and common coefficients. Unique coefficients reveal the amount of variance an independent variable contributes to the MLR equation on its own without sharing its contribution in predicting the dependent variable with other variables. Common coefficients reflect the contribution of an independent variable in combination with one or more independent variables. The commonality coefficients are used to give more information on the covariance between the different independent variables that could not be obtained when using β weights (Nathans *et al.*, 2012). According to Lorenzo-Seva *et al.* (2010) relative important weights (RIW) is a measure of the proportionate contribution of each independent variable to R^2, after correcting for the effects of the intercorrelation among independent variables. The sum of the RIW is equal to R^2. All the statistical parameters that were calculated with the SPSS programming software (Lorenzo-Seva *et al.*, 2010) are presented in Table 4.2.

Considering all the positives and negative associated with the various statistical parameters described above, it was decided to consider RIW values in greater detail, although other parameters will also be discussed. This was done, since RIW is likely regarded as the best to describe the contribution of an independent variable (correlating to species/parameters in Table 4.1), after correcting for the effects of the intercorrelation among independent variables. According to RIW values for reducing T_{soft}, K_2O content made the largest contribution to the variance, with a value of 20.8 %. K_2O has an r^2 value of 0.2532, indicating a 25.32 % contribution to the 99.96% variance (Figure 4.2a). It can also be seen from the commonality coefficients that K_2O contributed 14.51 % uniquely to the variance, and 10.82 % in combination with other independent variables. Independent variables that also have relatively large RIW values were H (20.4 %), P_2O_5 (12.3 %), O (11.6 %) and V_2O_5 (8.9 %). H had the largest unique contribution to variance (20.75 %) and a relatively lower common contribution (11.48 %). Kleynhans *et al*. (2017) concluded that H made a very significant contribution to variance in predicting pre-reduction. This was attributed to the ability of a reductant to release H that can induce reduction, and also to the belief that carbonaceous reductants used during FeCr pre-reduction can form H_2. In reducing atmosphere H clearly also has a substantial influence on the T_{soft}, which might be related to the ability of carbonaceous materials to act as a reductant. Ash had the largest common contribution (17.12 %) and also had a large unique contribution to the variance (18.08 %), but a RIW of only 7.1 %. From these results it can be seen that the intercorrelation between the different variables are very complex and even though the ash components (K_2O, V_2O_5, P_2O_5, etc.) contributed significantly to the variance (total of their RIW values = 47.5 %), they are not the only determining factor. It was also interesting to note that some ash species with a low content in the ash compositions (below 0.33 %) such as V_2O_5 and Sr contributed significantly to the variance (8.9 and 4.7 % RIW, respectively in Table 4.2).

As previously stated, elements occurring in the ash could occur in different phase as what is presented in the standard ash composition analysis (Table 4.2). To fully understand the impact of individual species and/or combinations of species on the reducing T_{soft}, additional investigations would be required. However, this would make the scope of the current work too extensive. Therefore, deductions from previous investigations were considered. For instance Wang *et al*. (2013) indicated that V_2O_3, rather than V_2O_5, is the most likely form of V in a reducing atmosphere. The melting point of V_2O_3 (1940 °C) is significantly higher than

that of V_2O_5 (690 °C) (Wang *et al*., 2013) which at least partially explaining why the small V content contributed to a higher T_{soft}.

For the Oxidising T_{soft}, P_2O_5 had the highest RIW value of 18.4 %. MnO and MgO had RIW of 14.3 and 13.2 %, respectively. Both MnO and MgO had a negative r values, indicating an inversely proportional correlation with oxidising T_{soft}. Van Dyk and Keyser (2005) and Song *et al* (2009) reported similar roles for MnO and MgO. Combined the ash components had a RIW contribution of 79.0 %. Considering the commonality coefficients P_2O_5 only contributes 8.8 % uniquely, but commonly contributed 20.67 %. MnO commonly contributed 53.35 % while uniquely only 0.11 %. For the oxidising T_{soft}, the unique contributions were relatively small. P_2O_5 had the largest unique contribution (8.8 %), while all the other variable contributions were less than 5 %. Van Dyk (2005) stated that an increase in acidic components such as Al would cause an increase in AFT's. This is also confirmed by the results in In Table 4.2, as Al_2O_3 had a RIW of 10.2 % and a positive r value showing a directly proportional relationship. However, commonly (total of "common" in Table 4.2) the ash components had a large contribution, showing that the interaction between the different ash components played a significant role in predicting AFT for an oxidising atmosphere. Even though there is some correlation to previous published data, understanding these complex interactions between the variables would require substantial additional investigation.

Table 4.2: Statistical parameters that were calculated with SPSS software for the interpretation of regression results and to determine the contributions of the different independent variables to the calculated AFTs.

	Variable	β	$r_s \cong r$	$(r_s)^2 \cong R^2_{yx}$	Unique	Common	RIW (%)
Red Soft Temp	MC	2.943	0.364	0.1325	0.1134	0.0191	5.3
	Ash	10.486	0.098	0.0097	0.1808	-0.1712	7.1
	C	14.367	0.41	0.1677	0.1847	-0.0169	8.1
	H	4.231	0.568	0.3222	0.2075	0.1148	20.4
	O	3.168	0.552	0.3037	0.1516	0.1521	11.6
	K_2O	-1.138	0.504	0.2532	0.1451	0.1082	20.8
	P_2O_5	0.556	0.385	0.1477	0.1481	-0.0004	12.3
	V_2O_5	0.263	0.161	0.0258	0.0197	0.006	8.9
	Sr	0.707	0.257	0.0658	0.0502	0.0156	4.7
	SO_3	-0.389	0.039	0.0015	0.0465	-0.0449	0.8
Ox Soft Temp	MC	-0.476	0.269	0.0724	0.0265	0.0459	3.4
	FC	-0.81	-0.409	0.1673	0.0125	0.1548	6.5
	H	-0.084	0.576	0.3323	0.0003	0.332	11
	Al_2O_3	0.516	0.199	0.0397	0.0484	-0.0087	10.1
	K_2O	-1.122	0.208	0.0432	0.1107	-0.0675	7.6
	MgO	-1.379	-0.417	0.1741	0.0448	0.1293	13.2
	MnO	0.097	-0.731	0.5346	0.0011	0.5335	14.3
	P_2O_5	-0.768	-0.543	0.2951	0.0883	0.2067	18.4
	ZrO_2	-0.416	0.481	0.2312	0.0191	0.212	5.9
	Ba	0.189	-0.524	0.2741	0.006	0.2681	6.2
	Sr	0.615	-0.185	0.0341	0.0207	0.0133	3.5

4.3 Conclusions related to pulverised fuel coal ash contribution to damring formation

By characterising an array of carbonaceous materials used in the FeCr industry, it was proven that the reducing and oxidising AFT of these materials differ substantially from one another (Table 4.1). It was postulated that lower AFTs would promote damring formation, therefore it would be advantages if these temperatures could be predicted/calculated. MLR analysis was used for determine optimum MRL equations for reducing T_{soft} and oxidising T_{soft} AFTs (Section 4.2.1). These calculated temperatures were proven to be accurate, at least within the accuracy limits of measured AFTs (Section 4.2.2). Such calculated reducing T_{soft} and oxidising T_{soft} AFTs can be used by FeCr producers, applying the pelletised chromite pre-reduction process, to more optimally select PF coals to limit damring formation.

The operational and financial benefits of prolonging the timespan between chromite pre-reduction kiln damring clean out are significant. Lastly, the mathematical information obtained by the MLR analyses were “translated” into chemically interpretable information, but considering the importance of the independent parameters included in the optimum MLR equations (Equation 4.1 and 4.2). Although this indicated that complex chemical interactions, which are not fully understood, are responsible for AFT variations, it was evident that the PF ash composition is important in the selection of PF materials with higher AFTs. Currently, the FeCr producers applying the pelletised chromite pre-reduction process do not consider ash composition during PF coal selection.

Chapter 5

Results and discussion

Chromite ore and composite pellet contributions to damring formation in chromite pre-reduction rotary kilns

In this chapter, high temperature softening of chromite ore and chromite composite pellets, as well as bentonite and anthracite that are included in these composite pellets, were investigated as possible contributors to damring formation in chromite pre-reduction rotary kilns. Seven different fine chromite ores, as well as an anthracite duff and bentonite was characterised (Section 5.1). The deformation temperatures (associated with softening) of the individual materials and composite pellet mixtures were then determined with sessile drop tests (Section 5.2). The composition of actual damrings obtained from a chromite pre-reduction kiln was also considered (Section 5.3). Finally, conclusions derived from the results were presented (Section 5.4).

5.1 Characterisation of chromite ores, and pellet components.

To facilitate investigating the possible contributions of chromite ore and pellet fragments to damring formation in chromite pre-reduction rotary kilns, 7 different fine chromite ores, as well as these ores in conjunction with bentonite clay (as the binder) and Nkomati anthracite duff (as the carbonaceous reductant) in composite pellet mixtures were considered in this study. At the time when this investigation was initiated, all these ores, as well as the clay and anthracite were sourced from South African ferrochrome (FeCr) smelters. As indicated in Section 3.3, the FeCr smelters requested anonymity; therefore the sources of these ores are not indicted. Table 5.1 presents the chemical analysis of the afore-mentioned 7 chromite ores. According to Cramer *et al.* (2004) South African chromite ores typically have Cr/Fe ratios of 1.5 to 2, while Upper Group 2 (UG2) ores (originating from the platinum industry)

typically have Cr/Fe ratios of 1.3 to 1.4. As is evident from the results presented in Table 5.1, the metallurgical grade ore samples had Cr/Fe ratios ranging from 1.41 to 1.58 and the UG2 ore sample had a chrome ratio of 1.4, which is all very typical. However, the sample "Met grade 6" had a Cr/Fe ratio similar to typical UG2 ore and it also had a relatively high SiO_2 content for a metallurgical grade chromite ore. This was expected, since this specific metallurgical grade ore (Met grade 6) originated from a test campaign conducted by one of the large South Africa FeCr and chromite producers, during which this producer tried to increase the Cr-recovery. This was achieved by increasing the width of the concentrate band (and decreasing the middling band width) that is recovered during spiral concentration of the fine chromite (Section 2.2.3.1), which is the most commonly applied large scale method to upgrade and recover fine chromite ore (Murthy *et al.*, 2011; Beukes *et al.*, 2017).

Table 5.1: Chemical analysis of the chromite ore samples

	***Met grade 1**	**#Met grade 2**	**Met grade 3**	**Met grade 4**	**Met grade 5**	**Met grade 6**	***UG2**
Cr_2O_3	44.19	45.37	43.94	43.29	44.98	42.18	41.82
FeO	24.68	25.39	26.75	24.41	25.26	26.32	26.2
SiO_2	2.96	1.72	2.42	4.43	2.40	4.46	3.38
Cr/Fe	1.58	1.57	1.45	1.56	1.57	1.41	1.40

*****Both these analyses were obtained from Glastonbury *et al*. (2015) since the same ore samples were used in this study.
#This analysis was obtained from Kleynhans *et al*. (2012), since the same ore sample was used in the current study.

Table 5.2 presents the chemical analysis of the bentonite clay and the Nkomati anthracite used as pellet binder and composite pellet carbonaceous source, respectively. The bentonite clay contained 53.5 % SiO_2 and 13.17 % Al_2O_3. The Nkomati anthracite had a 10.09 % SiO_2 content, 75.08 % fixed carbon (FC) content, 17.79 % ash content and 6.87 % volatile matter (VM) content (all on air-dried basis). As stated in Section 3.1.2, both these materials were used in the production of composite pellets in the pelletised chromite pre-reduction process by large FeCr producers, at the time that this study was initiated.

Table 5.2: Chemical analysis of the bentonite clay and Nkomati anthracite used in this study. The analyses correspond to that presented by Kleynhans *et al*. (2012), who used the same sample materials.

	Bentonite clay	**Nkomati anthracite**
% SiO_2	53.53	10.09
% Al_2O_3	13.17	3.13
% MgO	2.64	0.35
% CaO	4.77	0.80
% FC	-	75.1
% MC	-	0.3
% Ash	-	17.8
% VM	-	6.9

5.2 Sessile drop test of chromite, composite pellet mixtures and pellet components

In Chapter 4 ash fusion temperatures (AFTs) were used to assess the possible contribution of coal ash to damring formation in chromite pre-reduction kilns. However, as stated in Section 3.2.3, AFT measurements had a maximum measurement temperature of 1550 °C. Since it was expected that the softening temperature of chromite ore and composite pellets would be well above this temperature, another technique had to be used to assess the possible contribution of chromite ore and pellet fragments to damring formation. Sessile drop tests, as described in Section 3.2.3, were used for this purpose.

Ringdalen *et al.* (2010) used three points to define different stages of melting and/or reduction of manganese ores during sessile drop tests, i.e. a) initiation of melting, that is defined as the temperature at which liquid became visible on the surface of the ore; b) completion of melting, when the ore appeared to be completely liquid; c) start of reduction, when the first gas bubbles were evolved from the sample. None of the afore-mentioned temperatures can be directly correlated with the T_{soft} determined with AFT, which was used in Section 4.2 as a possible indication of the initiation of damring formation. Therefore, for the purpose of this study it was decided to consider the sessile drop test temperature at which any sign of deformation occurred as an indication of material softening, which was assumed to be the temperature at contribution to damring formation would occur. The afore-mentioned "deformation" can be in the form of bubbling, lifting, movement, rounding of corners, etc., of the sample as observed during heating. Therefore in this chapter the

temperature at which the first sign of deformation took place, is referred to as the deformation temperature.

As mentioned, sessile drop tests were done on composite pellet mixtures (Section 3.3), which were similar to what is used in the pelletised chromite pre-reduction process as feed material for the rotary kilns. Sessile drop tests were also done on the individual mixture components, i.e. chromite ores (the 7 different ores), reductant (Nkomati anthracite) and binder (bentonite clay). Figures 5.1 to 5.7 present images of how deformation of the small sample pellets (see Section 3.2.3 for details), considered during the sessile drop tests for the different ores investigated, as well as composite pellet mixtures containing each of these 7 ores, were detected. Figures 5.8 and 5.9 present similar images of the Nkomati anthracite and the bentonite clay respectively. In the following sections, the sessile drop tests of the different materials are briefly considered.

In Figure 5.1 (a) and (b) images of the observed deformation of the Met grade 1 metallurgical grade chromite ore, as well composite pellet mixtures containing Met grade 1 ore, are respectively presented. For the ore the first sign of deformation occurred as bubbling in the bottom left corner at 1757 °C (Figure 5.1 (a) top right pane). In contrast, deformation of the pellet mixture containing Met grade 1 was already observed at 1454 °C, as softening of the top of the pellet (top right pane of Figure 5.1 (b)). At 1757 °C the Met grade 1 pellet mixture softened to an extent that the sample lost its rectangular shape, with a lot of bubbling and rounding observed (Figure 5.1 (b) bottom left pane). The final melting temperatures of the ore and the composite pellet mixture did not differ significantly, but in the context of this study the temperature where the sample first started to deform is of importance. The composite pellet mixture had a significantly lower deformation temperature than the ore itself, since the clay and anthracite ash could reduce the liquidus temperature.

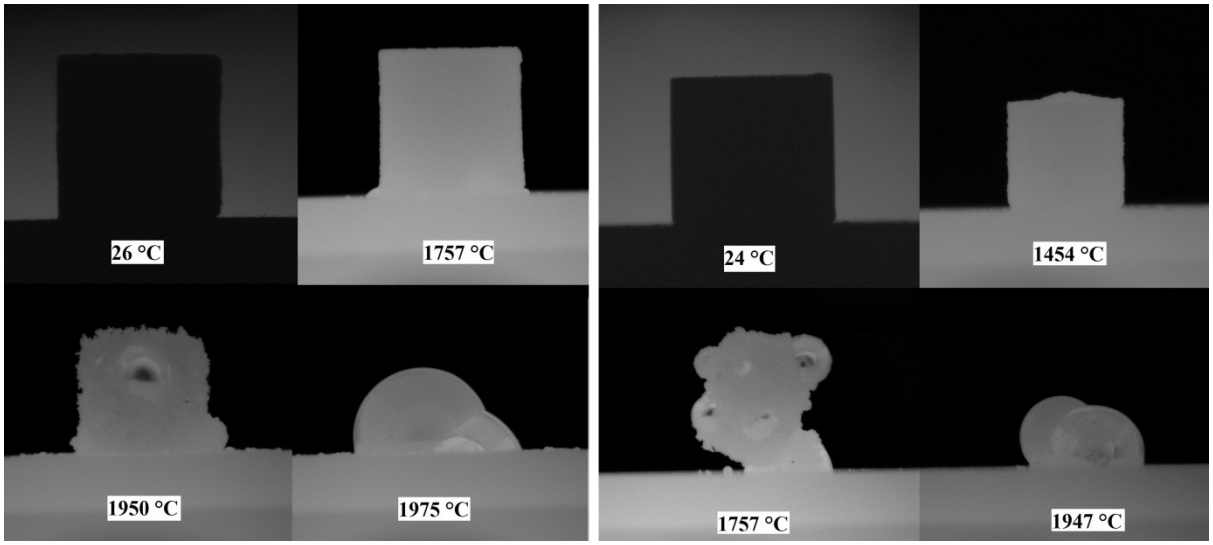

(a) **(b)**

Figure 5.1: Sessile drop test images of deformation/melting of Met grade 1 ore (a) and a composite pellet mixture containing this ore at different temperatures.

Figure 5.2 (a) and (b) presents the sessile drop test images of the Met grade 2 chromite ore and the composite pellet mixture containing this ore, respectively. Similar to what was observed for the Met grade 1 sample and its pellet mixture (Figure 5.1), the Met grade 2 pellet mixture (Figure 5.2 (b)) started deforming at a significantly lower temperature than the ore alone (Figure 5.2 (a)), but the final melting points were very similar. The first sign of deformation of the Met grade 2 ore was visible in the form of bubbling in bottom left corner at 1689 °C (Figure 5.2 (a) top right pane). For the pellet mixture this occurred in the form of extensive bubbling at the bottom of the pellet at 1443 °C (Figure 5.2 (b) top right pane).

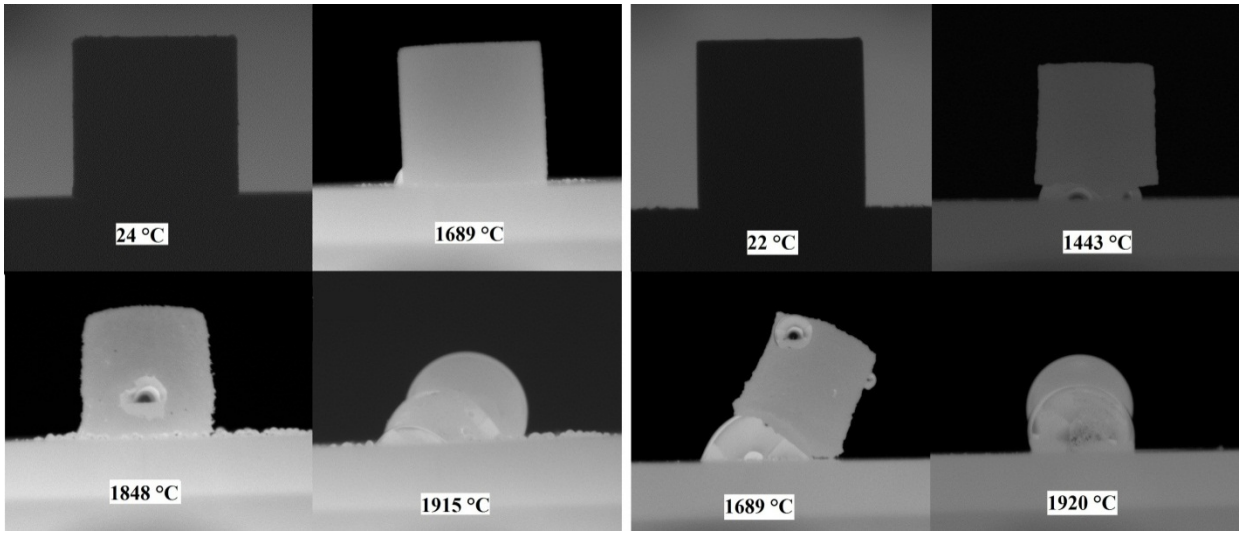

(a) **(b)**

Figure 5.2: Sessile drop test images of deformation/melting of Met grade 2 ore (a) and a composite pellet mixture containing this ore at different temperatures.

In the same manner in Figures 5.3 to 5.7, the deformation temperatures of the remaining ores (i.e. Met grade 3, Met grade 4, Met grade 5, Met grade 6 and) and their corresponding composite pellet mixtures were determined.

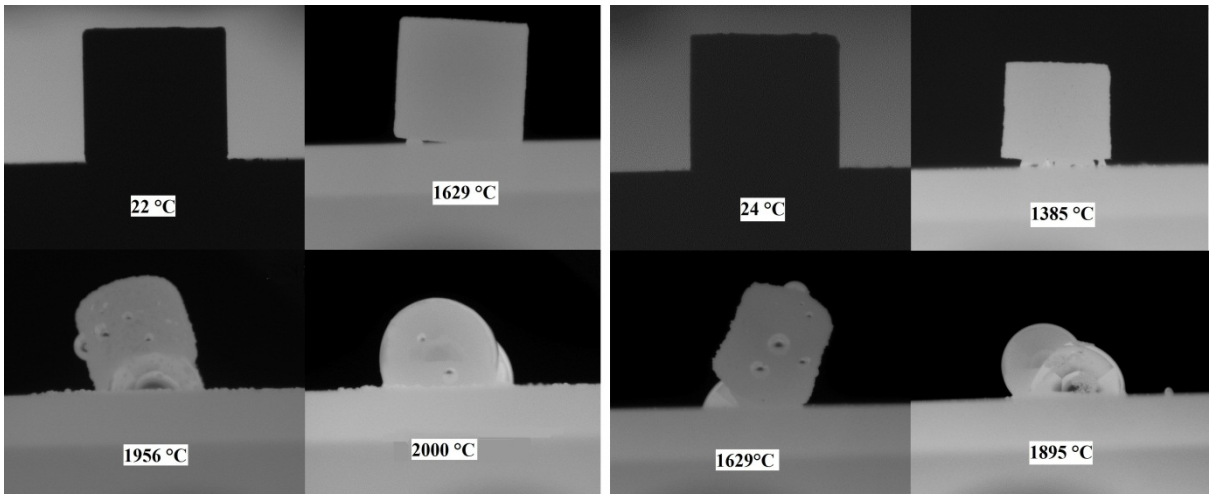

(a) **(b)**

Figure 5.3: Sessile drop test images of deformation/melting of Met grade 3 ore and a composite pellet mixture containing this ore at different temperatures.

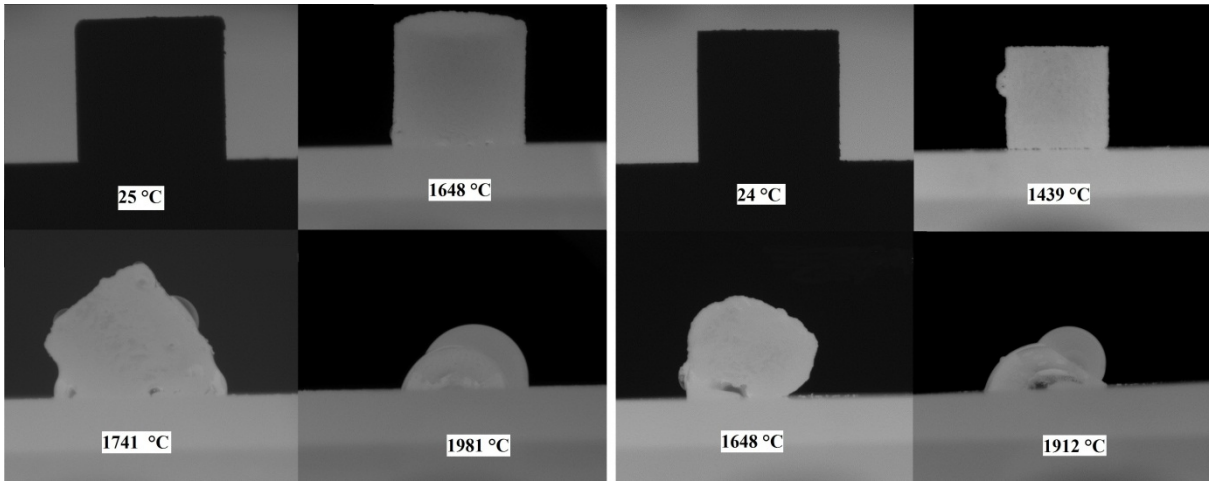

(a) **(b)**

Figure 5.4: Sessile drop test images of deformation/melting of Met grade 4 ore and a composite pellet mixture containing this ore at different temperatures.

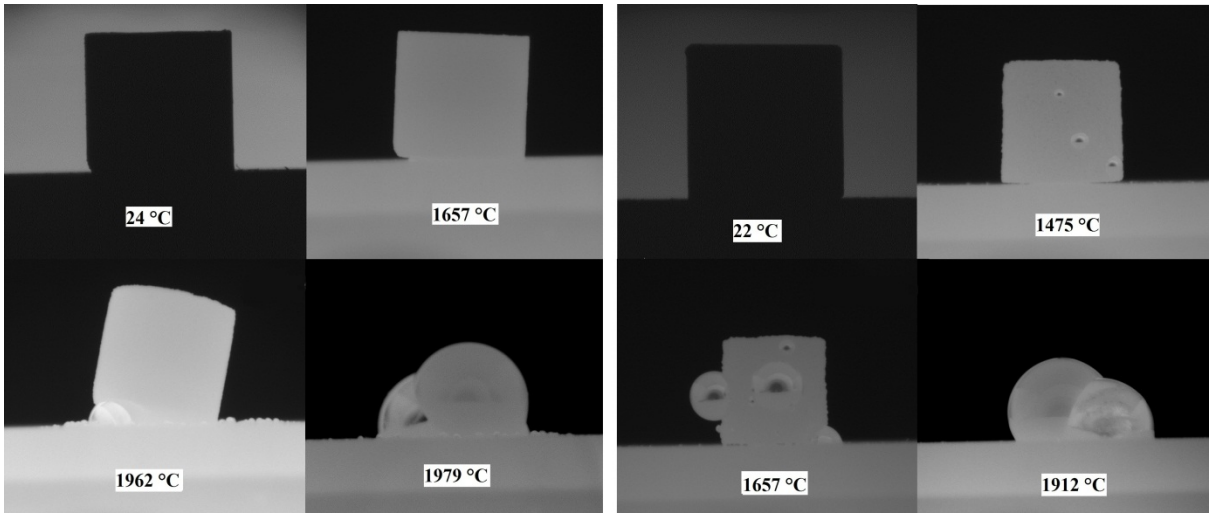

(a) **(b)**

Figure 5.5: Sessile drop test images of deformation/melting of Met grade 5 ore and a composite pellet mixture containing this ore at different temperatures.

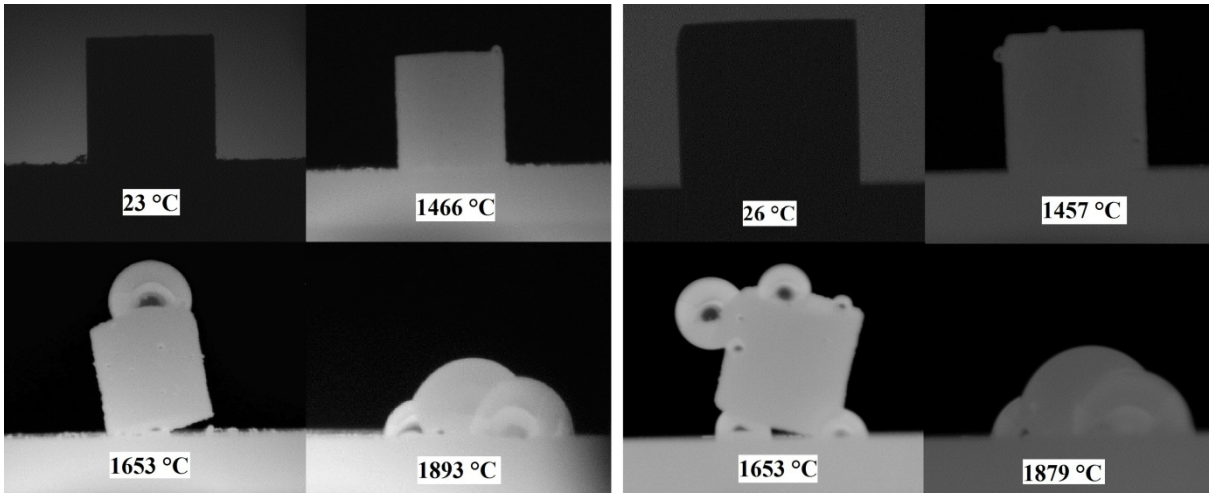

(a) **(b)**

Figure 5.6: Sessile drop test images of deformation/melting of Met grade 6 ore and a composite pellet mixture containing this ore at different temperatures.

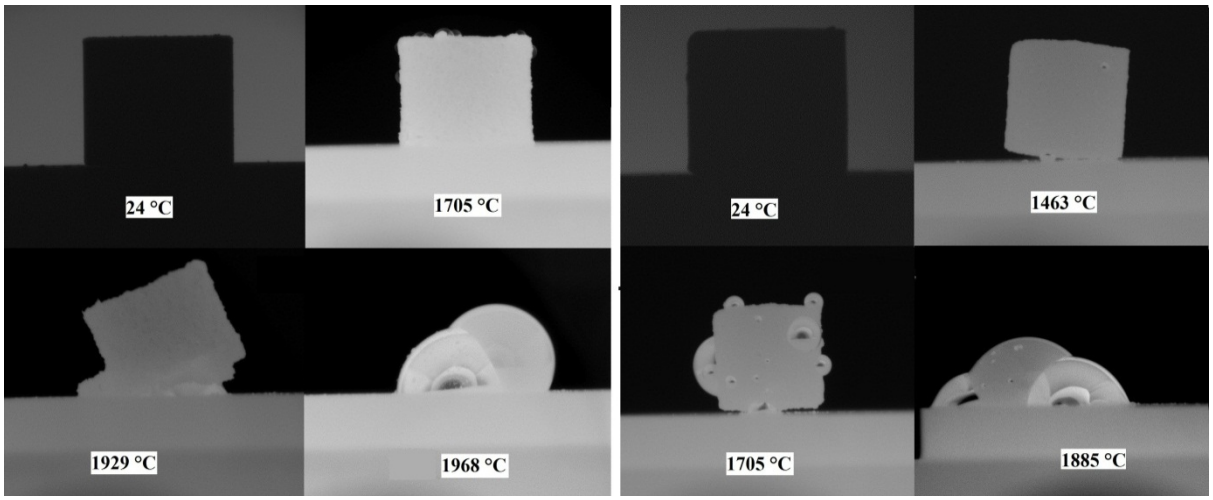

(a) **(b)**

Figure 5.7: Sessile drop test images of deformation/melting of the UG2 ore and a composite pellet mixture containing this ore at different temperatures.

In Figure 5.8 the high temperature deformation/melting behaviour of Nkomati anthracite, which was used as a carbonaceous reductant in the composite pellet mixtures, are presented. The first sign of deformation occurred at 1246 °C (Figure 5.8 top right pane) and the sample was completely melted at 1600 °C (Figure 5.8 bottom right pane). These temperatures are considerably lower than the corresponding temperatures of the ores and the pellet mixtures

(Figures 5.1 to 5.7). Since the sessile drop tests were conducted in a CO atmospheric environment (Section 3.2.3), it can be assumed that the Boudouard reaction (Equation 5.1) takes place. This reaction typically occurs above 900 or 1000 °C (depending on the CO_2-reactivity of the carbonaceous material), or even at lower temperatures (~800 °C) if alkalis are present (Tangstad et al., 2018). The consumption of carbon at temperatures exceeding the afore-mentioned temperatures will result in ever increasing concentration of ash being present in the sample, which will have lower deformation/melting temperatures that the ores, or pellet mixtures considered earlier.

$$C + CO_2(g) = 2\ CO(g) \qquad [5.1]$$

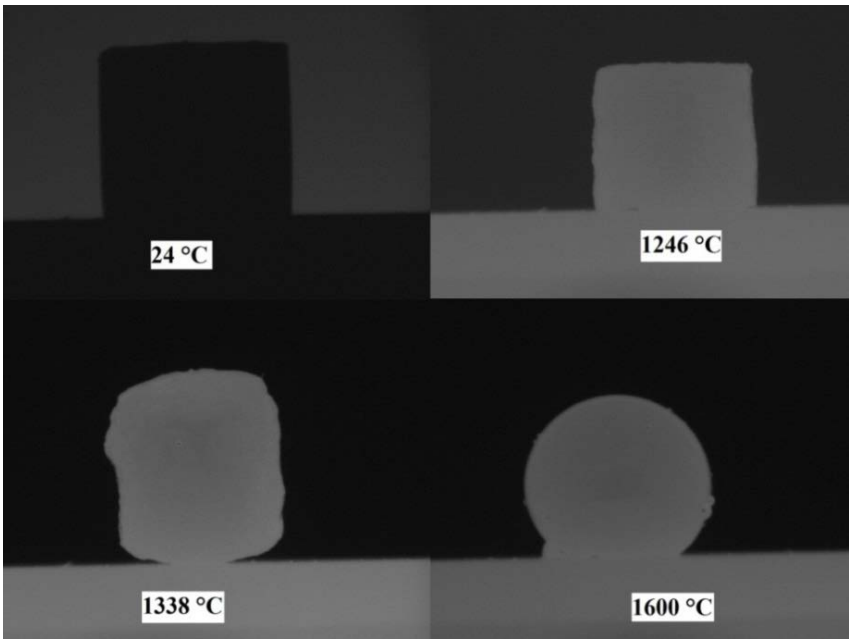

Figure 5.8: Sessile drop test images of the deformation/melting behaviour of Nkomati anthracite at different temperatures.

Figure 5.9 presents the sessile drop test images to determine the deformation/melting behaviour of the bentonite clay. The clay already started to deform at 1054 °C when swelling of the sample and softening of the edges occurred. The sample was completely melted at 1319 °C. Again, these temperatures are considerably lower than the corresponding temperatures of the ores and the pellet mixtures (Figures 5.1 to 5.7). This was expected,

since clays are essentially alumina silicates with lower melting temperatures than chromite ore.

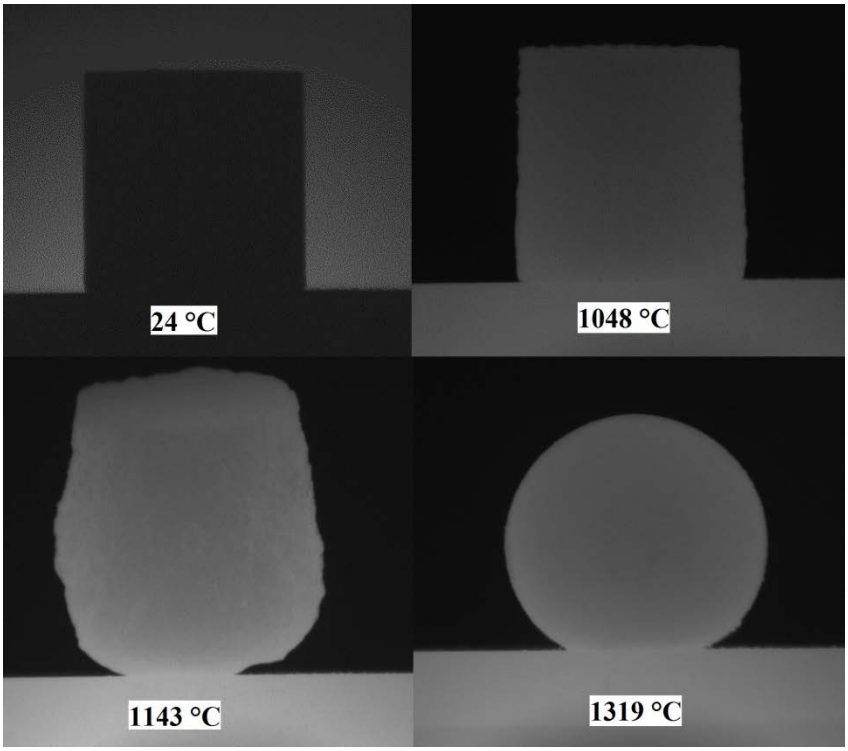

Figure 5.9: Sessile drop test images of the deformation/melting behaviour of the bentonite clay at different temperatures.

Table 5.1 presents a summary of the deformation temperatures that were derived from the sessile drop tests of all the samples considered (Figure 5.1 to 5.9). There are several important deductions that can be made from comparing these deformation temperatures, i.e.:

i) The deformation temperatures of all the ores ranged between 1466 °C and 1756 °C, which were significantly higher than the typical maximum temperature of the pellets being pre-reduced in a chromite pre-reduction rotary kiln, i.e.1300 °C (Dawson et al., 1986; Kleynhans et al. 2012). It is therefore unlikely that the ores alone will contribute to damring formation, unless the ores contain a significant fraction of liberated gangue minerals.

ii) The composite pellet mixtures had significantly lower deformation temperatures than the ores alone, which ranged from 1383 °C to 1463 °C. However, these temperatures were still above the typical maximum pellet pre-reduction temperature. Therefore, limited contribution to damring formation can be expected from composite pellets. However, fragmentation of composite pellets (pellet breakdown) due to various reasons (e.g. too high moisture content of green pellets, too fast heating in the heating chambers prior to the rotary kiln) can release small amounts of reductants and/or clay, which can contribute to damring formation, since the deformation temperatures of these materials were 1256 °C and 1054 °C, respectively.

iii) The UG2 ore and the UG2 containing composite pellet mixture did not have the lowest deformation temperatures, when compared with the other metallurgical grade chromite ores and the correlating composite pellet mixtures. The commonly held industry perception that UG2 ore will lead to quicker and/or more excessive damring formation is therefore not true. Each ore has to be evaluated separately and only then can conclusions be drawn with regard to possible damring formation.

iv) The Met grade 6 ore deformation occurred at a much lower temperature than that of the other ores. As indicated earlier (Table 5.1 and associated discussions), this ore had a higher SiO_2 content than the other metallurgical grade ores, due to being produced as part of test campaign to increase Cr-recovery. However, Met grade 6 and the UG2 ores had similar chemical compositions, yet the deformation temperatures of the Met grade 6 ore was approximately 240 °C lower than that of UG2 (Table 5.3). This significant difference was found to be due to the fact that the Met grade 6 ore contained a much larger fraction of liberated gangue particles (Figure 5.10 (a) left and right panes), than the UG2 where the gangue particles were often enclosed or attached to the chromite particles (Figure 5.10 (a) left and right panes). The gangue particles typically contain high concentrations of alumina silicates, which will have deformation/melting behaviours similar to that of the observed bentonite (Figure 5.9). Therefore, it stands to reason that although the chemical composition of the two ores were similar (Table 5.1), the liberated gangue particles in the Met grade 6 ore deformed/melted at much lower temperatures that the gangue that were at least partially protected from deformation/melting in the UG2 ore by the chromite (which is a refractory material) particles.

Table 5.3: Temperatures of deformation of the different ores, composite pellet mixtures and pellet components according to the sessile drop tests.

		First point of deformation (°C)	Sessile drop observation/description
Ore	Met grade 1	1757	Bottom left corner softening
	Met grade 2	1689	Bottom right corner lifting up
	Met grade 3	1629	Lifting at bottom left corner
	Met grade 4	1648	Bottom lifting up
	Met grade 5	1657	Lifting at bottom left corner
	Met grade 6	1466	Bubble on right upper corner
	UG2	1705	Bubbling at the top
Pellet ore mixtures	Met grade 1 mix	1454	Lifting at the top
	Met grade 2 mix	1443	Lifting at the bottom
	Met grade 3 mix	1385	Lifting at the right corner
	Met grade 4 mix	1439	Bubble on left
	Met grade 5 mix	1475	Small bubble in middle
	Met grade 6 mix	1457	Bubbles on top and left
	UG2 mix	1463	Lifting
	Nkomati anthracite	1246	Bubbling on the left side
	Bentonite clay	1054	Bubbling edges

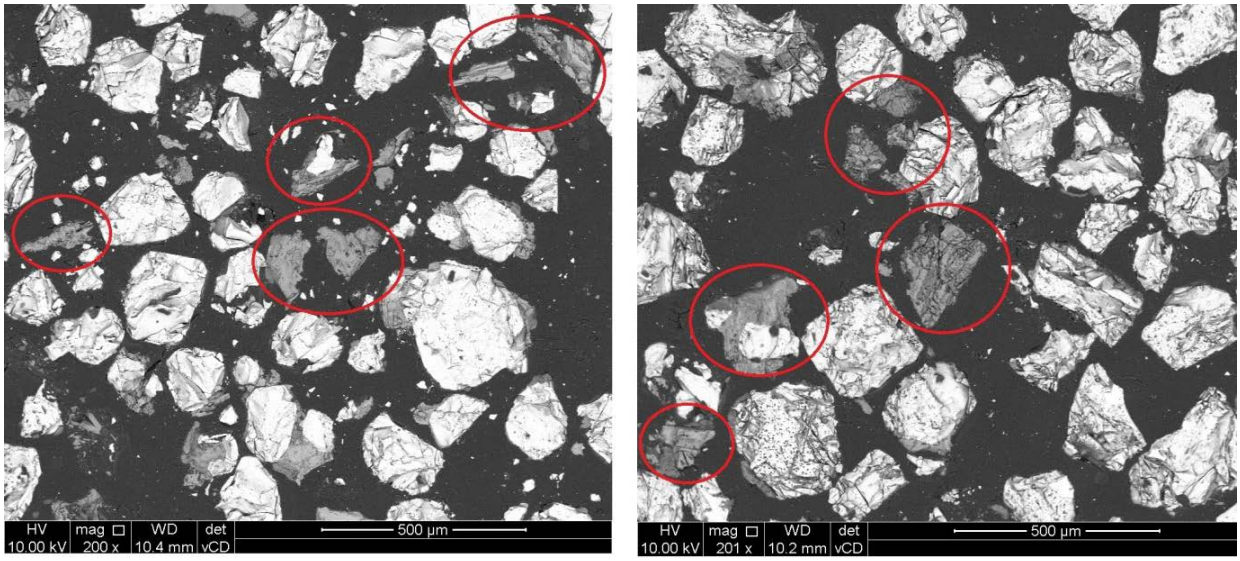

(a)

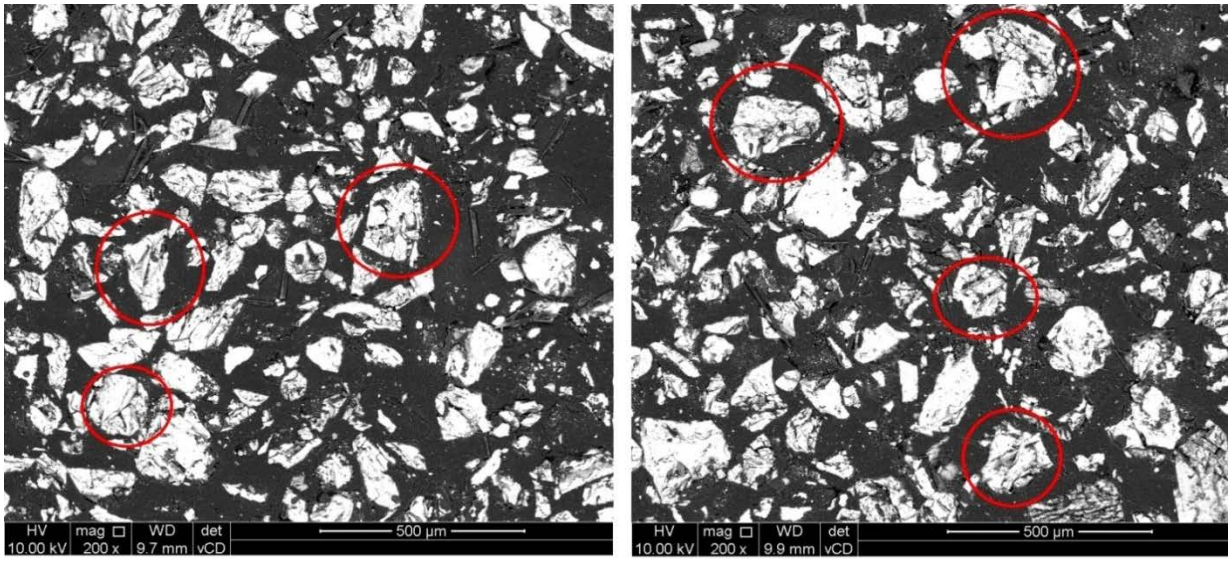

(b)

Figure 5.10: Scanning electron microscope (SEM) micrographs of Met grade 6 ore (a) and UG2 ore (b). The red circles indicate liberated gangue particles in the Met grade 6 ore (b) and gangue particles that are at attached or enclosed by the chromite particles in the UG2 ore.

5.3 Surface analysis of actual damrings

In order to augment the results derived from the AFT (Chapter 4) and sessile drop tests (Sections 5.1 and 5.2), actual damrings were also considered. Several damring fragments that were broken out of a pre-reduction kiln during a shutdown, were polished without the addition of resin to avoid carbon contamination and examined with scanning electron microscope and integrated energy dispersive x-ray spectroscopy (SEM-EDS). In Figure 5.11, a SEM micrograph of a cross sectional polished representative specimen is presented. From this micrograph is evident that the damrings consisted of lighter coloured particles (elements with higher atomic numbers) that are bonded together with a darker coloured matrix (elements with lower atomic numbers).

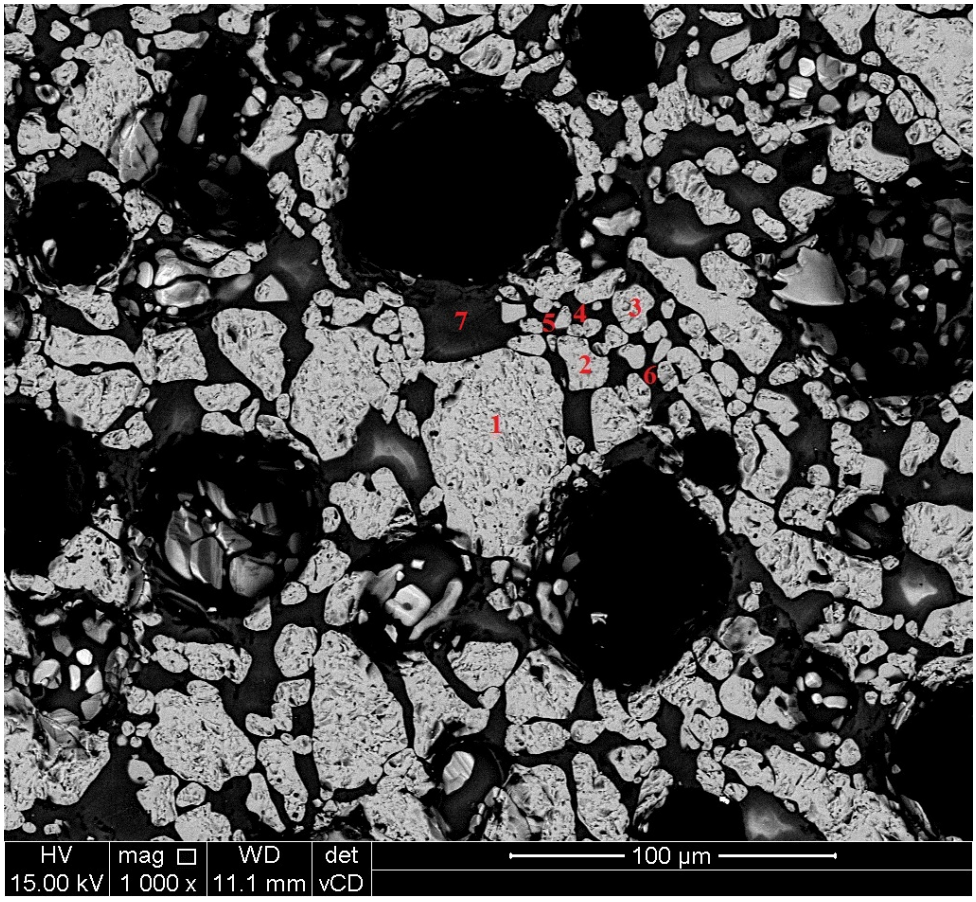

Figure 5.11: SEM micrograph of a polished section of damring fragment broken out of a chromite pre-reduction rotary kiln. Numbers 1 to 7 indicate areas that were analysed with EDS.

Average EDS analyses of the lighter coloured particles (points 1, 2 and 3 in Figure 5.11) and darker areas (points 4, 5, 6 and 7) are indicated in Table 5.4. From these results it can be deducted that the lighter coloured particles are mainly pellet fragments, since the Cr (24.6 wt. %) and Fe (16.0 wt. %) contents, and Cr/Fe ratio (1.54), resembled typical South African metallurgical grade chromite ore (Cramer *et al*., 2004). The small amount of C present in these particles can possibly originate from the carbon reductant included in the composite pellet mixture. This C can be present as free C, or as part of metal carbides that form during pre-reduction (Barnes *et al*., 1983). In contrast the darker matrix, which surrounded the afore-mentioned pellet fragments, only contained trace amounts of Cr and Fe. However, this matrix contained a significant amount of Si that is the most prevalent PF coal ash element (Table 4.1). The reductant used in the pellet mixtures contained 10.1 % SiO_2 and the bentonite clay contained 53.5 % SiO_2 (Table 5.2). Kleynhans *et al*. (2012) proposed that bentonite clay melts during the pre-reduction process and serves as flux to promote metal reduction. This could indicate the possibility that the Si in the damrings come from the clay binder. But this darker matrix also contained very high concentrations of C, which is indicative of unburned PF coal. Such high C contents will not be possible if the matrix was dominated by the clay binder and/or the gangue minerals included in the composite pellets. Therefore, the most obvious (and significant) source of the darker coloured matrix that bind the chromite (or chromite derived) particle together (Figure 5.11) is PF coal ash. Alternatively, as already indicated, liberated gangue minerals present in the ore could contribute significantly to damring formation.

Table 5.4: Average EDS analyses (wt.pct) of lighter (areas 1, 2 and 3) and darker areas (areas 4, 5, 6, and 7) in a micrograph of a cross sectional polished damring fragment.

Areas	C	O	Na	Mg	Al	Si	K	Ca	Ti	V	Cr	Fe	Total
1,2,3	8.28	39.41	-	5.04	6.50	0.26	-	-	-	-	24.58	15.92	100
4,5,6,7	36.73	42.5	0.15	0.54	3.21	13.84	0.28	0.91	0.56	0.18	0.16	0.96	100

5.4 Conclusions related to chromite ore and composite pellet contributions to damring formation

By using a sessile drop test method it was possible to determine the deformation temperatures (which was used as an indication of softening) of chromite ores, composite pellet mixtures containing these ores, as well as bentonite clay and anthracite included in the afore-mentioned mixtures (material characterisation presented in Section 5.1). It was found that the composite pellet mixtures had significantly lower deformation temperatures than the ores alone (Section 5.2). However, the deformation temperatures of the ores and pellet mixtures were above the maximum pellet temperature expected in a pre-reduction rotary kiln, therefore these materials are expected to contribute less significantly to damring formation than PF coal (Chapter 4). The deformation temperatures of the bentonite and anthracite samples considered (Section 5.2) were found to be below the typical pellet maximum temperature, therefore these materials could contribute to damring formation, if pellet breakup within or prior to the rotary kiln occurs. It was also demonstrated that UG2 ore will not necessarily contribute more to damring formation than metallurgical grade chromite ore, since the liberation of gangue minerals, which have much lower deformation/melting temperatures, need to be considered (Section 5.2). However, ore containing a significant amount of liberated gangue minerals could contribute significantly to damring formation. Lastly, by considering actual damrings obtained from a chromite pre-reduction rotary kiln, it was proven that although the damring contained significant amounts of Cr and Fe (chromite or chromite derived particles), it also contained a matrix that was most likely identified to originate from PF coal ash (Section 5.3). This significant Cr content, combined with the afore-mentioned result, implies that the PF ash is the “glue” that binds chromite particles originating from composite pellet fragments and/or disintegrated pellets together.

Chapter 6

Results and discussion

Commissioning of a large mass thermo-gravimetrical analyser and investigating thermo-mechanical analysis as an indicator of pre-reduction of chromite composite pellets

In this chapter the necessity for a large mass thermo-gravimetrical analyser (TGA) to better reproduce the complex environment inside the chromite pre-reduction rotary kiln is explained (Section 6.1). The design, construction, commissioning and testing of the large mass TGA instrument is described in Section 6.2. Although it is somewhat unusual to include the afore-mentioned work in a results chapter, the design, construction, commissioning and testing of the TGA was an important objective of this study, therefore the inclusion thereof in a results chapter. After the large mass TGA was tested, chromite composite pellets and pellet components were analysed with it (Section 6.3). Thermo-mechanical analysis (TMA) was also conducted on the composite pellets and the pellet components (Section 6.4). TMA measurements were then compared to TGA measurements to investigate the possibility of using TMA to follow chromite pre-reduction (Section 6.5). Lastly, conclusions are presented in Section 6.6.

6.1 The need for a large mass thermo-gravimetric analysis (TGA) instrument

One of the objective was aimed at determining whether TGA and TMA results were comparable, and if TMA, instead of TGA could be used to determine pre-reduction. TGA measures the change in mass of a sample as a function of temperature or time and can be used to investigate phase transitions, thermal decomposition, oxidation, reduction, etc. Industrially, rotary kilns are used to conduct pelletised chromite pre-reduction (Section 2.2.3.2). These kilns are continuously fed green (uncured) pellets in the range of 20 - 50 tons

per hour. Section 3.1 explained that the atmosphere inside the kiln is partially oxidising allowing for pulverised fuel (PF) combustion, and partially reducing inside the pellets due to the partial positive CO pressure inside the pellets themselves. Inside the pellet bed (Figure 1.1), between the pellets, reducing conditions also exist. Xiao *et al*. (2007) proposed the following mechanisms (Equations 6.1-6.3) to illustrate the overall reduction of chromite in a packed bed:

$FeCr_2O_4 + 4CO(g) \rightarrow 2\ Cr + Fe + 4CO_2$ (Solid-state reduction with CO) [6.1]

$CO_2(g) + C \rightarrow 2CO(g)$ (Boudouard reaction) [6.2]

$FeCr_2O_4 + 4C \rightarrow 2Cr + Fe + 4CO$ (Overall reaction) [6.3]

Recreating this rather complicated system on laboratory scale presented some difficulties. Firstly, the recommended sample mass for commercial TGAs is usually between 2 and 50 mg. The pre-reduction pellets that were investigated during this study had a mass of approximately 1 g per pellet. Therefore, not even one whole pellet could be analysed in the commercial TGAs that were available to the candidate. As discussed in Section 3.3, the pellet mixture used during this study consisted of ore, reductant and a clay binder. It is questionable if a 50mg sample of the pellet mixture, consisting of the afore-mentioned three heterogeneous materials, would be representative of the industrial process. Secondly, it would be impossible to recreate the externally oxidising (in kiln) and internally reducing (within pellet and pellet bed) conditions with such a small sample (50 mg). Therefore, it was decided that a large mass TGA should be developed as part of this PhD. The availability of such an instrument would not only contribute to this PhD, but would also contribute to future work done in the Chromium Technology group at the North-West University (NWU). In cooperation with Mintek (http://www.mintek.co.za/, accessed 25/05/2018) and the Instrument Makers of the NWU, an existing vertical tube furnace was therefore converted into fit-for-purpose large mass TGA.

6.2 Building, testing and commissioning of a large mass TGA

6.2.1 Materials and initial design

An existing Lenton Elite, UK model TSH15/75/610 ceramic tube furnace with a programmable temperature controller that can be used for temperatures up to 1500 °C, was redesigned into the large mass TGA instrument. Figure 6.1 shows an image of the front, side and 3D view of the TGA design. The figure also shows an enlarged view of the top of the TGA. The top of the tube was fitted with a stainless steel flange to hold the tube in place. A high temperature platinum wire thermocouple was obtained to record the temperature inside the tube furnace. The thermocouple was positioned inside a ceramic alumina sheath (ceramic alumina tube with an inside diameter of 8 mm) which was then placed inside the ceramic tube of the furnace through a hole in the flange. The flange allowed for a gas inlet, which was connected to a gas flow meter. Insulation wool that can withstand a maximum temperature of at least 1600 °C was obtained to insulate the top of the tube furnace, to keep the heat in the hot zone (middle of the tube) and to avoid heat distributing unevenly through the tube (which can cause it to crack). The insulation also protected the stainless steel flanch from melting.

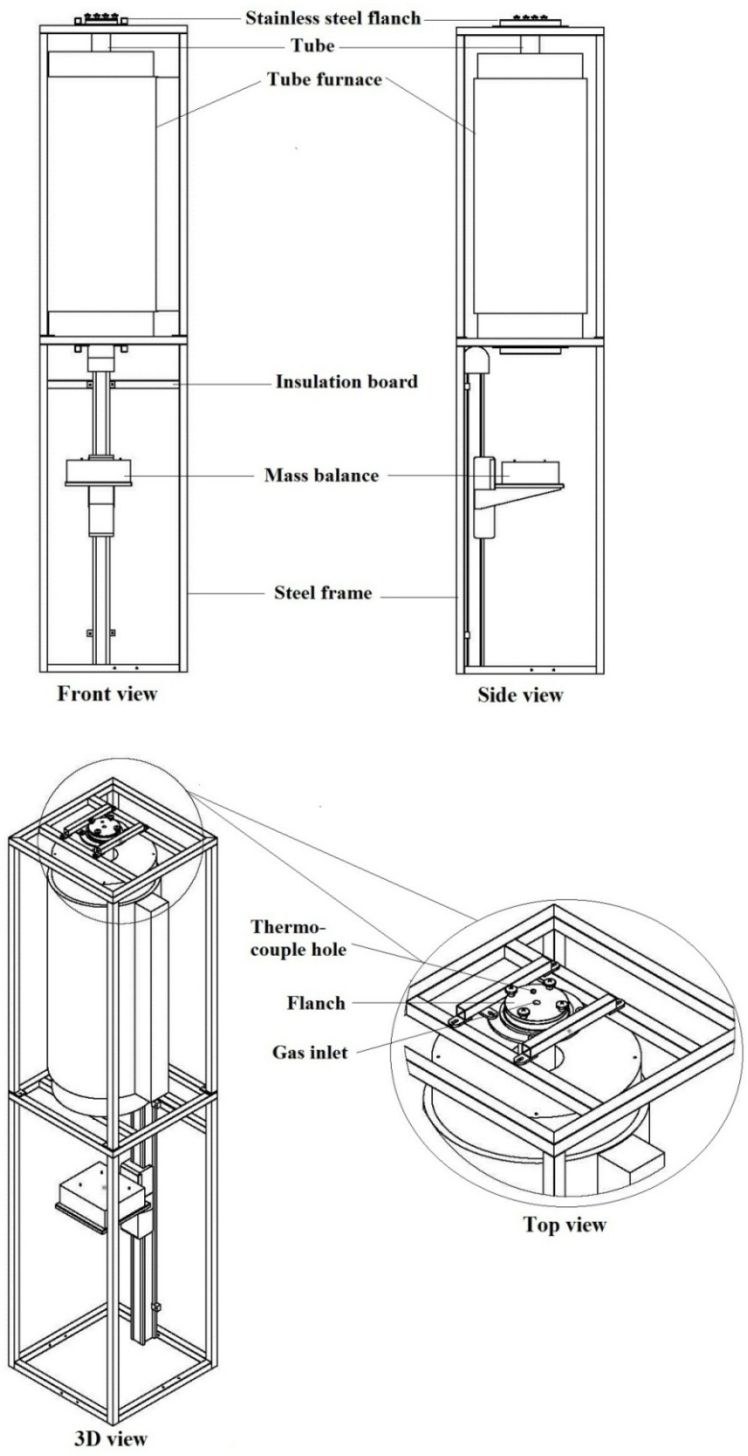

Figure 6.1: Design of the large mass TGA instrument. Front- (top left pane), side- (top right pane), 3D (bottom left pane) and top (bottom right) view.

An OHAUS Explorer EX2202 (version 2.01/2.01 S/N B520931006) balance with a maximum weight of 2200 g was obtained to determine the change in mass of the sample. An ceramic alumina rod was fitted onto the balance with a pedestal at the top end of the rod on which the sample holder would be placed. The initial idea for the pedestal, on which the sample holder would be placed, was to use a ceramic alumina disc. This however proved more difficult than anticipated, in terms of stability issues of the pedestal. To overcome this issue, a quartz pedestal that can fit over the ceramic rod on the balance was designed by the glassblowing service of the Instrument makers. It could withstand the high temperature and provide a more stable pedestal. Figure 6.2 shows a design of this quartz pedestal fitted over the alumina ceramic rod-end.

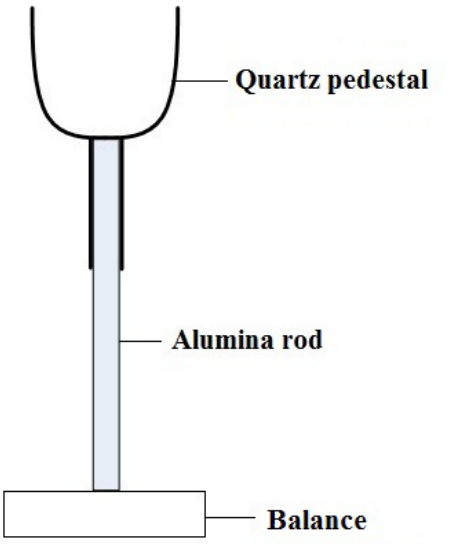

Figure 6.2: Illustration of the quartz pedestal used in the TGA design.

For the sample holder an alumina crucible with correct dimensions to fit into the tube furnace was used. A steel frame that is illustrated in Figure 6.1 was designed to house the TGA unit. Built into the steel frame is a flat stable platform onto which the balance unit is placed. The platform is connected to a mechanism to raise the crucible with the sample (which is then placed in the crucible holder that is connected to the balance) up into the furnace and lower it down out of the furnace once the analysis is complete. Between the mass balance and the furnace, an insulation board was placed to protect the balance from the radiation heat from the tube. Figure 6.3 presents an image where the above explained features of the TGA can be seen.

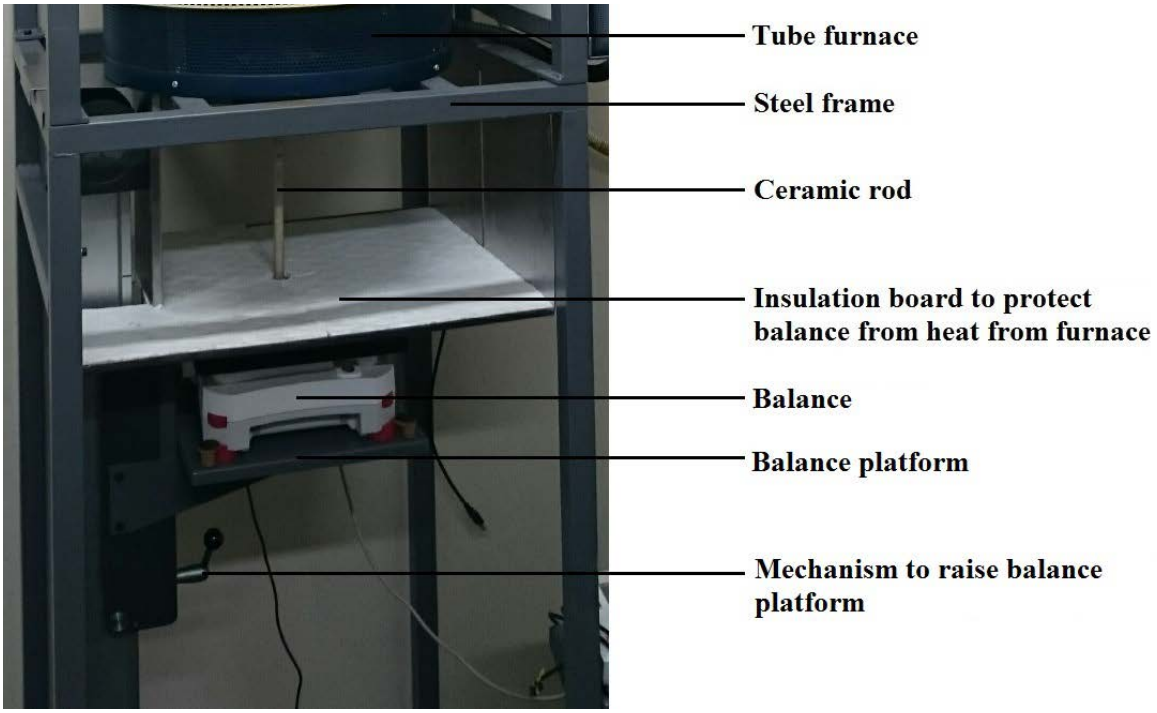

Figure 6.3: The mechanism used to raise the sample into the furnace, as well as the insulation board used to protect the balance from the radiation heat of the furnace.

A data acquisition system was required to process signals from the thermocouple, as well as from the balance during an analysis. For this purpose a cDAQ-9171, CompactDAQ Chassis was obtained together with LabVIEW Base Development System software to capture and export the data from the analysis.

6.2.2 Challenges encountered with the initial TGA design

After the initial testing of the TGA, a few problems were encountered with the design. The first few runs worked well. The data output given on the computer was only the temperature and corresponding mass loss. The software programming needed to be adapted to give the time, temperature and corresponding mass loss so that a differential thermo-gravimetric (DTG) curve (first derivative) could be plotted.

The furnace tube can be fragile when uneven heat distribution takes place, or if the furnace is heated up too quickly. Therefore to prolong the lifespan of the tube and protect it from cracking or breaking, the furnace was heated slowly as described in Section 3.5. After about 5 runs, the quartz sample holder (Figure 6.2) started to crack and small pieces broke off.

This resulted in incorrect mass loss results. The Instrument Makers made another quartz pedestal, which again after a few runs started cracking. This was a major problem since replacing the pedestal after every 5 runs was not financially viable.

The pedestal needed to consist of material that could withstand constant exposure to high temperatures without cracking, or influencing the mass loss of the sample in any way. Refractory material is used in high temperature application on industrial scale. The idea was then to cast refractory cement in a mould custom made to fit the specification of the pedestal. Vesuvius SA (Pty) Ltd, a refractory manufacturing company, donated 50 kg BetaCast refractory cement that could withstand a maximum temperature of 1600 °C. The Instrument Makers then built a custom mould to cast this refractory crucible pedestal. Figure 6.4 presents an image of this mould to cast the pedestal using the refractory cement. The white mould casing was made from high density polyethylene, the grey outer structure of the mould holding the casing in place was made from polyvinyl chloride (PVC) and the pen used to make a hole in the pedestal for the ceramic alumina rod was made from stainless steel.

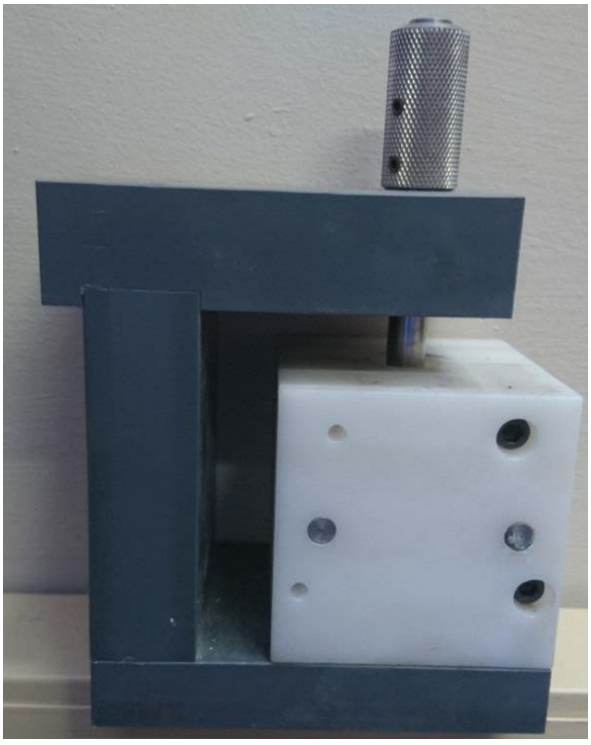

Figure 6.4: An image of the mould used to cast the refractory crucible pedestal

Figure 6.5 shows an image a ceramic crucible on top of the pedestal. The pedestal was cast and dried at 120 °C for a few hours and then heated in the TGA up to 1450 °C 3 times to make sure no mass loss from the refractory material would occur, which would influence the analysis. The new refractory pedestal was tested during the analyses of a few samples and no further issues occurred.

Figure 6.5: Refractory crucible pedestal

After a few more runs the temperature reading on the thermocouple inside the tube started to show values that were inconsistent with that of the furnace controller temperature. After extensive troubleshooting the conclusion was that the thermocouple had broken. As high temperature thermocouples are very expensive, this was a big setback. This instrument was taken apart to assess the damage. The top of the tube had a crack and the insulation wool was burned almost all the way through. It seemed that the thermocouple was oxidised. The thermocouple would need better protection against the environment in the furnace. The sheath that was used as protection for the thermocouple was an open ended ceramic alumina tube. In order to provide better protection, an ceramic alumina tube was obtained that was closed at one end. This would protect the thermocouple from the high temperature gaseous atmosphere during analysis. A new high platinum wire temperature thermocouple (type B) was obtained. Better insulation was needed to keep the heat isolated to the hot zone. For this

purpose a vacuum formed alumina fibre board was used. This material is more compact than the wool and would provide better heat insulation. Pieces of this board was cut out and fit into the top part of the furnace where the insulation wool was.

The instrument was reassembled and test runs were done to make sure that everything was in working order. After considerable testing it was clear that the modifications to the TGA design seemed to have resolved the problems. Figure 6.6 presents an image of the final operational large mass TGA that was used for the analysis presented in Section 6.3.

Figure 6.6: Image of the operational large mass TGA.

6.2.3 Comparing large mass TGA to commercial TGA

In order to evaluate the accuracy of the large mass TGA, the pellet mixture used to make the composite pellets was measured in a commercial TGA and the results were compared. This material is not a certified reference material or standard, it was merely a way to verify the accuracy of the large mass TGA, assuming that the calibrated commercial TGA would give correct results. Figure 6.7 presents a measurement run of the large mass TGA (sample consisting of 20 pellet, with total mass approximately 20 g), as well as the commercial TGA (sample mass of 50 mg un-pelletised material mixture), both in a nitrogen (N_2) gas atmosphere. Mass loss is presented as a function of temperature. As is evident from the figure, the mass loss trends are similar for both the instruments. The small differences in mass loss occurred at low temperatures, which are not relevant to iron (Fe) or chromium (Cr) reduction, and it can possibly be attributed to the significant different sample size of the two instruments. Since the two TGA curves were so similar, the measurements from the large mass TGA could be used with confidence.

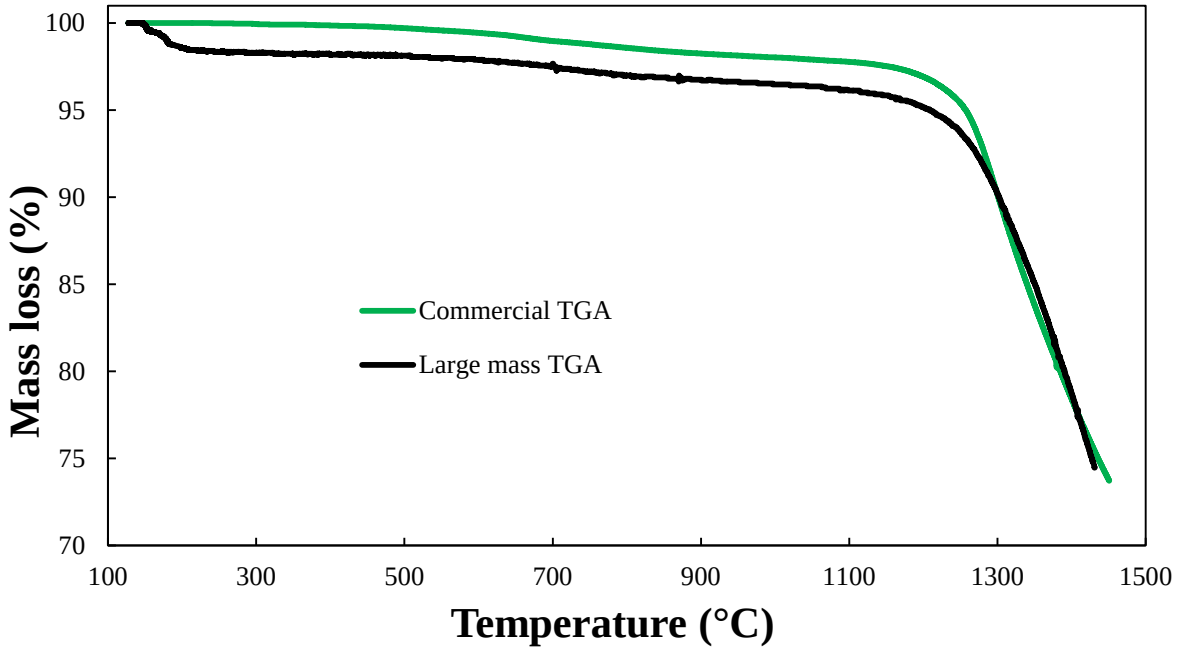

Figure 6.7: TGA curves from a commercial TGA using 45 mg composite pellet mixture and the large mass TGA using 20 composite pellets with an approximate weight of 20 g, both in a N_2 gas environment. The pellet mixture was milled and mixed as described in Section 3.3 and this mixture was pressed into pellets to form the composite pellets, as described in Section 3.5.

6.3 Thermo-gravimetrical analysis of composite pellets and pellet components

As mentioned in Section 3.5, Met grade 1 was used in composite pellets in the TGA measurements. In Figure 6.8 the mass loss (%) of the composite pellets and the pellet components (ore, Nkomati anthracite and bentonite clay) is presented as a function of temperature (°C). The overall mass loss trend can be compared in this figure. The ore didn't show any sign of mass loss for the temperature range investigated. This was expected since chromite is a well know refractory material (Papp, 2004) and the melting temperature of chromite ores investigated were in the range of 1885 to 1947 °C, as was found with the sessile drop tests (Section 5.2). Specifically, Ore 1 that was used in this pellet mixture had a deformation temperature of 1757 °C and melting temperature of 1975 °C. The high melting point and absence of any significant change in thermal behaviour at these temperatures is attributed to the strong spinel structure of the chromite ore. According to Xu and Dai (1992), even though the Cr, Fe and Mg contents of different ores vary considerably, the melting points of the spinel remain in the same high-temperature range. In contrast to the thermal behaviour of the ore over the investigated temperatures range (100 °C – 1450 °C), the composite pellets already started showing signs of mass loss below 300 °C. Further, a small mass loss was visible between 500 °C and 900 °C and significant mass loss above 1100 °C. For the Nkomati anthracite (which served as a reductant in the pellet mixture) mass loss also occurred below 300 °C, as with the pellet mixture and then again at about 500 °C, 700 °C and 1450 °C. Significant mass loss in the clay also occurred below 300 °C, but continued beyond 300 °C and then again at a few different temperatures up until 900 °C. In order to better understand the effects of the different pellet components and the composite pellets, TGA and DTG (Section 3.2.4) curves for each are presented and discussed separately.

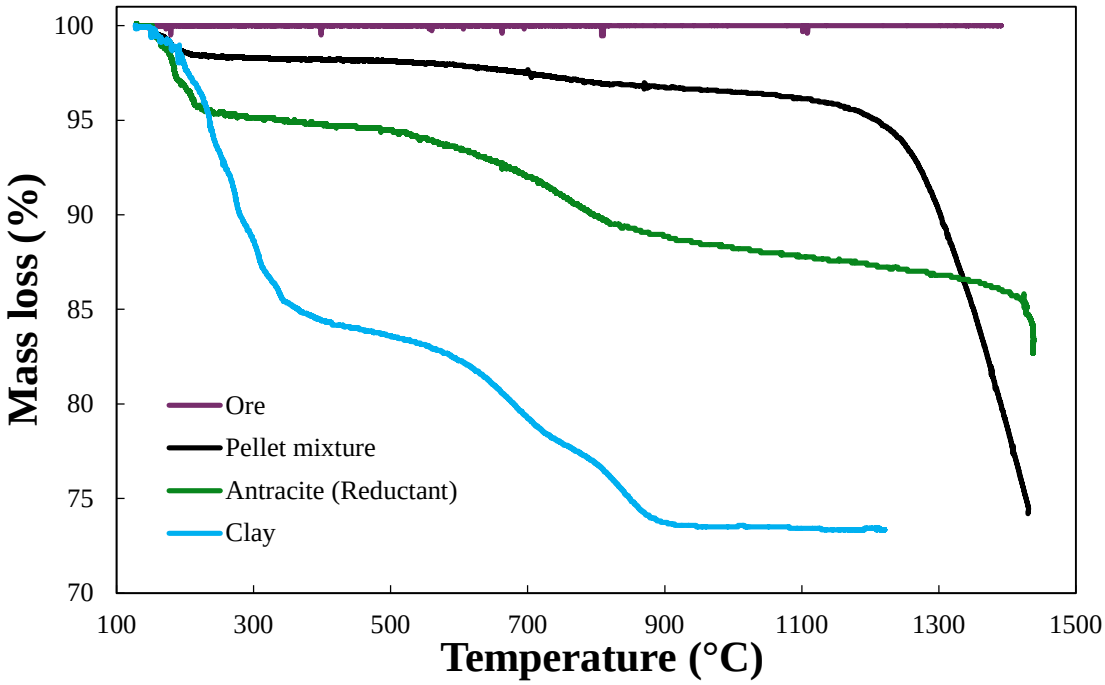

Figure 6.8: TGA curves of chromite composite pellets and pellet components. % Mass loss is presented as a function of temperature.

Figure 6.9 presents the TGA and DTG curves of Nkomati anthracite used as reductant in the pellet mixture. Considering the TGA curve, mass loss of about 4% can be observed between 152 °C and 200 °C with the DTG curve showing a maximum mass loss rate at 200 °C. The mass loss in this region can mainly be attributed to loss of moisture and light volatile matter (Xiao *et al*., 2015; Khare and Baruah, 2014). As mentioned in Section 3.5, a drop of water was added to the milled anthracite before pressing the pellet to ensure bonding. The added water therefor also contributed to the mass in this temperature range. The second stage of mass loss visible on the TGA curve is the fast pyrolysis region, where mass loss started at approximately 500 °C and had a maximum mass rate loss at approximately 750 °C (DTG minimum peak). The mass loss occurring in this temperature range can be ascribed to primary devolatilisation of the anthracite (Guangjun *et al*., 2017; Xiao *et al*., 2015; Khare and Baruah, 2014; Li *et al*., 2011). Secondary (slower) pyrolysis normally occurs in the temperature range of 750 °C to 1000 °C, or higher. The TGA curve shows a gradual mass loss from approximately 800 °C to 1400 °C, which correlates to the secondary pyrolysis region for this specific anthracite. The total mass loss during the primary and secondary pyrolysis regions (500 °C to 1400 °C) added up to about 10%. In Section 5.1 (Table 5.2) it

was indicated that the volatile matter content of Nkomati anthracite was 6.87. The remaining approximately 3% can possibly be ascribed to some carbonate minerals that would have started to decompose at about 850 °C (Xiao *et al*., 2015). The last mass loss stage of the anthracite started at approximately 1400 °C and was followed up to approximately 1450 °C, which was the maximum safe temperature at which the analysis could be conducted considering the instrumental limitations. The mass loss during this stage can be attributed to melting of the mineral assemblage (ash). This is supported by the results from the sessile drop test performed on Nkomati anthracite in Section 5.2. In Figure 6.10a and b sessile drop test images of the anthracite at 1400 and 1440 °C are presented, respectively. In Figure 6.10a the sample is starting to become more spherical, as the ash begins to melt. In Figure 6.10b the pellet has taken on a spherical shape, as the melting progressed. This, i.e. ash melting, would then be the source of the mass loss (TGA curve in Figure 6.9) at temperatures above approximately 1400 °C.

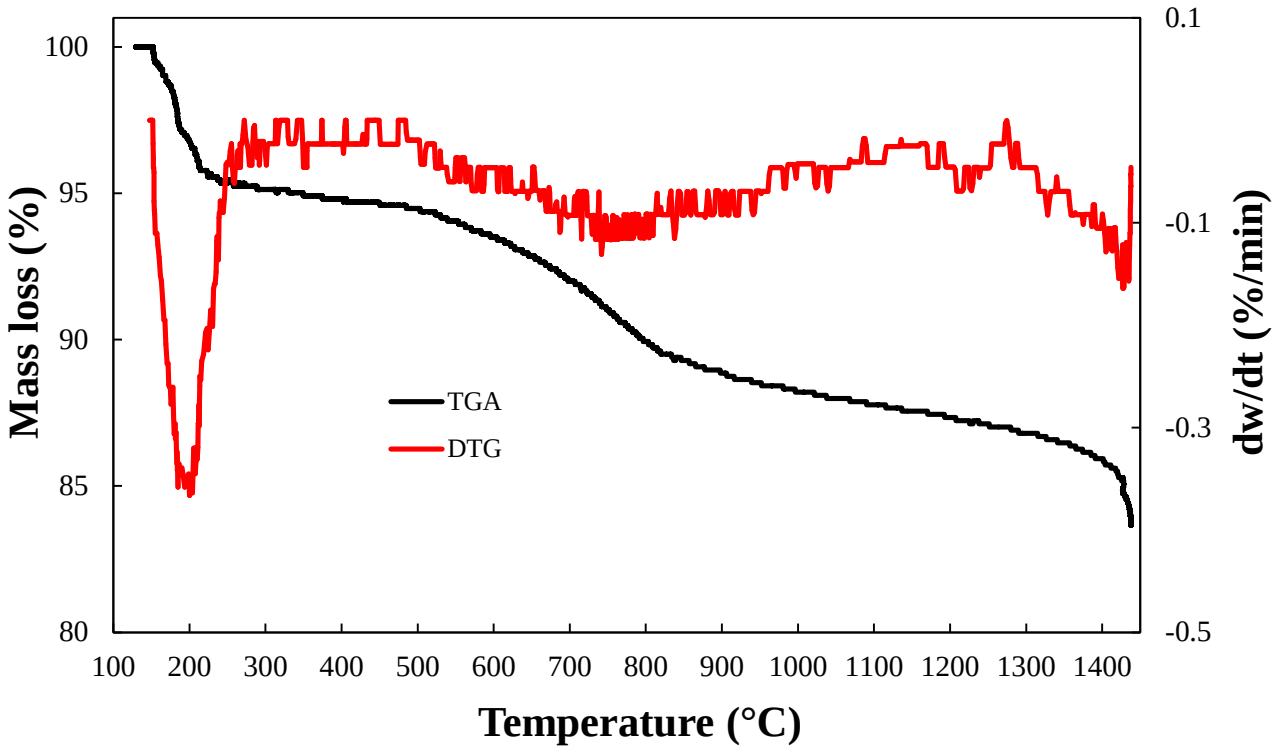

Figure 6.9: TGA and DTG curves of Nkomati anthracite as a function of temperature. Mass loss (%) is presented on the primary y-axis and differential mass loss (dw/dt) on the secondary y-axis. The noise on the DTG curves is due to small fluctuations of the TGA curve that are amplified in the DTG calculation – DTG curves were not smoothed.

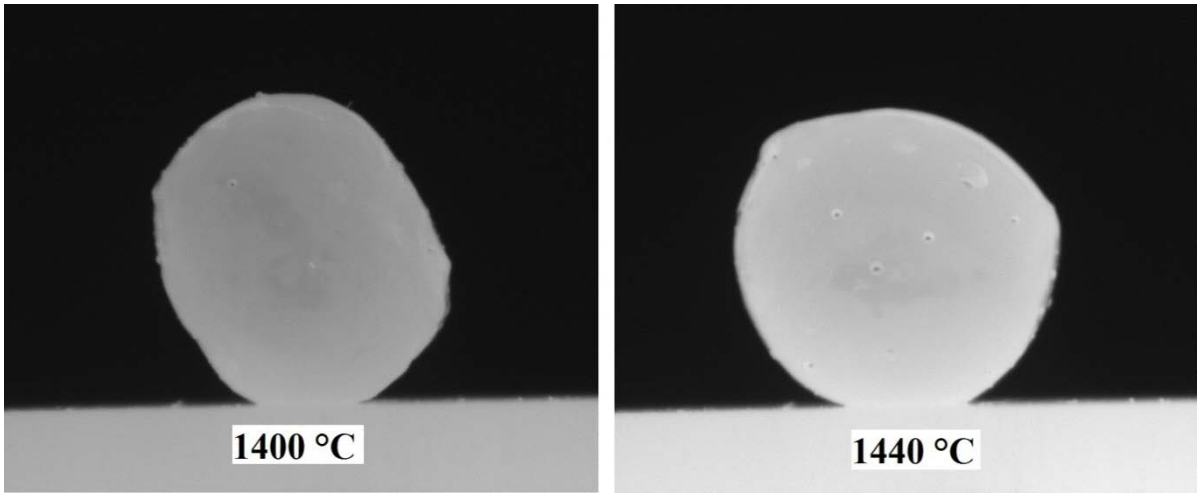

Figure 6.10: Sessile drop images of Nkomati anthracite at 1400 (a) and 1440 °C (b).

The TGA and DTG curves of the bentonite clay over the temperature range of 100 to 1250 °C are presented in Figure 6.11. The TGA curve shows an initial mass loss occurring from approximately 120 to 350 °C, with the DTG curve displaying a maximum mass loss rate at 280 °C. The mass loss in this region can be ascribed to a loss in moisture (Zuzana *et al*., 2012). According to Onal and Sarikay (2007), for bentonite clay dehydration of inter-particle water, adsorbed water and interlayer water occur at in this temperature range. These authors also state that mass loss occurring between 640 °C and 730 °C can be attributed to dehydroxylation. The DTG curve in Figure 6.11 shows a mass loss peak at 700 °C, which can then be ascribed to the release of hydroxyl groups. There is also a peak on the DTG curve at 890 °C. In Table 6.1 quantative XRD analysis of the bentonite clay is given. Amorphous phase was not taken in account in this analysis. The clay consists mainly of smectite clay group minerals. Kleynhans *et al*. (2012) stated that qualitative XRD analysis indicated that the smectite group contained montmorillonite. The structure of this component consists of two silica tetrahedral sheets and alumina octahedral sheet, which causes the clay to display properties such as swelling ability, plasticity, compressibility, and cation exchange properties (Zuzana *et al*., 2012). Onal and Sarikay (2007) explained that at about 900 °C decrystallisation of this structure occurs and therefore the peak mass loss at 890 °C can be attributed to the afore-mentioned occurrence of decrystallisation. Above this temperature, interparticle sintering takes place causing a phase transformation to a spinel structure (Onal and Sarikay, 2007; Grim and Bradley, 1940).

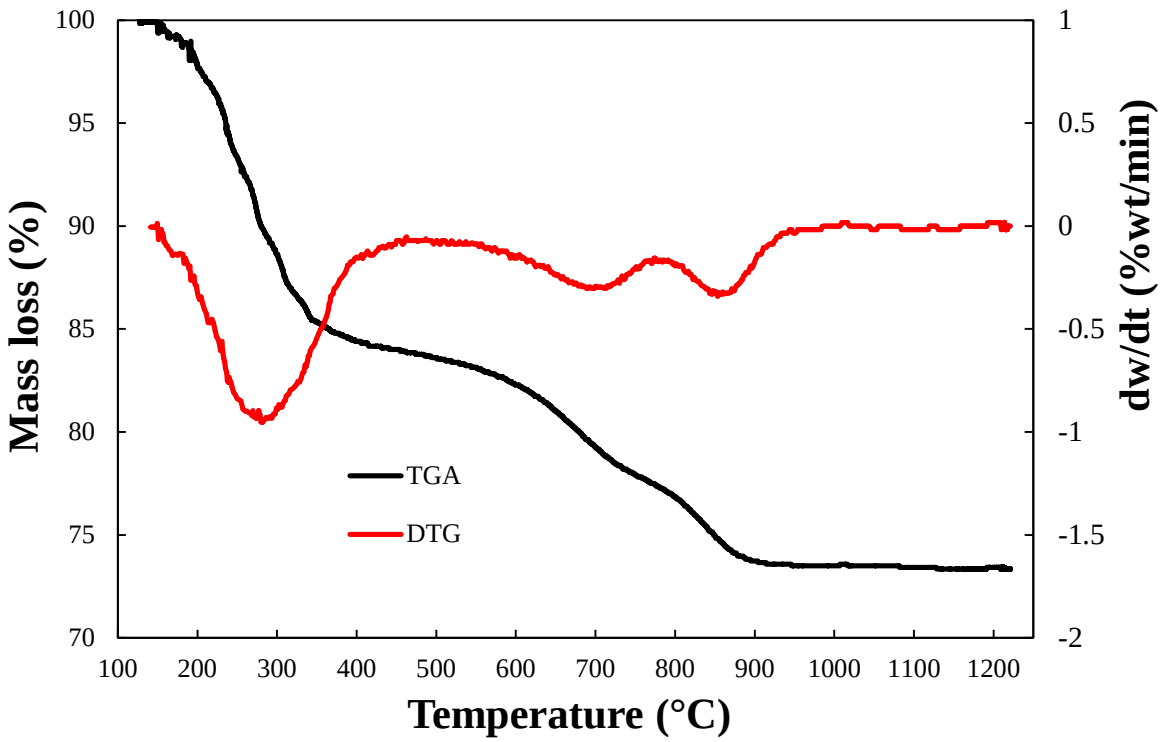

Figure 6.11: TGA and DTG curves of the bentonite clay as a function of temperature. Mass loss (%) is presented on the primary y-axis and differential mass loss (dw/dt) on the secondary y-axis.

Table 6.1: Quantative XRD analysis of the bentonite clay. This analysis was obtained from Kleynhans *et al*. (2012), since the same material was used.

Mineral phase	Content (%)
Augite	0.64
Calcite	6.34
Kaolinite	0.97
Muzcoivite	4.93
Orthoclase	4.25
Plagioclase	5.98
Quartz	14.39
Smectite	62.51

Figure 6.12 presents the TGA and DTG curves of the composite pellets for the temperature range between 120 °C to 1450 °C. From the TGA curve, a significant mass loss occurred from approximately 130 °C to 210 °C, with the DTG curve showing a maximum mass loss at 195 °C. This mass loss can be attributed to loss in moisture from the composite pellet mixture that was added during pelletisation (Section 3.2.4) , as well as light volatile matter from the anthracite (Figure 6.9) and dehydration of inter-particle water, adsorbed water and interlayer water from the bentonite (Figure 6.11). A second mass loss between 500 °C and 900 °C was observed, but is not clearly visible in this figure. Figure 6.13 presents an enlargement of Figure 6.12, so that the mass loss occurring over this temperature range is clearer. From the TGA curve in Figure 6.12 a gradual mass loss is visible from 210 reaching a maximum mass loss rate at 520 °C (DTG curve), which can be attributed to loss in volatiles from the reductant (Figure 6.9). Further mass loss occurred from approximately 520 to 820 °C with a DTG peak visible at approximately 700 °C, which is most likely the clay de-hydroxylation (Figure 6.11). Directly thereafter at approximately 780 °C another DTG peak is observe. Actually the afore-mentioned two peaks overlapped. Niemelä *et al*. (2004) and Kleynhans *et al*. (2016) presented Ellingham diagrams of metal oxides with carbon (C) and carbon monoxide (CO), where it was indicated that iron oxide reduction by carbon occurs above 710 °C. Thus the mass loss that peaked at 780 °C (according to DTG curve) indicated iron reduction in the chromite ore. The next stage of mass loss that can be seen on the TGA curve in Figure 6.12 begins at approximately 1200 °C and reaches a maximum at approximately 1380 °C, which can be ascribed to Cr reduction from the spinel (Niemelä *et al*., 2004; Kleynhans *et al*., 2016).

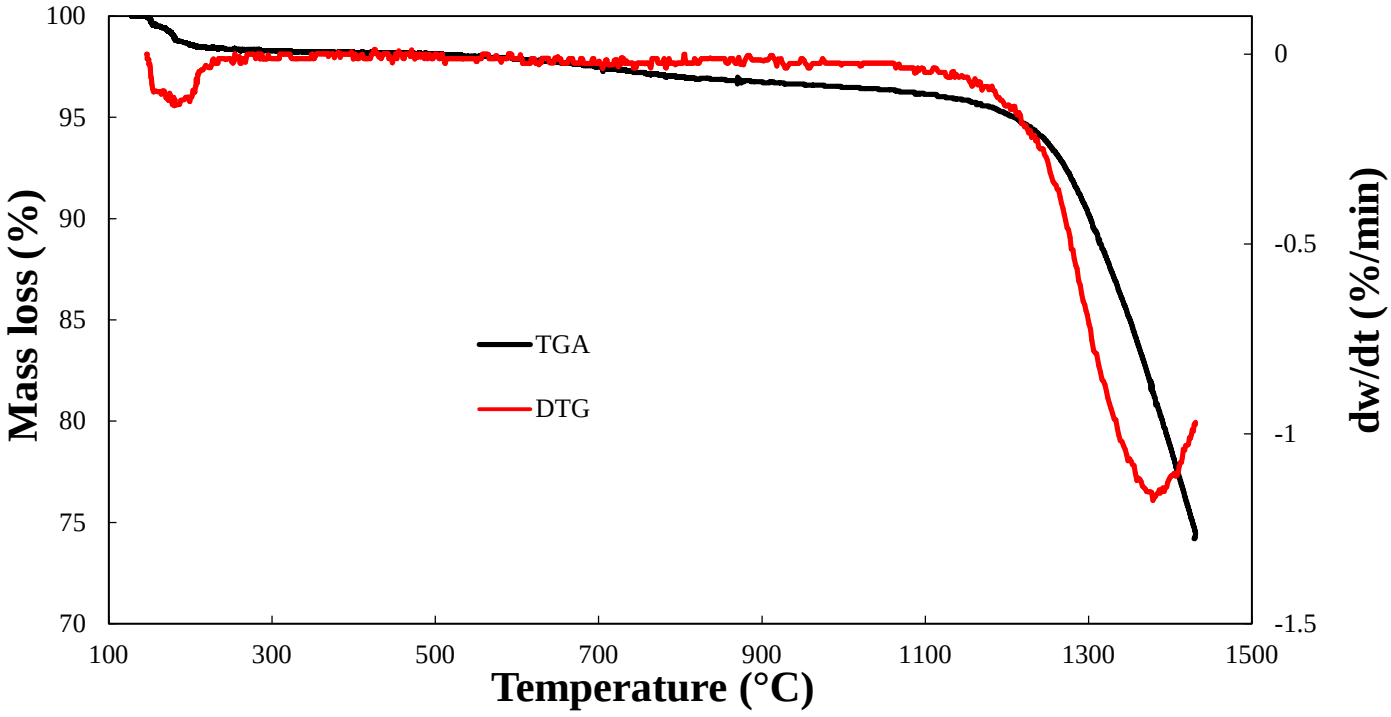

Figure 6.12: TGA and DTG curves of composite chromite pellets as a function of temperature, for a temperature range of 120 to 1450 °C. Mass loss (%) is presented on the primary vertical axis as a function of temperature and differential mass loss (dw/dt) on the secondary vertical axis.

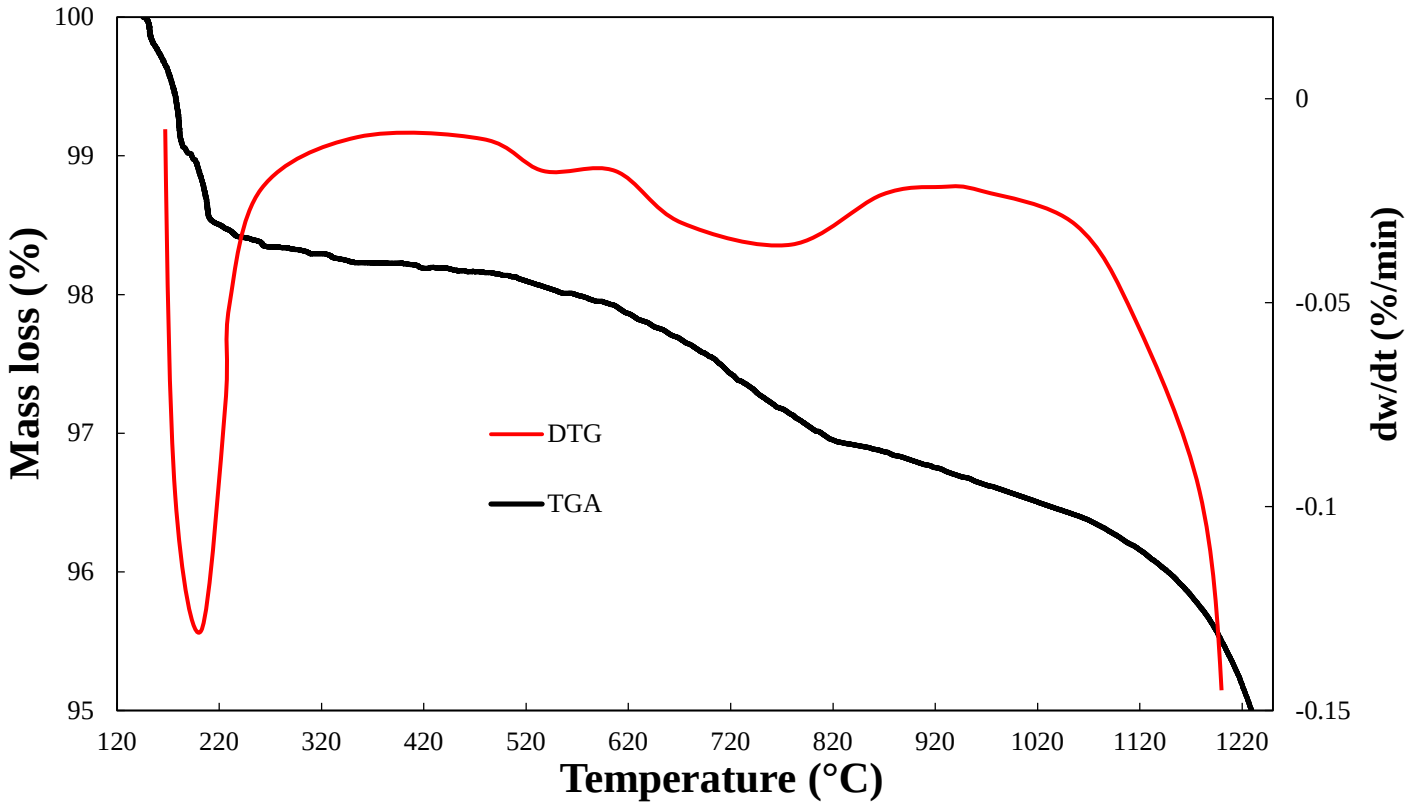

Figure 6.13: Enlarged TGA and DTG curves for composite chromite pellets between 120 and 1250 °C as a function of temperature. Mass loss (%) is presented on the primary y-axis and differential mass loss (dw/dt) on the y-axis.

6.4 Thermo-mechanical analysis of composite pellets and pellet components

As indicated in Section 3.2.5, TMA measurements are used to record the dimensional changes of a sample as a function of temperature or time. It can be used to study contraction or expansion of a sample, glass transitions, softening points, etc. It is well know that TGA and DTG curves are good indicators of pre-reduction of chromite (Dawson and Edwards, 1986; Nunnington and Barcza, 1989; Neuschütz, 1992; Kekkonen *et al.*, 1995). This was also proven in the preceding section (Section 6.3) with the large mass TGA instrument that was developed as part of this study. Kleynhans et al. (2016) suggested the possibility of using TMA measurements to indicate pre-reduction, however, no evidence could be found in literature that this has indeed been done. Therefore, in order to investigate this suggestion, TMA measurements were compared to the large mass TGA measurements. Even though the main idea of this investigation was to evaluate the possibility of following pre-reduction

using dimensional changes, the dimensional changes of the pellet components was also discussed briefly.

Figure 6.14 presents the dimensional changes of a composite chromite pellet, as well as those of each of the pellet components over the temperature range of 25 °C to 1450 °C. The ore TMA curve show that the ore gradually expands from ambient temperature to 1100 °C. This expansion could be the attributed to the ore acting as a solid material that expands when heated, without any significant chemical/compositional change. The TGA curve of the Nkomati anthracite showed gradual expansion from ambient temperature until approximately 200 °C. This expansion could be ascribed to the material acting as a solid, just as for the ore, that expands upon heating. From approximately 200 °C until 500 °C the expansion of the sample correlated with the TGA data in Figure 6.8, where primary devolatilisation started to takes place. Thereafter the sample contracted until approximately 690 °C, as it approached the end of the primary devolatilisation region. The anthracite gradually expanded again from 690 °C until 1250 °C, during which secondary devolatilisation took place. The TGA curve for the bentonite clay showed a gradual expansion through the entire temperature range investigated. Clay undergoes significant swelling when heated and forms a hardened spinel structure as inter-particle sintering takes place and phase transformation occurs (Onal and Sarikay, 2007; Grim and Bradley, 1940). The TMA curve of the composite pellet indicated an initially expansion up to approximately 500 °C. This expansion could be attributed to most of the material present in the pellet acting as a solid by expanding when heated. Additionally, it can partially be attributed to the primary devolatilisation that occurs in the anthracite and would therefore also occur in the mixture. After approximately 500 °C the composite pellet contracted up until approximately 860 °C and again after 1200 °C. The complete dimensional change of the composite pellet is not visible in Figure 6.14 as the % change was too large for the scale to fit on the figure with the pellet components. The dimensional changes occurring in the composite pellet was discussed in more detail in comparison to TGA measurements in the next section (Section 6.5).

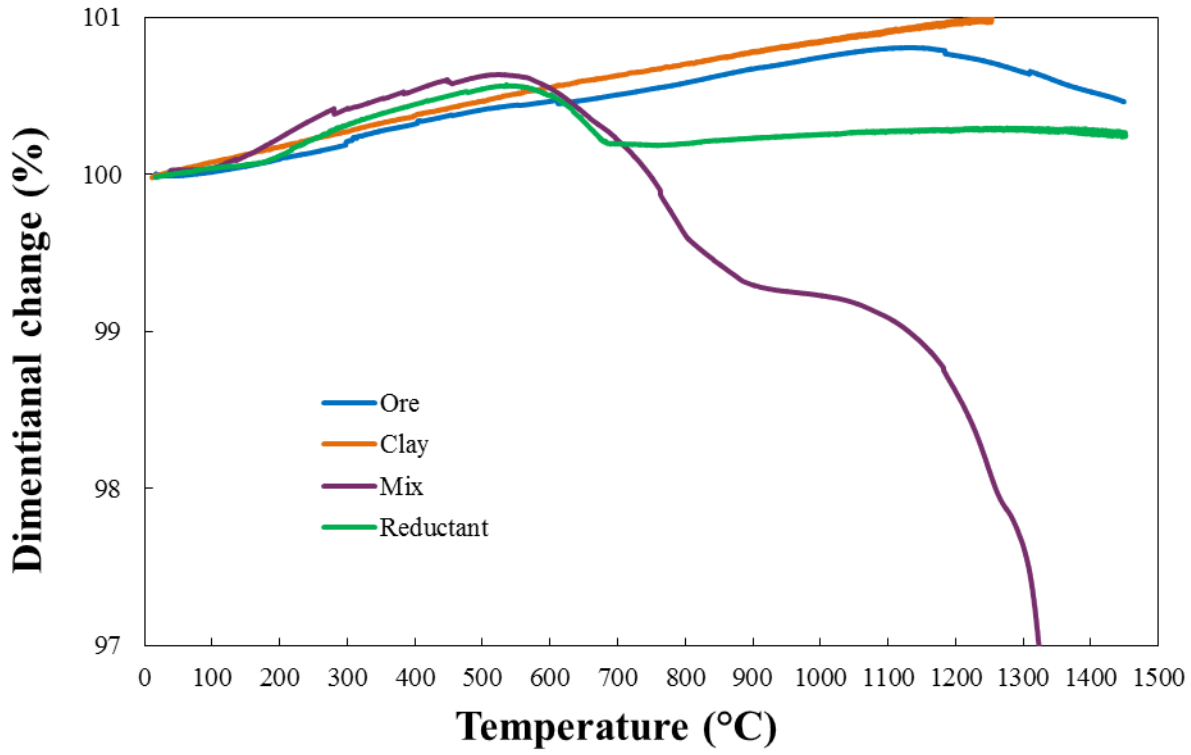

Figure 6.14: The dimensional change (%) of a composite chromite pellet, as well as the individual pellet components as a function of temperature.

6.5 Comparison of thermo-gravimetrical and –mechanical analyses in relation to chromite pre-reduction.

Figure 6.15 presents the dimensional change (TMA), as well as the mass loss (TGA) of composite chromite pellets, as a function of temperature on the primary y-axis. The differentials of both the TMA and TGA are also presented in the figure on the two secondary y-axes. From this figure it is evident that there is a very good relationship between the two different analyses. As discussed in Section 6.3, Fe reduction takes place above 710 °C, and on the TGA curve 780 °C was identified as the temperature at which Fe reduction peaked in the composite pellets. The TMA curve indicated contraction over the temperature range where Fe reduction occurred and the differential dimensional change (DTMA) also peaked at 780 °C. The DTG and DTMA curves are not clear on this figure due to the scale, but an enlarged DTG and DTMA curves confirmed that afore-mentioned statement. Cr reduction was indicated in Figure 6.12 (TGA/DTG curves of the composite pellet) to peak at 1380 °C. The TMA also indicated contraction over the temperature range relevant to Cr reduction and

the DTMA curve also peaked at approximately 1380 °C. Considering there results, it seems that TMA and DTMA can be used successfully to follow chromite pre-reduction of composite chromite pellets.

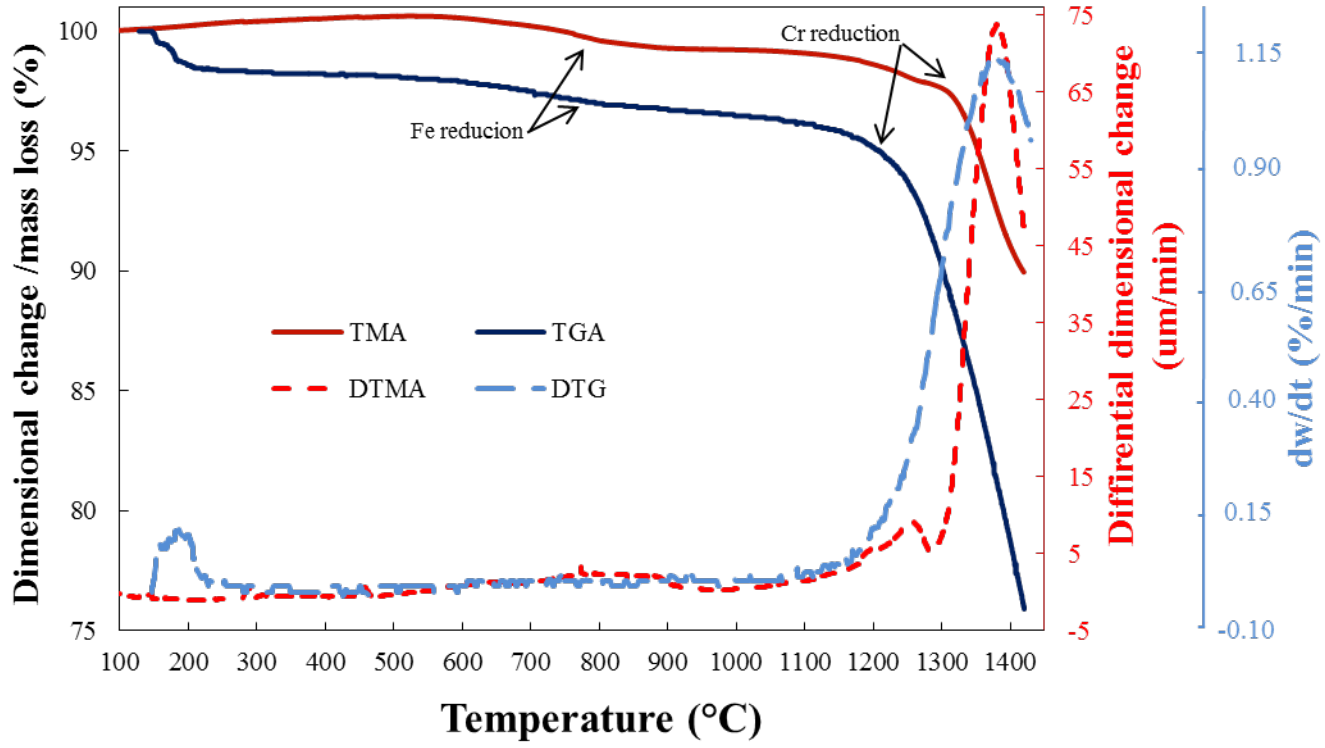

Figure 6.15: The % dimensional change (TMA) and mass loss (TGA) of composite chromite pellets as a function of temperature on the primary y-axis. The differential dimensional change (um/min) (DTMA) and the differential mass loss (%/min) (DTG) are presented on the first (red) and second (blue) y-axis, respectively.

6.6 Conclusions

A large mass TGA was successfully designed, constructed and commissioned (Section 6.2). TMA curves of composite chromite pellets (analysed in the large mass TGA) and pellet mixture (analysed in a commercial TGA) compared well (Section 6.2). Samples with a mass of up to 1900 g could be analysed using the large mass TGA, which made the results much more relevant to the industrial application, since a pellet bed could be simulated. Fe and Cr reduction, taking place in the composite chromite pellets, could clearly be identified with the large mass TGA (Section 6.3). Studying the TGA behaviour of the pellet component complimented the results. The sessile drop test results presented in Chapter 5 supported the results further (e.g. confirming the melting temperature of the anthracite ash). Lastly, and most significantly, TMA and DTMA curves compared very well with TGA and DTG curves, proving that it is possible to follow chromite pre-reduction with TMA measurements. As far as the candidate could assess from literature, this is the first such proof presented. Both measurement methods indicated Fe and Cr reduction to peak at 780 and 1380 °C, respectively. However, it should be remembered that these temperatures are ore (and composite pellet mixture) specific.

Chapter 7

Project evaluation and future perspectives

In this chapter, the project evaluation is presented in Section 7.1. This was done by repeating each objective proposed in Chapter 1, where after the main findings and conclusions were discussed, as well as how these contributed to achieving that specific objective. Thereafter recommendations for future work is discussed (Section 7.2).

7.1 Project evaluation

The general aims of this study were the investigation of damring formation in pre-reduction rotary kilns used in ferrochrome (FeCr) production and assessing if thermo-mechanical analysis (TMA) can be used as an alternative method to follow pre-reduction of composite chromite pellets. In order to achieve these aims, specific objectives and strategies were formulated, which were stated in Chapter 1, Section 1.2. The project evaluation, which is presented here, was done by stating each objective and the strategies linked to it, as presented in Chapter 1. Thereafter, the major findings associated with each objective are discussed, as well as the successes and shortcomings/challenges.

i) Objective 1: *Assess the possible contribution of pulverised fuel (PF) coal ash to damring formation in chromite pre-reduction kilns. The strategy to fulfil this objective was to obtain a wide range of different PF coal samples, which could then be characterised in detail. It was assumed that the softening temperature (T_{soft}), determined with ash fusion temperature (AFT) analysis, could be used to indicate possible contribution to damring formation. However, ATFs are not routinely determined by the FeCr industry, therefore a multivariate statistical method will be used to related more commonly measured PF coal characteristics to its ash softening behaviour.*

Twenty different carbonaceous materials were obtained from FeCr producers. Currently only coal is used to fire pre-reduction rotary kilns, since it is less expensive than other carbonaceous materials (e.g. coke, char and anthracite) and it is easier to ignite due to the general higher volatile matter content. However, only three coal samples used as PF could be obtained. Therefore, apart from coal; char, coke and anthracite samples were also obtained. Including a wider selection of carbonaceous materials made it possible to make more significant deductions on general trends and relating (T_{soft}) to PF characteristics that are more commonly measured. Therefore, the results could be applied to a wide range of carbonaceous materials with different compositions. This should give FeCr producer confidence to apply the results, even if PF coal composition change due to fluctuations in the coal deposit, coal beneficiation inconsistencies, or if suppliers/coal deposit change.

The carbonaceous materials were characterised by conducting the following analyses: proximate, ultimate, total sulphur, calorific value, ash composition (16 different species) and AFTs under oxidising and reducing atmospheres. AFTs were the obvious characteristics that could be used as indicators for the contribution of a specific carbonaceous material to damring formation. From the results (Table 4.1) it was evident that the oxidising and reducing AFTs of some carbonaceous samples were below the typical temperature of pre-reduced pellets the chromite pre-reduction process, i.e. 1300 °C. Also, it was attempted to identify general trends, relating the characterisation data to the AFTs. However, no consistent relationship(s) could be identified that could be used as a basis for selecting PF coals more optimally. This was expected, since it is highly unlikely that the AFTs will be dependent on only one or two general carbonaceous material characteristics. Multiple-linear regression (MLR) analysis was therefore used to establish a mathematical relationship between the general carbonaceous material characterisation data and ash fusion temperatures. This technique has been successfully applied in many scientific and engineering disciplines, including pyrometallurgical applications. Specifically, T_{soft} was used as an indication of the temperature where PF ash would start to contribute to damring formation, since ash softening represent be the lowest temperature where it could bond to the kiln refractory and other particles. MLR calculations were done for both oxidising and reducing T_{soft}, since both atmospheres are relevant to pelletised chromite pre-reduction kilns (as described in Section 4.1). In each MLR calculation T_{soft} was considered as the dependent variable and the other characterisation data as independent variables. Optimal MLR equations, containing the least number of independent variables, with the best possible correlation to the actual

measured T_{soft} values, were determined. Root mean squared error (RMSE) values were used to quantify the difference between calculated and measured values, and additionally four carbonaceous materials that were omitted from the MLR calculations were used to verify the accuracy of the calculated/predicted T_{soft} values. These optimised MLR equations for oxidising and reducing T_{soft} (Equations 4.1 and 4.2) can be used by FeCr producer to select PF coals more optimally in future, if AFTs are not available during the selection process.

Instead of just presenting the deduced optimised MLR equations, the candidate attempted to scientifically interpret the meaning thereof. This was done by using SPSS programming software to further derive several statistical parameters (i.e. β weights; structure coefficients, r_s; squared structure coefficient, r_s^2; unique and common commonality coefficients, and the relative important weights, RIW) that was used to evaluate the contribution of each independent variable and the combined contribution to the calculated T_{soft}. Of these, RIW is likely regarded as the best to describe the contribution of an independent variable (correlating to species/parameters in Table 4.1), after correcting for the effects of the intercorrelation among independent variables. Evaluation of RIW and the other statistical parameters indicated that the intercorrelations between the different variables are very complex, which confirmed the earlier conclusion that it is not possible to relate the general characteristics (proximate and ultimate analyses, ash composition, etc.) of carbonaceous material to its AFTs without using a multi-variant technique (e.g. MLR) that takes intercorrelations and other complex factors into consideration.

Specifically for the reducing T_{soft}, K_2O ash content was found to make the largest contribution (20.8 %) to the variance in calculating T_{soft}, with the combined ash components (K_2O, V_2O_5, P_2O_5, etc.) contributing 47.5 % to the variance (Table 4.2). These results indicate that ash composition, not only ash wt.% content and PF composition as currently considered by FeCr producers when selecting a PF, are very important. It was also found that some ash species such V_2O_5, which had very low ash contents (below 0.33 wt.%), contributed significantly to the variance (8.9 and 4.7 % RIW, respectively). This was related to the fact that V_2O_3, rather than V_2O_5, is the most likely form of vanadium (V) in a reducing atmosphere. The melting point of V_2O_3 (1940 °C) is significantly higher than that of V_2O_5 (690 °C) (Wang *et al.*, 2013).

For the oxidising T_{soft}, P_2O_5 had the highest RIW value of 18.4 %, with MnO and MgO having RIW values of 14.3 and 13.2 %, respectively. Both MnO and MgO had a negative r

values, indicating an inversely proportional correlation with oxidising T_{soft}. Van Dyk and Keyser (2005) and Song *et al.* (2009) reported similar roles for MnO and MgO. Combined the ash components had a RIW contribution of 79.0 %, which again proved that ash composition, not only ash wt.% content as is currently considered by FeCr producers when selecting a PF, is very important. Van Dyk (2005) stated that an increase in acidic components such as Al would cause an increase in oxidising AFT's. This was also confirmed by the results (Table 4.2), as Al_2O_3 had a RIW of 10.2 % and a positive r value showing a directly proportional relationship. However, commonly (total of "common" in Table 4.2) the ash components had a large contribution, showing that the interaction between the different ash components played a significant role in predicting AFT for an oxidising atmosphere.

Considering all the above-mentioned, Objective 1 was successfully achieved since the possible contribution of PF coal ash was established, and optimised MLR equations were deduced that can be used to calculate oxidising and reducing atmosphere T_{soft} relatively accurately for a PF, if the basic characteristics are known. If FeCr producers want to limit damring formation, AFTs have to be specified as selection criteria for procurement of PF. Currently, only proximate analysis characteristics and cost considerations are used to select PFs. If determining AFTs is not practical, the optimised MLR equations derived in this study can be used to estimate the oxidising and reducing T_{soft}.

ii) Evaluate the possible contribution of chromite ore, as well as composite chromite pellet fragments to damring formation in chromite pre-reduction kilns. In order to achieve this, several typical chromite ores will be obtained from FeCr producers, as well as a typical clay binder and carbonaceous reductant used in the production of composite chromite pre-reduced pellets. These raw materials will be characterised in detail. The thermal softening behaviours of the composite chromite pellets and individual raw materials will then be evaluated by performing sessile drop tests, which will be related to possible damring formation contribution. It is also foreseen that actual damrings will be analysed to verify conclusions made from Objective i) and ii).

Seven typical fine South Africa chromite ores used as feed material in FeCr production processes (specifically pre-reduction or oxidative sintered pellet processes) were obtained, as well as a reductant and clay binder sample used in pelletised chromite pre-reduction processes. These materials were characterised by conducting chemical analyses, as well as proximate analysis of the reductant (result presented in Tables 5.1 and 5.2).

To achieve Objective 1, T_{soft} values determined with AFT analyses were used to assess the possible contribution of PF coal ash to damring formation. However, the AFT method had a maximum measurement temperature of 1550 °C. The softening temperatures of chromite ore and composite pellets were expected to be well above this temperature, therefore another technique had to be used. The high temperature behaviour of the composite pellet mixtures (with similar composition that industrially produced pellets) containing ore, reductant and clay, as well as the pellet components individually, were therefore assessed using the sessile drop test method, since it has a maximum operating temperature of 2400°C.

With the sessile drop test method, the temperature where the first sign of deformation of the sample was observed, was defined as the deformation temperature. This temperature was assumed to be the temperature where the material could start contributing to damring formation. The deformation temperatures of the ores were found to be in the range of 1466 °C to 1757 °C, which are much higher than the typical material temperature inside the rotary kiln (~1300 °C). The deformation temperatures of the composite pellet mixtures ranged between 1385 °C and 1475 °C. Although lower than that of the ores, these temperature were still above the typical material temperature inside the rotary kiln (~1300 °C). It is therefore unlikely for that the ores, or composite pellets fragments will significantly contribute to damring formation, unless the ore contains significant amounts of liberated gangue minerals. However, the deformation temperatures of the clay and reductant were 1054 °C and 1246°C, respectively. Therefore, clay and reductant ash released by pellet fragments could contribute to damring formation, if pellet breakup occurs.

Actual damring samples were also obtained from a chromite pre-reduction rotary kiln that was broken out during a shutdown. Scanning electron microscope (SEM) and associated energy dispersive x-ray spectroscopy (EDS) surface microanalysis of polished damring samples were undertaken. It proved that the damrings consisted of composite pellet fragments (with a Cr/Fe ratio of 1.54, which is typical for South African met grade ore), bonded together with a darker coloured matrix (indicating dominance of elements with lower atomic numbers). This matrix contained a significant amount of Si (> 13.8 wt.%), which is the most prevalent PF coal ash element (Table 4.1). The reductant used in the pellet mixtures contained 10.1 % SiO_2 and the bentonite clay contained 53.5 % SiO_2 (Table 5.2). This could indicate the possibility that the Si in the damrings come from the clay binder. But this darker matrix also contained very high concentrations of C, which is indicative of partially unburned PF coal. Such high C contents will not be possible if the matrix was dominated by the clay

binder and/or the gangue minerals included in the composite pellets. Therefore, the most obvious (and significant) source of the matrix that bind the chromite (or chromite derived particle) together is PF coal ash. Since the damring samples were not set in resin and not carbon coated prior to SEM analysis, the afore-mentioned C analyses were relatively accurate and could be used in this assessment.

Another interesting and very important finding was that UG2 ore does not necessarily contribute more to damring formation than metallurgical grade chromite ore, as is the general industry perception. For instance, it was found that the Met grade 6 sample and the UG2 ore had similar chemical compositions (Table 5.1), yet the deformation temperatures of the Met grade 6 ore was approximately 240 °C lower than that of UG2 (Table 5.3). This significant difference was found to be due to the fact that the Met grade 6 ore contained a much larger fraction of liberated gangue particles, than the UG2 where the gangue particles were often enclosed or attached to the chromite particles. The gangue particles typically contain high concentrations of alumina silicates, which will have deformation/melting behaviours similar to that of the observed bentonite. Therefore, it stand to reason that although the chemical composition of the two ore were similar, the liberated gangue particles in the Met grade 6 ore deformed/melted at much lower temperature that the gangue that were at least partially protected from deformation/melting in the UG2 ore by the chromite (which is a refractory material) particles. Therefore, FeCr producers should not only rely on the chemical composition to choose an ore to limit damring formation, but should consider if the gangue present in the ore is liberated or not.

Considering all the above-mentioned, Objective 2 was achieved successfully. The sessile dropt test results and the analyses of actual damrings (all conducted to achieve Objective 2), in conjunction with the results presented to achieve Objective 1, proved that PF coal ash is likely the “glue”, without which damring formation would be much less significant. Also, it was found that the comparison of chemical composition of ores is not necessarily a good indicator of the possible contribution to damring formation. The liberation, or lack thereof, of the gangue minerals, seem to be a much better indicator.

iii) *Compare thermo-mechanical (TMA) and thermo-gravimetrical (TGA) measurements of chromite composite pellets, in order to assess if TMA can also be used to follow chromite pre-reduction occurring in such pellets. The pelletisation method presented by Kleynhans et al. (2012) and Neizel et al. (2013) will be used to simulate the formation of green (uncured) pellets for the purpose of further experimentation. However, the atmosphere in a pre-reductions kiln is partially oxidising to allow PF combustion, while a partial positive CO pressure existing inside the pellets themselves, causes a reducing atmosphere inside and around the pellets. To recreate this system, the ideal would be to be able perform TGA measurements on a couple of pellets in packed bed, which will not be possible with a commercial TGA since the typical maximum sample mass is usually 50 mg. Therefore as part of this study, a large mass TGA (able to analyse approximately 100 g) will be designed, constructed commissioned and tested. The results from this large mass TGA could then be compared to TMA measurements conducted on full size pellets.*

A large mass TGA was successfully designed, constructed and commissioned to better recreate the complex gas atmosphere inside a chromite pre-reduction rotary kiln. Some initial teething problems occurred, but these were resolved. Thereafter the large mass TGA was compared with a commercial TGA, by analysing a similar chromite composite pellet mixture and applying comparable experimental conditions (gas atmosphere and heating rate). The TGA curves of these experiments correlated very well, indicating the accuracy of the large mass TGA. As envisaged, the large mass TGA permitted the analysis up to 20 composite pellets at a time, which allowed the recreation of a pellet bed similar to what occurs in the industrial pre-reduction kilns – where the pellets form a partially reducing atmosphere, notwithstanding the partially oxidising conditions required to achieve PF combustion.

Large mass TGA measurements were done on composite pellets, as well as individual pellet components. Fe and Cr reduction, taking place in the composite chromite pellets, could clearly be identified with the large mass TGA. Although such reduction observations with TGA are not novel, these results are some of the only currently available in the peer reviewed literature, where a bed of composite pellets in an industrially relevant gas atmosphere has been studies. Most of the previous published chromite TGA publications were based on the use of small scale commercial TGA instruments, which typically only allow sample mass up to 50 mg. Such small scale studies have made significant contributions to understanding the fundamental reaction mechanism. But, such results are not always directly relevant to the

industrial process, due to: a) the common use of Argon (Ar) gas atmosphere, b) the use of graphite, or another non-industrially relevant reductant, and c) the omission of a clay binder in the material analysed. Most of these limitations have been overcome with the large mass TGA instrument developed in this study.

TMA measurements of composite pellets, as well as individual pellet components, were also undertaken and the results explained. Thereafter, TGA and TMA curves (as well as their derivatives) of composite chromite pellets were compared. From the results it was evident that the TMA measurements compared very well with that obtained with the large mass TGA. Therefore, it seem feasible that thermo-dimensional changes, measure with TMA, can successfully be used to follow pre-reduction of composite chromite pellets. As far as the candidate could assess, such prove has not yet been published in the peer-reviewed public domain. Considering all the afore-mentioned, Objective 3, i.e. investigating whether TMA measurements can be used to follow pre-reduction, was also achieved successfully.

7.1.1 Summary of project evaluation and current status of publications

In summary, the overall project outcome of this study can be considered as successful, since the specific objectives set for this study was achieved. Furthermore, the results presented in Chapters 4 and 5 were published in a high impact, internationally accredited, peer-reviewed journal, i.e. Metallurgical and Materials Transactions B (a Springer journal), which proved that the candidate made a contribution to science, which is likely the most important criteria for a PhD study. The results presented in Chapter 6 are currently also being written up as a paper that will be submitted to internationally accredited, peer-reviewed journal.

7.2 Future prospective

Although this study was completed successfully, with the objectives achieved, the study did not manage to address all relevant research gaps. In addition, a PhD study has to be confined to a limited scope of work to make it feasible, and it is bound by time and resource limitations. Also, new insights/information raise new question gathered. Therefore, to stimulate relevant future research, remaining and/or identified research gaps were identified, i.e.:

i) As indicated in the discussions relevant to Objective 1 (Section 7.1), some light was shed on the scientific meaning of the optimised MLR equations to calculate T_{soft} of PF coal ash. However, understanding the complex interactions between the independent variables would require substantial additional investigations, which were beyond the scope of the current study. In future, mono-variant addition of selected ash species to synthetic ash (or real ash) can to be investigated, in order to systematically quantify the influence of each ash species, as well as interactions between ash species, on the oxidising and reducing T_{soft}. Additionally, thermodynamic modelling (e.g. with FactSage) can be undertaken to better understand the high temperature chemistry associated with the prediction/calculation of oxidising and reducing T_{soft}.

ii) The sessile drop test results (part of Objective 2) proved that the comparison of chemical composition of ores is not necessarily a good indicator of the possible contribution to damring formation. The liberation, or lack thereof, of the gangue minerals, seem to be a much better indicator. However, in future the effect that the degree of gangue mineral liberation has on ore softening should be quantified if possible, as well as the influence of gangue mineralogical composition.

iii) As stated in the results, the mineral phases reported by chemical analysis are in the standard reporting format, e.g. Cr content is usually expressed as Cr_2O_3. However, in future it should be attempted to identify the actual mineralogical phase in which elements occur. This should preferably be done for both the PF ash (actually the ash composition in the PF before it is combusted) and the ore (to determine the liberated gangue mineral phases).

iv) Although the deformation temperatures determined with the sessile drop method proved to be valuable, there is currently no reference available to indicate the standard deviation/error associated with this method. Therefore, this should be determined.

v) Since it was proven in this study that thermo-dimensional changes, measured with TMA, can successfully be used to follow pre-reduction of composite chromite pellets (Objective 3), such in-depth investigations with a large variety of ores and reductants, as well as binders, should be conducted.

vi) Lastly it is recommended that the large mass TGA that was developed as part of this study be used by the Chromium Technology group at the North-West University (NWU) to conduct more industrially relevant pyro-metallurgical research, which include, but are not limited to chromite pre-reduction research.

Bibliography

Awang, N.R., Ramli, N.A., Yahaya, A.S. and Elbayoumi, M. Multivariate methods to predict ground level ozone during daytime, nighttime, and critical conversion time in urban areas. *Atmospheric Air Pollution Research*, 6:726-734.

Bao, S., Tang, K., Kvithyld, A., Tangstad, M. and Engh, T.A. 2011. Wettability of aluminum on alumina. *Metallurgical and Materials Transactions B*, 42B:1358-1366.

Barnes, A.R., Finn, C.W.P., Algie, S.H. 1983. The prereduction and smelting of chromite concentrate of low chromium-to-iron ratio. *Journal of the South African Institute of Mining and Metallurgy*, 49-54.

Basson, J., and Daavittila, J. 2013. High Carbon Ferrochrome Technology-Chapter 9. (*In* Gasik, M. (ed.) Handbook of ferroalloys: theory and technology. United Kingdom: Elsevier. p. 317-363).

Beukes, J.P., Dawson, N. & Van Zyl, P.G. 2010. Theoretical and practical aspects of Cr (VI) in the South African ferrochrome industry. *Journal of the South African Institute of Mining & Metallurgy*, 110 (12):743.

Beukes, J.P., Du Preez, S.P., Van Zyl, P.G., Pactunc, D., Fabritus, T., Päätalo, M. and Cramer, M. 2017. Review of Cr(VI) environmental practices in the chromite mining and smelting industry - Relevance to development of the Ring of Fire, Canada. *Journal of Cleaner Production*, 165:874-889.

Biermann, W., Cromarty, R.D. and Dawson, N.F. 2012. Economic modelling of a ferrochrome furnace. *The Journal of The Southern African Institute of Mining and Metallurgy*, 112:301-308.

Bhonde, P.J., Ghodgaonkar, A.M. and Angal, R.D. 2007. Various techniques to produce low carbon ferrochrome. (*In* Proceedings of The 11th International Ferro Alloys Congress, New Delhi. p.85-90).

Brynjulfsen, I., Bakken, A., Tangstad, M. and Arnberg, L. 2010. Influence of oxidation on the wetting behavior of liquid silicon on Si_3N_4-coated substrates. *Journal of Crystal Growth*, 312:2404-2410

Carter, C. and Liang, S. 2018. Comprehensive evaluation of empirical algorithms for estimating land surface evapotranspiration. *Agricultural and Forest Meteorology*, 256–257: 334–345.

Chakravarty, S., Mohanty, A., Banerjee, A., Tripathy, R., Mandal, G.K., Basariya, M.R. and Sharma, M. 2015. Composition, mineral matter characteristics and ash fusion behavior of some Indian coals. *Fuel*, 150:96-101.

Chong, J., 2014. Resource Development in Canada: a case study on the ring of fire. http://www.lop.parl.gc.ca/content/lop/ResearchPublications/2014-17-e.htm#a3. (Date of access 3 May 2018).

Ciftja, A., Engh, T.A. and Tangstad, M. 2010. Wetting properties of molten silicon with graphite materials. *Metallurgical and Materials Transactions B*, 41A:3183-3195.

Conradie, A. 2016. Mining of chrome and production of ferrochrome. Africa business Information. https://www.whoownswhom.co.za/store/info/4460?segment=Mining. Date of access: 25 May 2018.

Cramer, L.A., Basson, J. & Nelson, L.R. 2004. The impact of platinum production from UG2 ore on ferrochrome production in South Africa. *The Journal of The South African Institute of Mining and Metallurgy*, 104(9):517-527.

Creamer, M. 2017. South Africa crucial to global chrome supply, Chromium 2017 hears. Mining weekly. 10 Nov 2017. http://www.miningweekly.com/article/south-africa-crucial-to-global-chrome-supply-chromium-2017-hears-2017-11-10. Date of access: 28 May 2018.

Daavittila, J., Honkaniemi, M. & Jokinen, P. 2004. The transformation of ferrochromium smelting technologies during the last decades. *The Journal of The South African Institute of Mining and Metallurgy*, 541–549.

Dawson, N.F. & Edwards, R.I. 1986. Factors Affecting the Reduction Rate of Chromite. (*In* Proceedings of the 4th International Ferro-alloys Congress, Sao Paulo. p. 105-113).

Ding, Y.L. & Warner, N.A. 1997b. Reduction of carbon-chromite composite pellets with silica flux. *Ironmaking and Steelmaking*, 24(4):283-287.

Dennison, P.E. and Roberts, D.A. 2003 Endmember selection for multiple endmember spectral mixture analysis using endmember average RMSE. *Remote Sensing of Environment*, 87 (2003) 123 – 135.

Ding, Y.L. and Warner, N.A. 1997. Catalytic reduction of carbon-chromite composite pellets by lime. *Thermochimica Acta*, 292:85-94.

Du Preez, S.P., Beukes, J.P. and Van Zyl, P.G. 2015. Cr(VI) Generation During Flaring of CO-Rich Off-Gas from Closed Ferrochromium Submerged Arc Furnaces. *Metallurgical and Materials Transactions B*, 46:1002-1010.

Edwards, R. & Atkinson, K. 1986. Ore deposit geology. London: Chapman and Hall. 446p.

Gaal, S., Lou, D., Wasbø, S., Ravary, B. & Tangstad, M. 2007. Melting phenomena in ferromanganese production. (*In* Proceedings of the 14th International Ferro-alloys Congress, Delhi. p. 247-257).

Germeca, M. , Karhana M., Bialkab, K.L., Demircib, A. and Turhana, I. Mathematical modeling of lactic acid fermentation in bioreactor with carob extract. *Biocatalysis and Agricultural Biotechnology* 14 (2018) 254–263

Gibbs, B.M. and Thomson, D. and Argent, B.B. 2004. A thermodynamic equilibrium comparison of the mobilities of trace elements when washed and unwashed coals are burnt under pf firing conditions. *Fuel*, 83(17-18):2271-2284.

Glastonbury, R., Van der Merwe, W., Beukes, J.P., Van Zyl, P.G., Lachmann, G., Steenkamp, C.J.H., Dawson, N.F. and Stewart, H.M. 2010. Cr(VI) generation during sample preparation of solid samples – A chromite ore case study. *Water SA*, 36(1), 105-110.

Glastonbury, R.I., Beukes, J.P., Van Zyl, P.G., Sadiki, L.N., Jordaan, A., Campbell, Q.P., Stewart, H.M. and Dawson, N.F. 2015 Comparison of physical properties of oxidative sintered pellets produced with UG2 or metallurgical grade South African chromite: a case study. *The Journal of The Southern African Institute of Mining and Metallurgy*. 115:1-8.

Goel, R.P. 1997. Smelting Technologies for Ferrochromium Production-Recent Trends. *Ferro Alloy Industries in the Liberalised Economy*:37-50.

G&W Base (Pty) Ltd. http://www.gwminerals.com/ Date of access:20 May 2018.

Grim, R.E., Bradley, W.F. 1940. Investigation of the effect of heat on the clay minerals illite and montmorillonite. *The Journal of the American Ceramic Society*, 23(8):242-248.

Haggerty, S.E. 1991. Oxide mineralogy of the upper mantle. *Reviews in Mineralogy and Geochemistry*, 25 (1):355-416.

Hong, T., Kim, C., Jeong, J., Kim, J., Koo, C., Jeong, K. and Lee, M. 2016. Framework for approaching the minimum CV(RMSE) using energy simulation and optimization tool. *Energy Proccedia*, 88:265-270.

Howat, D.D. 1986. Chromium in South Africa. *Journal of the South African Institute of Mining and Metallurgy*, 86 (2):37-50.

Howat. D.D. 1994. Chromium in South Africa. *The Journal of the South African Institute of Mining and Metallurgy*, 86(2), 37-50.

ICDA. 2013. Statistical Bulletin 2013. International Chomium Development Association. Paris, France.

ICDA. 2018. Chronology of Chrome. http://www.icdacr.com/index.php?option=com_content&view=article&id=135&Itemid=340&lang=en. Date of Access: 20 May 2018.

Jacobs, J.A. & Testa, S.M. 2005. Overview of chronmium(VI) in the enviroment background and history. (*In* Guertin, J., Jacobs J.A. & Avakian C.P., eds. Chromium(VI) handbook. USA: CRC Press. p. 1-21).

James, N. 2016. South Africa's chrome industry wel placed to "grow and prosper'. Creamer media's mining weekly. 21 Oct. http://www.miningweekly.com/print-version/south-africas-chrome-industry-well-placed-to-grow-and-prosper-2016-10-21. Date of access: 28 May 2018.

Jones, R.T. 2018. Pyrometallurgy in Southern Africa - List of Southern African Smelters. http://www.pyrometallurgy.co.za/PyroSA/. Date of access: 25 May 2018.

Katayama, H.G., Tokuda, M. and Ohrani, M. 1986. Promotion of the Carbothermic Reduction of Chromium Ore by the Addition of Borates. *The Iron and Steel Institute of Japan*, 72(10):1513-1520.

Kekkonen, M., Xiao, Y. and Holappa, L. 1995. Kinetic study on solid state reduction of chromite pellets. (*In* Porceedings of The 7th International Ferroalloys Congress, Trondheim. p.351-360.)

Khan, D.M.A. 2013. Pre-reduction of chromite by thermogravimetric (TG) analysis. *Materials Science Forum*, 760:23-32.

Khosravi, A., Machado, L and Nunes, R.O. 2018. Estimation of density and compressibility factor of natural gas using artificial intelligence approach. *Journal of Petroleum Science and Engineering*, 168. DOI:10.1016/j.petrol.2018.05.023

Kleynhans, E.L.J.., Beukes, J.P, Van Zyl, P.G, Kestens, P.H.I. & Langa, J.M. 2012. Unique challenges of clay binders in a pelletised chromite pre-reduction process. *Minerals Engineering*, 34:55-62.

Kleynhans, E.L.J., Neizel, B.W., Beukes, J.P. and Van Zyl, P.G. 2016a. Utilisation of pre-oxidised ore in the pelletised chromite pre-reduction process. *Minerals Engineering*, 92:114-124.

Kleynhans, E. 2016b. Development and improvement of pretreatment technologies to enhance ferrochrome production. Potchefstroom: NWU. (Thesis-PhD).

Kleynhans, E.L.J., Beukes, J.P., Van Zyl, P.G. and Fick, J.I.L. 2017a. Techno-economic feasibility of pre-oxidation process to enhance pre-reduction of chromite. *Journal of the Southern African Institute of Mining and Metallurgy*, 117(5):457-468.

Kleynhans, E.L.J., Beukes, J.P, Van Zyl, P.G, Bunt, J.R., Nkosi, N.S.B., and Venter, M. 2017b. The Effect of Carbonaceous Reductant Selection on Chromite Pre-redcution. *Metallurgical and Materials Transactions B*, 48B:827-840.

Kotz, J.C., Treichel, P.M. and Weaver, G.C. 2006. Chemistry and chemical reactivity. 6th ed. Canada: Thomson Brooks/Cole. 1145 p.

Kraha, A., Turner, H., Nimon, K., Zientek L.R., and Henson R.K. 2012. Tools to Support to support interpreting multiple regression in the face of multicollinearity. *Frontiers in Psychology*, 3(44), pp.1-16.

Latypov, R., Chistyakova, S., Page, A. and Hornsey, R. 2015. Field Evidence for the In Situ Crystallization of the Merensky Reef. *Journal of Petrology*, 56(12):(2341-2372).

Lorenzo-Seva, U., Ferrando, P.J. and Chico E. 2010. Two SPSS programs for interpreting multiple regression results. *Behavior Research Methods*, 42(1), pp.29-35.

Lui, Y.P., Wu, M.G. and Qian, J.X. 2007. Predicting coal ash fusion temperature based on its chemical composition using ACO-BP neural network. *Thermochimica Acta*, 454:64–68.

McCullough, S., Hockaday, S., Johnson, C. & Barcza, N.A. 2010. Pre-reduction and smelting characteristics of Kazakhstan ore samples. (*In* Proceedings of The 12th International Ferroalloys Congress. Helsinki. p. 249-262).

Mohale, G.T.M., Beukes, J.P., Kleynhans, E.L.J., Van Zyl, P.G., Bunt, J.R., Tiedt, L.R, Venter, A.D. and Jordaan, A. 2017. SEM image processing as an alternative method to determine chromite pre-reduction. *Journal of Southern African Institute of Mining and Metallurgy*, 117(11).

Mondal, S.K. and Mathez, E.A. 2006. Origin of the UG2 chromite layer, Bushveld Complex. Journal of petrology 48(3), 495-510. http://petrology.oxfordjournals.org/content/48/3/495.full.pdf+html. Date of access; 27 Mei 2018.

Motzer, W.E. 2005. Chemistry, Geochemistry, and Geology of Chromium and Chromium Compunds. (*In* Guertin, J., Jacobs J.A. & Avakian C.P., eds. Chromium(VI) handbook. USA: CRC Press. p. 23-75).

Murthy, Y.R., Tripathy, S.K. & Kumar, C.R. 2011. Chrome ore beneficiation challenges & opportunities–A review. *Minerals Engineering*, 24 (5):375-380.

Naiker, O. & Riley, T. 2006. Xstrata Alloys in Profile. (*In* Jones, R.T., ed. Southern African Pyrometallurgy organised by Johannesburg, South Africa: South African Institute of Mining and Metallurgy. p. 297-306).

Naiker, O. 2007. The development and advantages of Xstrata's Premus Process. (*In* Roy, T.K., ed. Proceedings of The Eleventh International Ferroalloys Congress, New Delhi. p. 112-118).

Nathans, L.L., Oswald F.L and Nimon K. 2012. Interpreting multiple linear regression: A guidebook of variable importance. *Practical Assesment, Research & Evaluation*, 17(9), pp.1-19.

Nel, M. V., Strydom, C.A., Schobert, H.H., Beukes, J.P. and Bunt, J.R. 2014. Reducing atmosphere ash fusion temperatures of a mixture of coal-associated minerals-The effect of inorganic additives and ashing temperature. *Fuel Processing Technology*, 124:78-86.

Neizel, B.W., Beukes, J.P., van Zyl, P.G. & Dawson, N.F. 2013. Why is $CaCO_3$ not used as an additive in the pelletised chromite pre-reduction process? Minerals Engineering, 45:115–120.

Neuschütz, D., JanBen, P., Friedrich, G. & Wiechowski, A. 1995. Effect of Flux Additions on the Kinetics of Chromite Ore Reduction with Carbon. (*In* Proceedings of the 7th International Ferroalloys Congress, Trondheim. p. 371-381)

Niayesh, M.J. and Dippenaar, R.J. 1992. The solid-state reduction of chromite. (*In* Proceedings of The 6th International Ferroalloys Congress, Cape Town. p. 57-63)

Niemelä, P., Krogerus, H., Oikarinen, P., 2004. Formation, characterisation and utilisation of CO-gas formed in ferrochrome smelting. (*In* Proceedings of the The Tenth International Ferroalloys Congress, Cape Town. p. 68-77.)

Nriagu, J.O., 1988. Historical perspectives. (*In* Nriagu, J. O. and Nieboer, E., eds. Chromium in the natural human environment. New York: Wiley. pp 1-12.).

Nunnington, R.C. & Barcza, N.A. 1989. Pre-reduction of fluxed chromite-ore pellets under oxidizing conditions. (*In*. Proceedings of the 5th International Ferroalloys Congress New Orleans.. p. 55-68)

Onal, M. and Sarikay, Y. 2007. Thermal behavior of a bentonite. *Journal of Thermal Analysis and Calorimetry*, 90 (1):167–172.

Outotec. 2018. https://www.outotec.com/globalassets/company/investors/2008/q3_2008_en_final-version.pdf. Date of access : 20 Apr. 2018.

Özbayoğlu, G. and Özbayoğlu, M.E. 2006 A new approach for the prediction of ash fusion temperatures: A case study using Turkish lignites. *Fuel*, 85(4):545-552.

Papp, J.F. 2004. Chromium use market in the United States. (*In* Proceedings of the 10th International Ferroalloys Congress, Cape Town. p. 770-778.)

Papp, J.F. and Lipin, B.R. 2006. Chromite (*In* Kogel, J.E., Trivedi, N.C., Barker, J.M. and Krukowski, S.T. eds. Industrial Mineral & Rocks: Commodities, Markets and Uses. Colorado: Society for Mining, Metallurgy and Exploration, Inc. p. 309-334).

Pham, B.T., Son, L.H., Hoang, T., Nguyen, D. and Bui, D.T. 2018. Prediction of shear strength of soft soil using machine learning methods. *Catena*, 166:181-191.

Perrit, S. and Roberts, M. 2007 Flexural-slip structures in the Bushveld Complex, South Africa? *Journal of Structural Geology*, 29(9):1422-1429.

Pohl, W.L., 2011. Economic Geology: Principles and Practices. UK: Wliey-Blackwell. 680p.

Rao, D.S. 2010. Valuble waste. Recovery of chromite values from ferrochrome industry flue dust. *AT Mineral Processing English edition*, 55:2-6. http://www.at-online.info/download/215793/12_Research_Development.pdf. Date of access: 15 Jul. 2017.

Reifenstein, A.P., Kahraman, H., Coin, C.D.A, Calos, N.J and Uwins, M.P. 1999. Behaviour of selected minerals in an improved ash fusion test: quartz, potassium feldspar, sodium feldspar, kaolonite, illite, calcite, dolomite, siderite, pyrite and apatite. *Fuel*, 78:1449-1461.

Riekkola-Vanhanen, M. 1999. Finnish expert report on best available techniques in ferrochromium production. Helsinki.

Ringdalen, E., Gaal, S., Tangstad, M. & Ostrovski, O. 2010. Ore melting and reduction in silicomanganese production. *Metallurgical and MaterialsTtransactions B,* 41 (6):1220-1229.

Roza, G., 2008. Understanding the elements of the periodic table-Chromium. New York: The Rosen publishing group, Inc. 49 p.

Safarian, J., Kolbeinsen, L., Tangstad, M. & Tranell, G. 2009. Kinetics and mechanism of the simultaneous carbothermic reduction of FeO and MnO from high-carbon ferromanganese slag. *Metallurgical and Materials Transactions B,* 40 (6):929-939.

Salkind, N. J. 2010. Root Mean Square Error. (*In* Encyclopedia of research design Thousand Oaks, CA: SAGE Publications Ltd. http://dx.doi.org/10.4135/9781412961288.n392. Date of access 22 May 2018.)

Schouwstra, R.P. and Kinloch, E.D. 2000. A Short Geological Review of the Bushveld Complex. *Platinum Metals Review*, 44(1):33-39.

SEAISI. 2017. Record high for global stainless steel production in 2017. South East Asia Iron and Steel Institute. http://www.seaisi.org/News/6952/Record+high+for+global+stainless+steel+production+in+2017. Date of access: 28 May 2018.

Seggiani, M. Empirical correlations of the ash fusion temperatures and temperature of critical viscosity for coal and biomass ashes. *Fuel*, 78:1121-1125.

Sentula mining: Nkomati Anthracite (Pty) Ltd, http://www.sentula.co.za/?page_id=28, Date of access: 15 Aug 2017.

Song, W.J., Tang, L.H., Zhu, X.D., Wu, Y.Q., Zhu, Z.B. and Koyama, S. 2009. Effect of coal ash composition on ash fusion temperatures. *Energy Fuels*, .24, pp.182-189.

South African National Standard. SABS ISO 11722:1999 (SANS 11722:2005). Solid mineral fuels - Hard coal - Determination of moisture in the general analysis test sample by drying in nitrogen. South African Bureau of Standards.

South African National Standard. SABS ISO 1171:2010 (SANS 131:2011). Solid mineral fuels - Determination of ash. South African Bureau of Standards.

South African National Standard. SABS ISO 562:2010 (SANS 50:2011). Hard coal and coke - Determination of volatile matter. South African Bureau of Standards

South African National Standard. SABS ISO 29541:2010 (SANS 29541:2014). Solid mineral fuels - Determination of total carbon hydrogen and nitrogen content – Instrumental method. South African Bureau of Standards.

South African National Standard. SABS ISO 19579:2006 (SANS 19579:2007). Solid mineral fuels - Determination of sulfur by IR spectrometry. South African Bureau of Standards.

South African National Standard. SABS ISO 1928:2009 (SANS 1928:2009). Solid mineral fuels - Determination of gross calorific value by the bomb calorific method, and calculation of net calorific value. South African Bureau of Standards.

South African National Standard. SABS ISO 540:2008 (SANS 43:2008). Hard coal and coke - Determination of ash fusibility. South African Bureau of Standards.

Soykan, O., Eric, R.H. and King, R.P. 1991a. The Reduction Mechanism of a Natural Chromite at 1416 °C. *Metallurgical and Materials Tansactions B*, 22(1):53-63.

Soykan, O., Eric, R.H. and King, R.P. 1991a. Kinetics of the reduction of bushveld complex chromite ore at 1416 °C. *Metallurgical and Materials Tansactions B*, 22(6):801-810.

Sundar Murti, N.S., Shah, K., Gadgeel, V.L. & Seshadri, V. 1983. Effect of lime addition on rate of reduction of chromite by graphite. *Transactions of the Institution of Mining and Metallurgy: Section C: Mineral Processing and Extractive Metallurgy*, 92:172-174.

Takano, C., Zambrano, A.P., Nogueira, A.E.A., Mourao, M.B. and Iguchi, Y. 2007. Chromites reduction reaction mechanisms in carbon-chromites composite agglomerates at 1773 K. *ISIJ international*, 47 (11):1585-1589.

Tangstad, M., Beukes, J.P., Steenkamp, J., Ringdalen, E., Chapter 13. Coal-based reducing agents in ferroalloys and silicon production. (*In* New Trends in Coal Conversion (Elsevier), eds. Suárez-Ruiz,I., Rubiera, F and Diez, M.) (in press).

Thirumalai, K., Singh, A. and Remash, R. A MATLAB™ code to perform weighted linear regression with (correlated or uncorrelated) errors in bivariate data. *Journal of Geological Society of India*, 77(4):377-380.

USGS. 2018. U.S Geology Survey. Mineral commodity summeries 2018 edition. https://minerals.usgs.gov/minerals/pubs/mcs/. Date of access: 27/05/2018.

Van Deventer, J.S.J. 1988. The effect of additives on the reduction of chromite by graphite. *Thermochimica Acta*, 127:25-35.

Van Dyk, J.C., Baxter, L.L., Van Heerden, J.H.P. and Coetzer, R.L.J. 2005. Chemical fractionation tests on South African coal sources to obtain species-specific information on ash fusion temperatures (AFT). *Fuel*, 84 (14-15):1768-1777.

Van Dyk, J.C., Keyser, M.J. 2005. Characterization of inorganic material in Secunda coal and the effect of washin on coal properties. T*he Journal of The South African Institute of Mining and Metallurgy*, 105 (1):1-6.

Van Dyk, J.C. 2006. Understanding the influence of acidic component (Si, Al, and Ti) on ash flow temperature of South African coal sources. *Minerals Engineering*, 19(3):280-286. https://doi.org/10.1016/j.mineng.2005.06.018.

Van Dyk, J.C. and Waanders, F.B. 2007. Manipulation of gasification coal feed in order to increase the ash fusion temperature of the coal enabling the gasifiers to operate at higher temperatures. *Fuel*, 86(17-18):2728-2735.

Van Dyk, J.C., Waanders, F.B., Benson, S.A., Laumb, M.L. and Hack, K. 2009. Viscosity predictions of the slag composition of gasified coal, utilizing FactSage equilibrium modelling. *Fuel*, 88(1):67-74.

Venter, A.D., Beukes, J.P., Van Zyl, P.G., Brunke, E.G., Labuschagne, C., Ebinghaus, R. and Kock, H. 2015. Statistical exploration of gaseous elemental mercury (GEM) measured at Cape Point from 2007 to 2011. *Atmospheric Chemistry and Physics*, 15:10271-10280.

Wang, Z., Bai, J. Kong, L., Bai, Z. and Li, W. 2013. Effect of V and Ni on Ash Fusion Temperatures. *Energy & Fuels*, 287:7308-7313.

Wang, Y., Wang, L. & Chou, K.C. 2015. Effects of CaO, MgO, Al_2O_3 and SiO_2 on the carbothermic reduction of synthetic $FeCr_2O_4$. *Journal of Mining and Metallurgy, Section B: Metallurgy*, 51(1):17-24.

Weber, P. & Eric, R.H. 1992. Solid state fluxed reduction of LG-6 chromite from the bushveld complex. (*In* Proceedings of the 6th International Ferroalloys Congress, Cape Town. p. 71-77).

Weber, P. & Eric, R.H. 1993. The Reduction Mechanism of Chromite in the Presence of a Silica Flux. *Metallurgical Transactions B*, 24B(December):987-995.

Weber, P. & Eric, R.H. 2006. The reduction of chromite in the presence of silica flux. *Minerals Engineering*, 19 (3):318-324.

Williams, K. 2014. Why is Ontario's ring of fire on the back burner? Geology for Investors. https://www.geologyforinvestors.com/ontarios-ring-fire-burner/. Date of access: 20 May 2018.

Winegartner, E.C. and Rhodes, B. T. 1975. An Empirical study of the relation of chemical properties to ash fusion temperatures. *Journal of Engineering for Power*:395-403.

Xiao, Y. Yang, Y., Holappa, L. and Boom, R. 2007. Microstructure changes of chromite reduced with CO Gas. (*In* Proceedings of the 14th International Ferro-alloys Congress, Delhi. p.133-144).

Xu, S. and Dai, W. 1992. The melting behaviour of chromite ores and the formation of slag in the production of high-carbon ferrochromium. (*In* Proceedings of the 6th International Ferro-alloys Congress, Cape Town. p.87-92).

Zaouche, M., Bel, L. and Vaudour, E. 2017. Geostatistical mapping of topsoil organic carbon and uncertainty assessment in Western Paris croplands (France). *Geoderma Regional*, 10 (2017) 126–137

Zhang, B., Shi, P. and Jiang, M. 2016. Advances towards a clean hydrometallurgical process for chromite. *Minerals*, 6(1):1-12.

Damring Formation During Rotary Kiln Chromite Pre-reduction: Effects of Pulverized Carbonaceous Fuel Selection and Partial Pellet Melting

Y. VAN STADEN, J.P. BEUKES, P.G. VAN ZYL, E. RINGDALEN, M. TANGSTAD, E.L.J. KLEYNHANS, and J.R. BUNT

Electricity consumption is the largest cost contributing factor in the production of ferrochrome. Currently the pelletized chromite pre-reduction process (solid-state reduction of chromite) is the process option with the lowest specific electricity consumption (MWh/ton). In this process, pelletized chromite is fed into a rotary kiln at 1573 K (1300 °C), where partial pre-reduction takes place. Damring formation (material build-up) in the rotary kiln causes routine shutdowns, resulting in loss of revenue. The damring formation is possibly caused by melting of the ash of the pulverized coal used to fire the kiln and/or the partial melting of the chromite pellets. Ash fusion temperatures of twenty different samples were evaluated to assess the temperature at which the pulverized coal ash will start to contribute to damring formation. Sessile drop tests were used to assess the softening behavior of different ore types (*e.g.*, UG2, MG, and LG metgrade), as well as softening of composite chromite pellets made from these ores. Actual damrings were also analyzed using scanning electron microscopy with energy dispersive X-ray spectroscopy. Results indicate that it is mainly the pulverized coal ash that will contribute to damring formation, and not ore or pellet softening. Multiple-linear regression was used to derive equations to predict the ash fusion temperatures of the pulverized coal ash, which can be used by ferrochrome producers to optimize pulverized coal selection.

https://doi.org/10.1007/s11663-018-1376-7

I. INTRODUCTION

CHROMITE is a mineral with a spinel crystalline structure with the formula $[(Mg,Fe^{2+})(Al,Cr,Fe^{3+})_2O_4]$.[1] Chromite is of great importance since it is the only commercially viable source of new chromium (Cr) units.[2,3] Cr has many applications in the metallurgical, chemical, and refractory fields. The application of importance in this study is the production of ferrochrome (FeCr). FeCr is an alloy used mainly in the production of stainless steel, which is a vital alloy in modern society. According to Rao,[4] approximately 90 pct of all mined chromite is utilized in the production of FeCr.

The single largest cost component in FeCr production is electricity consumption.[5,6] It is therefore important for FeCr producers to apply processes to minimize energy use. Several of these processes have been developed.[7–9] One of these processes, known as Chrome Direct Reduction (CDR), was commercialized in South Africa in the late 1980s and entailed the direct reduction (which is complete or almost complete pre-reduction) of fine chromite ores.[9] However, due to operational difficulties, the process was abandoned fairly quickly. Another process implemented commercially was developed by Showa Denko in the 1970s, *i.e.*, solid-state reduction of chromite (SRC) or otherwise known as pelletized chromite pre-reduction. This process was modified and is being applied by Glencore Alloys at two very large smelters in South Africa (Lydenburg operations and the Lion Ferrochrome smelter).[10] FeCr smelters applying this process have also relatively recently been developed in China, but information regarding these smelters is not yet available in the public peer-reviewed domain. Glencore Alloys refer to their application of pelletized chromite pre-reduction as the Premus process.[10] This process has the lowest energy consumption (specific electricity

Y. VAN STADEN, J.P. BEUKES, P.G. VAN ZYL, E.L.J. KLEYNHANS, and J.R. BUNT are with the Chemical Resource Beneficiation, North-West University, Potchefstroom, Private Bag X6001, Potchefstroom, 2520, South Africa. Contact e-mail: paul.beukes@nwu.ac.za E. RINGDALEN is with the Sintef, Materials and Chemistry, 7465 Trondheim, Norway. M. TANGSTAD is with the Norweigian University of Science and Technology (NTNU), 7465 Trondheim, Norway.

Manuscript submitted November 23, 2017.

Published online: 07 August 2018

consumption (SEC), *i.e.*, MWh/ton FeCr), high Cr recovery, as well as being more environmentally friendly than the conventional process in some respects.[10]

In the pelletized chromite pre-reduction process, raw materials (chromite ore, reductants, and clay binder) are dry milled, pelletized, and pre-heated, after which the pellets are fed into a counter current rotary kiln where chromite pre-reduction takes place. These hot, pre-reduced pellets are then fed directly into a closed submerged arc furnace (SAF), with the required fluxes and reductants. Feeding the hot, pre-reduced pellets into the SAF reduces the amount of energy required for smelting.[10,11] The pre-reduction achieved relates to metallization of up to 90 pct for iron (Fe) and 50 pct for Cr, and results in reduced SEC during the smelting process by up to 40 pct.[9] Other advantages associated with the pelletized chromite pre-reduction process include the consumption of fine chromite ores and reductants, significant replacement of coke with less expensive reductants such as anthracite, as well as the production of a low silicon (Si)- and sulfur (S)-containing FeCr product.[8,10] Disadvantages associated with this process are the higher capital cost[10] and the extensive operational control that is required due to the variation in pre-reduction levels and carbon (C) contents of the pre-reduced pelletized furnace feed material.[12]

Previous studies related to chromite pre-reduction focused on aspects such as the fundamental reaction mechanisms[8] and enhancing pre-reduction by the use of different conditions and/or additives.[13–16] Kleynhans *et al.*[17,18] also investigated the effect of different clay binders and carbonaceous reductants.

Chromite pre-reduction applied on an industrial scale takes place in a counter current rotary kiln. Pellets are fed into the kiln and heated to approximately 1573 K (1300 °C). Cross- and longitudinal sectional cut illustrations of a typical rotary kiln with pelletized feed that is used in the chromite pre-reduction process are presented in Figure 1.

During chromite pre-reduction, damrings (material build-up) are formed in the kiln (Figure 1). These damrings can have positive and/or negative impacts on the process. Limited damring formation can protect the refractory lining of the kiln. It is also known that limited damring formation in strategic areas (*e.g.*, marked with "a" in Figure 1) can increase the retention time of the pellets in the kiln hot zone, therefore enhancing pre-reduction levels. However, if damring formation is too extensive, it compromises material throughput. Also, excessive damring formation in certain areas (*e.g.*, marked with "b" in Figure 1) can actually increase the effective slope that the pelletized chromite pellets experience in the kiln, which will lead to shorter retention time and lower pre-reduction levels. Currently, routine shutdowns have to be performed on chromite pre-reduction kilns to break out the damrings in order to maintain the desired throughput. Figure 2 presents a photo taken during a recent shutdown of a chromite pre-reduction kiln, which clearly illustrates the extent of the problem.

One of the possible reasons for damring formation is melting of pulverized fuel (PF) coal ash that originates from the coal used to fire the kiln. Therefore, the ash fusion temperatures (AFTs) of the PF coal ash can be used as an indication of the temperature at which the ash will start to contribute to damring formation. AFTs, *i.e.*, initial deformation (T_{indef}), softening (T_{soft}), hemispherical (T_{hem}), and fluid temperature (T_{fluid}), can be determined experimentally.[19] However, AFTs are not always readily available, since AFT analyses are time-consuming and special instrumentation is needed. In contrast, proximate, ultimate, total S, calorific value (CV), and ash composition analyses are routinely conducted in industry. Therefore, there have been a number of studies done on the prediction of AFT based on chemical composition. Previously Liu *et al.*[20] predicted AFT for steam boiler operations of power plants based on chemical composition. These authors used a neural network method, *i.e.*, ACO-BP neural network based on ant colony optimization, to predict the AFT. Chakravarty *et al.*[21] used thermodynamic modeling to predict and understand ash fusion behavior and Winegartner and Rhodes[22] used regression analysis to calculate AFT of coal ash from chemical composition.

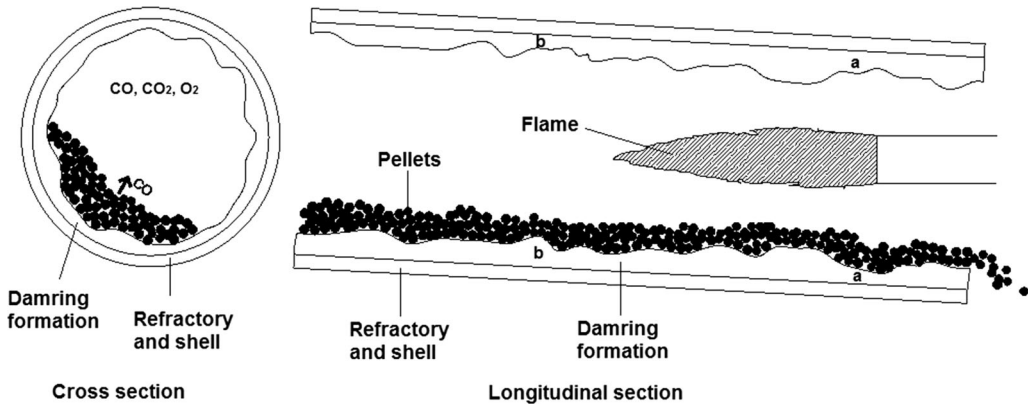

Fig. 1—Illustration of the cross and longitudinal sections of a rotary kiln used in pelletized chromite pre-reduction.

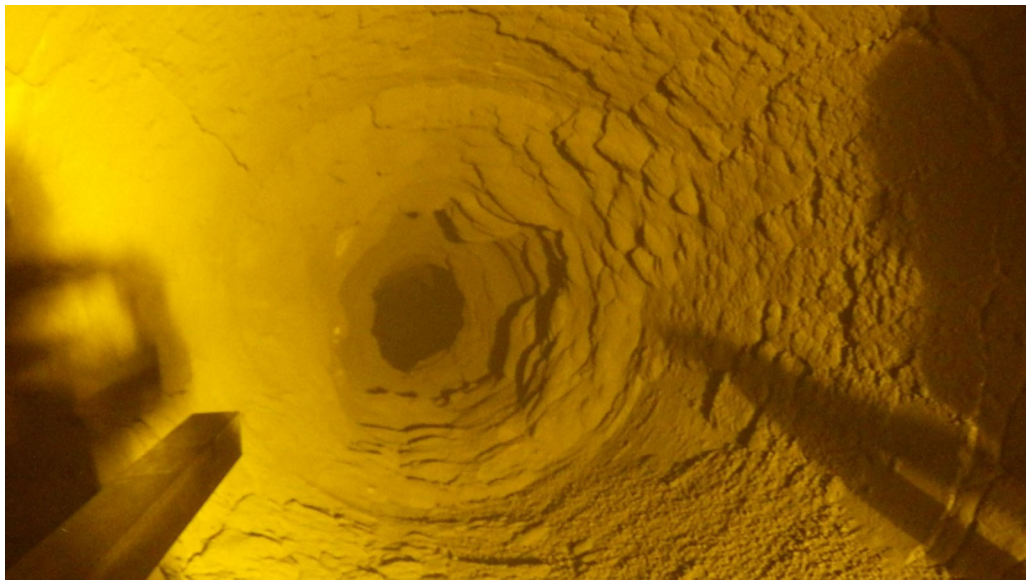

Fig. 2—A picture of damrings inside a pelletized chromite pre-reduction kiln.

The possibility exists that damring formation can also be caused by partial melting of pellets being fed into the kiln and/or pellet fragments formed in the kiln. Extensive sessile drop test work has been conducted for manganese ores,[23–25] in order to observe their behavior during heating. The sessile drop test is used to measure the melting and reduction temperatures of materials.[24] As far as the authors could assess, no such work has been published for chromite ores.

In this paper, it is indicated how multiple-linear regression (MLR) analysis, using proximate, ultimate, total S, CV, and ash composition analyses as independent parameters, can be used to calculate the AFT of carbonaceous materials. The calculated AFT can be used by FeCr producers to select PF coals that will contribute less to damring formation, which will increase the kiln operational time between damring break-out shutdowns. This will enhance production output and improve profitability. The possible contribution of pellet softening to damring formation was also investigated, by using sessile drop tests to observe the melting behavior of the composite pellets and the individual pellet components.

II. EXPERIMENTAL METHODS

A. *Carbonaceous Materials and Characterization Thereof*

Although only coal (which is less expensive than, *e.g.*, coke and anthracite) is currently used as PF to fire pre-reduction rotary kilns, a wider selection of materials was included in this study to assess if the developed method would be applicable for a wider selection of carbonaceous materials. These materials consisted out of twenty coals, anthracites, chars, and cokes. At the time when this research was initiated the afore-mentioned carbonaceous materials were either used as PF to fire the rotary kilns or as reductants in the composite pre-reduced pellets at FeCr producers applying the pelletized chromite pre-reduction process.

During the proximate analysis (air-dried basis), the inherent moisture content (MC) was determined according to SABS ISO 11722:1999 and was done by placing a 1 g sample in an air-oven at 378 K (105 °C) for 1 hour until the mass remained constant. The ash content was determined according to SABS ISO 1171:2010 and it entailed heating 1 g of sample to 1088 K ± 10 K (815 °C ± 10 °C) for at least 1.5 hours. The volatile matter (VM) content was determined according to SABS ISO 562:2010. In this method, the sample is heated in inert atmosphere at 1173 K ± 10 K (900 °C ± 10 °C) for 7 min. The pct mass fraction of VM is calculated from the loss in mass after deducting the loss of mass due to moisture. The fixed carbon (FC) was calculated by deducting the MC, ash content, and VM from the total weight.

The ultimate analysis was undertaken according to SABS ISO 29541:2010 in which the C, hydrogen (H), nitrogen (N), and oxygen (O) contents were determined. The C and H contents were determined by heating the sample in a stream of O_2 at 1623 K (1350 °C) and converting C and H into their corresponding gases, *i.e.*, carbon dioxide and water. Magnesium perchlorate was used to absorb the water and sodium hydroxide to absorb the carbon dioxide, which was then determined gravimetrically. For the determination of N, the sample was heated with concentrated sulfuric acid in the presence of a mixed catalyst to convert N into ammonium sulfate. The ammonia in the solution is then released using steam distillation after which it was absorbed in boric acid and the N was then determined by titration with sulfuric acid. The sum of these elements, *i.e.*, C, H, and N, together with the ash, and MC, expressed as mass percentage, was used to calculate the O content (adding up to a total of 100).

The determination of the total S content was done according to SABS ISO 197579:2006 using a LECO Sulfur analyzer. The sample was combusted at 1623 K (1350 °C) in a stream of oxygen. Thereafter, particulates and water vapor are removed from the gas stream. The gas stream then passes through a cell in which sulfur dioxide is measured by an infrared absorption detector. The S in the sample is then calculated from the results.

The gross CV was determined (according to SABS ISO 1928:2009) by burning a sample of solid fuel in high-pressure oxygen in a bomb calorimeter. The gross CV is calculated from the corrected temperature rise and the effective heat capacity of the calorimeter. The ash composition was determined using X-ray fluorescence (XRF) as specified in ASTM D4326. For the afore-mentioned analysis, only contents above the detection limit of the various ash components were retained.

The samples used in the AFT determination were sized and ashed in the same method as described earlier, using SABS ISO 1171:2010, prior to the analysis. AFT tests were performed according to the SABS ISO 540:2008, which involves heating of a cone of the ash sample. Four different temperatures are then recorded according to the specific shape of the ash cone, *i.e.*, the T_{indef} when the corners of the cone first become rounded; T_{soft} when the top of the cone first become rounded; T_{hem} when the entire cone took on a hemispherical shape; and the T_{fluid} when the cone collapsed to a flattened button on the furnace floor.[19] According to SABS ISO 540:2008, the standard deviation of AFTs measured in this manner is typically ± 30 K.

AFT tests were conducted in both oxidizing (normal air) and reducing atmospheres (CO/CO_2), since both atmospheres are relevant to chromite pre-reduction kilns.[17] The atmosphere inside the kiln is partially oxidizing to allow PF combustion, while the high carbon content inside the pellets causes a partial positive CO pressure inside the pellets themselves, preventing oxygen from entering the pellets (therefore a reducing environment inside the pellets).[17]

B. *Computational Methods*

A simple linear regression model includes a constant (c), an independent variable (x), and a dependent variable (y). The objective is then to establish the relationship between the independent (x) and the dependent (y) variables by fitting a linear equation to the data. In MLR, there is more than one independent variable (x) and the relationship between the dependent variable (y) and the independent variables (x) is given by the following equation.[26]

$$y = c_0 + c_1x_1 + c_2x_2 + \cdots\cdots c_px_p. \quad [1]$$

In this paper, the individual AFTs were considered as the dependent variable, while the proximate, ultimate, total S, CV, and the ash composition data as independent variables. The root mean squared error (RMSE) between the calculated independent variable and the experimental value was calculated to quantify the difference.[26–28] Sixteen of the twenty samples were used in the MLR calculation, while the remaining four samples were used to assess how well the method performed.

SPSS programming software was used to calculate parameters that could be used to interpret the MLR results and to determine the contributions of the different independent variables to the calculated AFTs.

C. *Sessile Drop Analysis of Chromite, Composite Pellet Mixtures, and Pellet Components*

The maximum temperature of the AFT test instrument was 1823 K (1550 °C). Due to the spinel crystalline structure of chromite, the melting temperature thereof is higher than the afore-mentioned temperature. Therefore in order to determine the temperatures at which softening of the ores, or ore mixtures took place, an alternative method, *i.e.*, sessile drop, was used. The sessile drop furnace has a maximum operating temperature of 2673 K (2400 °C).[23–25]

For the sessile drop study, seven typical metallurgical grade ores were obtained from FeCr producers across South Africa. Since more than a quarter of chromite consumed by the FeCr industry outside South Africa originate from South Africa,[29] results obtained from these ores will also be of international relevance. The afore-mentioned ores were individually mixed with a carbonaceous reductant and a clay binder to form pellet mixtures, as industrially applied.[17] Anthracite breeze from Nkomati Anthracite (Pty) Ltd[30] was used as the reductant in the mixtures and bentonite clay as the binder. Both these materials were previously characterized[17] and such details are therefore not repeated here. The softening temperatures of the anthracite breeze and the bentonite clay were also investigated individually, using the sessile drop test method.

The chromite ore samples were dry milled to the particle size applied in the pre-reduction process, *i.e.*, 90 pct smaller than 75 μm (d_{90} = 75 μm). A Siebtechnik laboratory disc mill with a tungsten carbide grinding chamber was used, to avoid possible iron contamination. The particle size distribution was determined using a Malvern Mastersizer 2000. Each pellet mixture consisted of 3 wt pct clay, ~ 20 wt pct anthracite (to ensure 15 wt pct FC content), and the remainder was made up with chromite ore. These pellet mixtures were also dry milled to the same particle size as previously indicated for the ores (d_{90} = 75 μm).

The above-mentioned milled samples were pressed into small pellets of approximately 3 mm in diameter and height. An investigated pellet was placed on a graphite substrate disk (diameter of 10 mm and height of 3 mm), which was then placed in the sample holder in the sessile drop furnace. The furnace was heated at 300 K/min (300 °C/min) up to 1173 K (900 °C) and then at 10 K/min (10 °C/min) up to 2223 K (1950 °C). The furnace was continuously purged with 0.5 Nl/min of carbon monoxide for the entire duration of the experiment. A firewire digital video camera with a telocentric zoom lens was used to record images at a resolution of

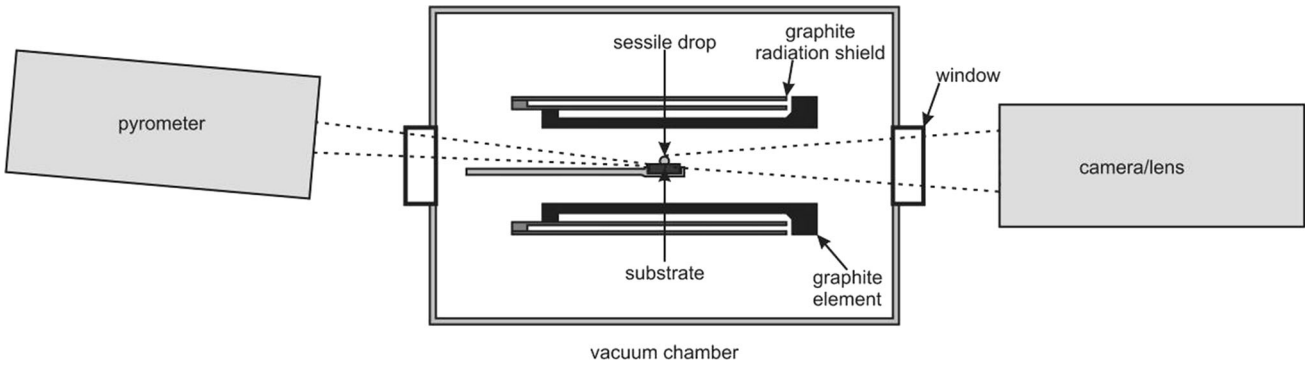

Fig. 3—A schematic of the sessile drop furnace Reprinted from Refs. [24] and [25]

1280 × 960 pixels, to determine the different stages of melting. Figure 3 presents an illustration of the sessile drop furnace.

D. *Surface Analysis of Actual Damrings*

Actual damrings broken out during a kiln shutdown were obtained from a South African ferrochrome smelter applying the pelletized chromite pre-reduction process. Several pieces of the damrings were polished and analyzed with a FEI Quanta 200 scanning electron microscope (SEM) with an integrated Oxford Instruments INCA 200 energy dispersive X-ray spectroscopy (EDS) microanalysis system.

III. RESULTS AND DISCUSSION

A. *Carbonaceous Material Characterizations*

Table I presents the proximate- and ultimate analyses, total S contents, CVs, ash compositions, as well as the reducing and oxidizing AFTs of all the carbonaceous materials considered. Obviously, elements occurring in the ash could occur in a different phase than what is presented; however, the reported species are standard for this type of analysis.

As expected, the coal samples had the lowest FC and highest VM content, while the char samples had the highest ash contents. There are many factors influencing the melting point of carbonaceous materials; hence, it is difficult to relate the measured parameters directly to AFTs. However, some authors have made general observations. Van Dyk and Keyser,[31] found that low ash melting temperatures were generally accompanied by high CaO and high Fe_2O_3. Song *et al.*[32] investigated the effect of coal ash composition on AFTs. According to these authors, AFTs decrease with increasing CaO, Fe_2O_3, and MgO contents, and then increases again after reaching a minimum value. In our own results (Table I), An-4, An-8, Ch-2, Coal-1, and Coal-2 generally had the highest AFTs and these samples also had very low Fe_2O_3 contents in comparison to the other samples. Also, Co-5 had the lowest T_{indef} and T_{soft} and contained 14.87 pct Fe_2O_3, which is fairly high in comparison to the other samples. Additionally, SiO_2 seemed higher in the samples with higher AFTs. However, the afore-mentioned observations from our results are somewhat crude and can certainly not be used as the basis for selecting carbonaceous PF to reduce damring formation during chromite pre-reduction. A more systematic approach is required, as there are too many variables and interactions between the variables that need to be taken into consideration. Therefore, MLR was used to establish mathematical relationships between the different factors.

B. *Multiple-Linear Regression Analysis to Predict AFTs of Carbonaceous Materials*

In this study, T_{soft} was considered as the temperature at which PF ash will start contributing to damring formation in the kiln. Therefore, oxidizing T_{soft} and reducing T_{soft} were considered as the dependent variables, while the other parameters presented in Table I (excluding the AFTs) were considered as independent parameters in MLR calculations. The relationship between the number of independent variables included in the optimum MLR solutions and the RMSE between the calculated T_{soft} values and the experimental values (Table I) are presented in Figures 4(a) and (b), for the reducing T_{soft} and the oxidizing T_{soft}, respectively. As is evident from the results for the reducing T_{soft} (Figure 4(a)), the RMSE for the optimum MLR equation containing one independent variable was approximately 75 K. This could be reduced to approximately 55 K, if an optimum MLR equation containing two independent variables was calculated. The inclusion of more independent variables in the optimum MLR solution further reduced the RMSE. Additional independent variables were included until the relative improvement {(RMSE for equation with x−1 independent variable − RMSE for equation with x independent variable)/(RMSE for equation with 1 independent variable − RMSE for equation with all possible independent variables)} in RMSE was less than 1 pct. For the reducing T_{soft} (Figure 4(a)), this was found to be a MLR equation containing 10 independent variables for which the RMSE was approximately 1.7 K. In a similar manner, the optimum MLR solution for oxidizing T_{soft} (Figure 4(b)), which had a relative improvement in RMSE of less than 1 pct (approximately 0.5 K), contained 11

Table I. Proximate and Ultimate Analysis, Total S, Gross CV, Ash Composition, and Reducing and Oxidizing AFT of Materials Considered

	An-1	An-2	An-3	An-4	An-5*	An-6	An-7	An-8	An-9*	An-10	Ch-1	Ch-2
Proximate Analysis (Air-Dried) (Pct)												
MC	3.8	1.9	2.9	2.1	1.4	1.3	3.2	1.2	1.6	3.2	4.4	5.6
Ash content	15.7	20.3	11.8	12.1	15.5	15.9	15.0	16.0	11.7	16.3	34.9	22.1
VM	5.0	9.7	4.9	4.5	6.5	8.6	4.0	7.6	5.1	5.0	8.4	4.7
FC	75.5	68.1	80.4	81.3	76.6	74.2	77.8	75.2	81.6	75.5	52.3	67.6
Ultimate Analysis (Air-Dried) (Pct)												
C	74.10	70.63	78.29	79.88	76.07	75.30	76.20	75.79	80.10	73.63	54.68	67.34
H	1.62	2.60	2.12	2.01	2.49	3.06	1.54	2.95	2.29	1.69	0.97	0.45
N	1.63	1.69	1.77	1.41	1.55	1.60	1.60	1.63	1.45	1.64	1.05	1.14
O	2.01	2.14	2.05	1.80	2.15	2.03	1.81	1.86	2.12	2.12	3.59	3.12
Total S (Air-Dried) (Pct)	1.14	0.74	1.07	0.70	0.84	0.81	0.65	0.57	0.74	1.42	0.41	0.25
Gross CV (Air-Dried) (MJ/kg)	27.21	27.24	29.49	29.51	29.35	29.59	28.13	29.69	30.5	27.4	19.49	23.45

	Co-1*	Co-2	Co-3	Co-4	Co-5	Coal-1	Coal-2	Coal-3*
Proximate Analysis (Air-Dried) (Pct)								
MC	1.2	0.2	0.6	0.4	0.4	4.0	2.3	2.8
Ash content	20.4	7.7	16.5	9.8	12.4	10.7	10.3	13.1
VM	1.6	0.6	0.8	0.8	0.9	30.9	35.5	32.2
FC	76.8	91.5	82.1	89.0	86.3	54.4	51.8	51.9
Ultimate Analysis (Air-Dried) (Pct)								
C	75.51	89.14	81.03	87.45	84.74	69.41	71.80	68.57
H	0.20	0.03	0.01	0.10	0.01	4.65	5.23	4.56
N	0.87	1.33	0.67	1.02	1.19	1.92	1.59	1.57
O	1.04	0.80	0.37	0.72	0.48	8.87	7.57	8.96
Total S (Air-Dried) (pct)	0.78	0.80	0.82	0.51	0.78	0.46	1.12	0.45
Gross CV (Air-Dried) (MJ/kg)	23.33	29.25	22.76	27.82	27.03	27.9	29.3	27.7

	An-1	An-2	An-3	An-4	An-5*	An-6	An-7	An-8	An-9*	An-10	Ch-1	Ch-2
Ash Composition (Pct)												
Al_2O_3	22.70	19.70	28.59	28.85	17.97	19.25	25.35	21.03	28.58	25.92	19.80	28.77
CaO	1.22	4.99	2.35	3.08	4.18	1.82	6.29	2.07	2.88	0.97	2.65	2.66
Cr_2O_3	6.79	16.40	0.38	0.08	1.45	0.06	0.09	0.04	0.09	3.14	26.20	6.53
Fe_2O_3	21.03	16.20	10.44	4.85	7.28	5.90	5.36	4.15	4.05	13.61	17.50	6.94
K_2O	1.33	1.00	2.42	2.03	1.69	1.77	1.79	1.64	1.57	1.49	0.33	0.45
MgO	3.31	5.28	1.30	1.43	1.33	0.87	1.59	0.86	1.29	2.39	6.25	3.52
MnO	0.11	0.14	0.10	0.07	0.11	0.07	0.10	0.07	0.06	0.07	0.17	0.09
Na_2O	1.27	1.14	2.37	1.52	0.36	0.70	3.13	1.19	1.11	1.49	0.08	0.04
P_2O_5	0.08	0.11	0.15	0.08	0.19	0.21	1.83	0.31	0.08	0.08	0.08	0.07
SiO_2	40.57	29.00	48.52	54.13	61.78	67.04	50.17	67.36	55.60	49.36	23.70	48.94
TiO_2	1.41	1.09	1.76	1.24	0.96	0.94	1.31	0.84	1.14	1.25	0.86	1.25
V_2O_5	0.13	0.18	0.15	0.06	0.08	0.06	0.04	0.05	0.06	0.07	0.21	0.10
ZrO_2	0.07	0.04	0.12	0.07	0.05	0.05	0.06	0.03	0.06	0.06	0.03	0.05
Ba	0.20	0.16	0.12	0.11	0.14	0.13	0.16	0.13	0.09	0.23	0.04	0.07
Sr	0.15	0.18	0.33	0.32	0.08	0.07	0.31	0.08	0.29	0.13	0.05	0.05
SO_3	0.72	4.32	1.77	2.85	3.18	1.50	2.33	1.32	3.89	0.86	2.31	1.20
AFT (Red. Atmos.) (K)												
T_{indef}	1591	1581	1499	1690	1517	1596	1501	1665	1743	1479	1515	1717
T_{soft}	1602	1598	1531	1711	1534	1619	1510	1679	1789	1527	1565	1729
T_{hem}	1571	1573	1517	1703	1520	1611	1483	1671	> 1823	1599	1563	1731
T_{fluid}	1662	1743	1699	1773	1657	1716	1581	1750	> 1823	1711	1757	1757
AFT (Oxid. Atmos.) (K)												
T_{indef}	1597	1591	1617	1739	1543	1639	1525	1675	> 1823	1665	1582	1729
T_{soft}	1611	1603	1671	1769	1561	1659	1538	1706	> 1823	1697	1595	1737
T_{hem}	1632	1617	1694	1781	1587	1685	1556	1724	> 1823	1712	1617	1771
T_{fluid}	1759	1795	1763	1819	1705	1785	1633	1803	> 1823	1759	1803	1817

Table I. continued

	Co-1*	Co-2	Co-3	Co-4	Co-5	Coal-1	Coal-2	Coal-3*
Ash Composition (Pct)								
Al_2O_3	17.41	24.88	19.77	24.89	22.42	24.39	19.23	23.59
CaO	1.69	1.78	1.55	5.32	3.74	3.52	0.99	2.28
Cr_2O_3	5.64	1.79	0.88	2.20	4.57	0.44	0.44	0.13
Fe_2O_3	12.16	17.00	9.01	15.09	14.87	3.75	5.66	2.77
K_2O	0.95	1.95	1.16	1.72	2.25	1.08	1.03	1.19
MgO	1.93	1.09	0.78	3.03	2.30	1.51	0.55	1.03
MnO	0.16	0.12	0.12	0.20	0.13	0.02	0.08	0.01
Na_2O	0.09	0.92	0.11	1.37	1.25	0.27	0.22	0.16
P_2O_5	0.17	0.33	0.21	1.11	0.29	0.27	0.11	0.09
SiO_2	57.45	48.34	63.35	40.21	46.15	59.43	68.66	65.97
TiO_2	1.43	1.25	1.69	1.00	0.93	1.28	1.76	1.00
V_2O_5	0.16	0.11	0.14	0.10	0.11	0.05	0.12	0.03
ZrO_2	0.14	0.04	0.17	0.04	0.04	0.11	0.18	0.08
Ba	0.08	0.12	0.12	0.31	0.19	0.08	0.08	0.05
Sr	0.04	0.11	0.06	0.19	0.11	0.11	0.05	0.04
SO_3	1.02	0.68	0.90	2.72	1.32	3.20	0.76	1.36
AFT (Red. Atmos.) (K)								
T_{indef}	1547	1463	1607	1498	1409	1651	1719	1727
T_{soft}	1593	1491	1642	1517	1415	1681	1739	1785
T_{hem}	1575	1500	1639	1561	1429	1662	1721	1769
T_{fluid}	1729	1671	1729	1748	1727	1735	1775	> 1823
AFT (Oxid. Atmos.) (K)								
T_{indef}	1621	1638	1652	1539	1505	1736	1758	1781
T_{soft}	1645	1651	1670	1561	1541	1768	1777	1817
T_{hem}	1654	1667	1703	1651	1581	1792	1798	> 1823
T_{fluid}	1793	1731	1777	1795	1787	1822	1823	> 1823

*These samples were excluded from the MLR calculations but were used to verify the accuracy of the MLR calculations.

independent variables. Considering that the uncertainty associated with AFT measurements is 30 K (SABS ISO 540:2008), the afore-mentioned RMSE differences between calculated T_{soft} values and the experimental values (1.7 and 0.5 K, respectively) could be considered as over-fitting of the data. However, the differences in T_{soft} between the applied rule (1 pct relative improvement in RMSE) and if a 30 K RMSE limitation was considered were found to be approximately 50 to 100 K for the T_{soft}. Within the context of industrial application and optimum selection of PF coal, 50 to 100 K lower/higher T_{soft} can have a significant effect on damring formation. Therefore, it was decided to rather implement a relative improvement in RMSE as described, which is quantifiable (is associated with a rule) and gave more accurate calculated T_{soft} values. These two optimized equations for calculating reducing T_{soft} and oxidizing T_{soft} are presented in Eqs. [2] and [3], respectively.

$$T_{soft(reducing)} = \begin{aligned} &-1.4286E4 + (1.7570E2 \times MC) + (1.5738E2 \times Ash) + (1.6621E2 \times C) \\ &+(2.5337E2 \times H) + (1.3008E2 \times O) + (-1.8626E2 \times K_2O) + \\ &(-1.1178E2 \times P_2O_5) + (-5.0067E2 \times V_2O_5) + (7.1129E2 \times Sr) + \\ &(-3.5258E1 \times SO_3) \end{aligned} \quad [2]$$

$$T_{soft(oxidizing)} = \begin{aligned} &2.1568E3 + (-2.4588E1 \times MC) + (-5.1311E0 \times FC) + (-3.4287E0 \times H) + \\ &(1.2248E1 \times Al_2O_3) + (-1.4721E2 \times K_2O) + (-6.4158E1 \times MgO) + \\ &(1.5306E2 \times MnO) + (-1.2579E2 \times P_2O_5) + (-6.9090E2 \times ZrO_2) \\ &+(1.8523E2 \times Ba) + (4.8366E2 \times Sr) \end{aligned} \quad [3]$$

In order to assess the accuracy of the method, calculated reducing and oxidizing T_{soft} values were plotted against the experimentally determined values, as indicated in Figures 5(a) and (b), respectively. As mentioned in Section II–B, four samples were not included in the computation of the MLR equation. The T_{soft} values for these four samples were calculated using the MLR equations obtained. The measured as well as the calculated T_{soft} values (using Eqs. [2] and [3])

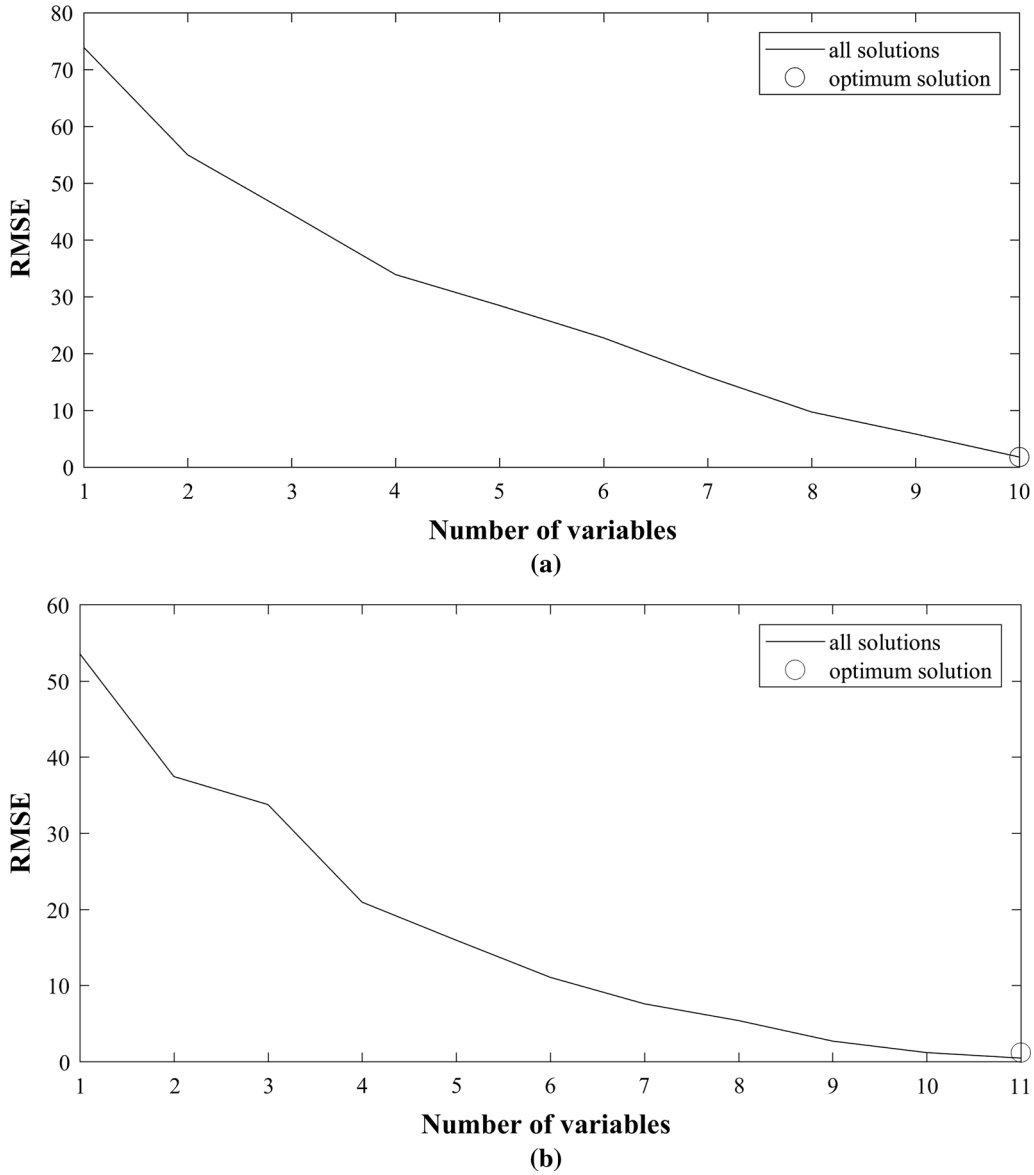

Fig. 4—RMSE between the calculated and experimental T_{soft} for reducing (*a*) and oxidizing (*b*) atmospheres.

of these samples are shown in Figures 5(a) and (b). An-9 was not included in the MLR calculations because its oxidizing T_{soft} was above the AFT test limitation of 1823 K (1550 °C). However, its reducing T_{soft} value was within the limit and could still be used as an assessment of the accuracy of Eq. [2]. The other three samples that were left out from the MLR calculation (*i.e.*, An-5, Co-1, and Coal-3) were selected randomly to assess both Eqs. [2] and [3].

As is evident from Figure 5(a), the reducing T_{soft} of the four additional samples (An-9, An-5, Co-1, and Coal-3) compared relatively well with the linear relationship derived from the optimized MLR equation, although two of the values (An-9 and Coal-3) differed by just more than the 30 K standard deviation associated with AFTs.[19] However, within the context of the absolute values of reducing T_{soft}, which ranged between 1415 and 1789 K, the calculated T_{soft} of even these samples that did not fit perfectly on the predicted line would still be useful for selecting PF coal better (to reduce damring formation). For the oxidizing T_{soft} (Figure 5(b)), the values of two of the three additional samples (Co-1 and Coal-3) correlated very well with the linear relationship derived from the MLR calculations, while An-5 was still a good fit if the 30 K standard deviation[19] is taken into account. The calculated oxidizing T_{soft} of An-9 (using Eq. [3]) was also added to the figure, even though the experimental value could not be determined.

Chen and Jiang introduced equations cited by Liu *et al.*[20] that differ from those determined during this study, for predicting oxidizing AFTs of Chinese coal. The method that is suggested in Liu *et al.*[20] consists of four different equations, with the one that has to be applied selected based on the compositional content of the sample. As a comparison, this method was applied to calculate the oxidizing T_{soft} of the samples that was left out of the MLR calculations (*i.e.*, An-5, An-9, Co-1,

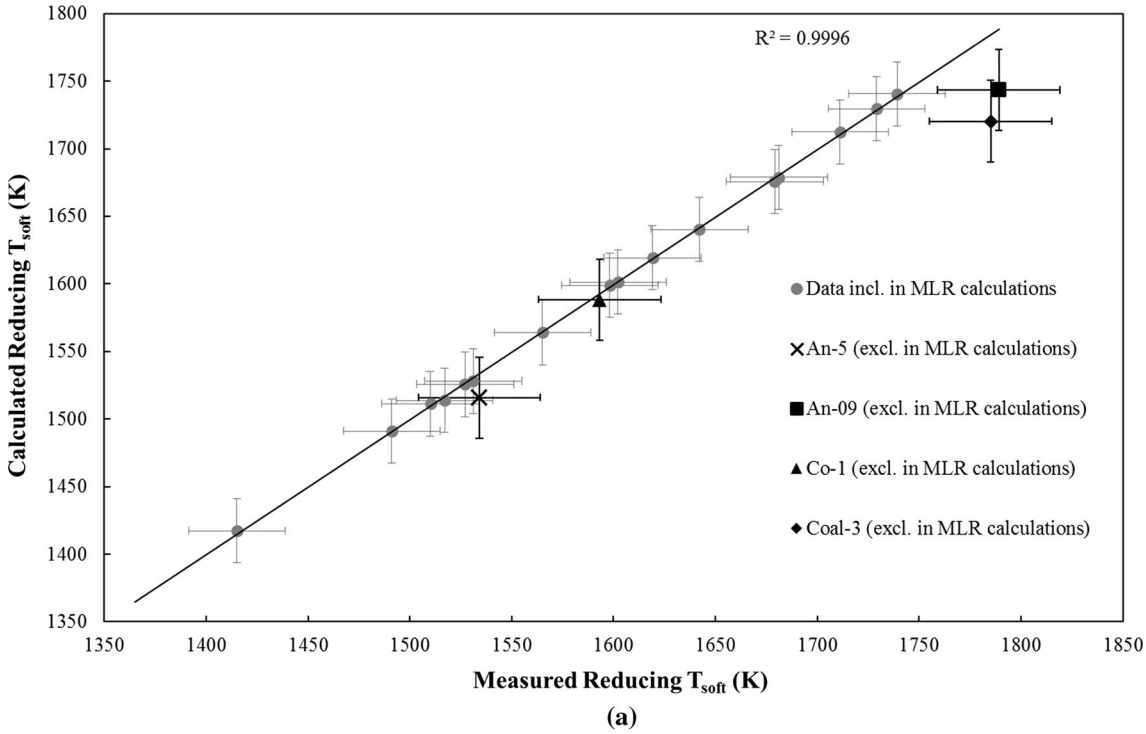

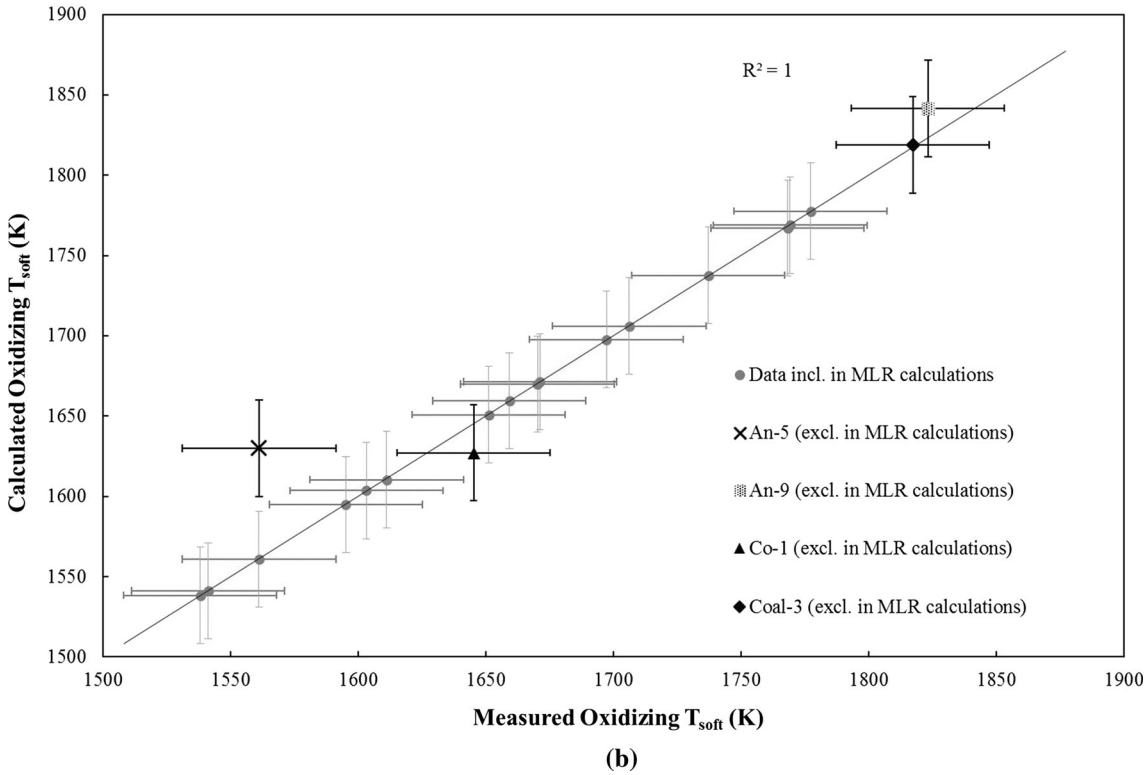

Fig. 5—Correlations of calculated (Eqs. [2] and [3]) and experimental (Table I) T_{soft} values for reducing (*a*) and oxidizing (*b*) environments using a bivariate correlation method.[33] The error bars indicate the 30 K standard deviation that is common for AFT measurements.

and Coal-3). Since the equations given by Liu *et al.*[20] was only for oxidizing T_{soft}, Eq. [3] was used to calculate the T_{soft} so that the two methods can be compared. The experimental value of the oxidizing T_{soft} for An-9 is given as $>$ 1823 K (1550 °C). Using the equation proposed Chen and Jiang as cited by Liu *et al.*,[20] the oxidizing T_{soft} was calculated as 1710 K (1437 °C), which is too low. An-5 had an experimental value of 1561 K (1288 °C) and with the equation in Liu *et al.*[20] it was calculated as 1575 K (1303 °C), which is fairly

accurate. Co-1 and Coal-3 had experimental values of 1654 K and 1817 K (1372 °C and 1544 °C), which were calculated with the Liu *et al.*[20] equations as 1588 K and 1721 K (1315 °C and 1447 °C), respectively. Even though the calculated values seem to be reasonable, the average error using the equation by Liu *et al.*[20] is more than 3 pct. Therefore, the equations proposed in this paper seem to enable similar, or even better accuracy, to calculate T_{soft} than what has been proposed before. The higher accuracy might be due to the inclusion of more independent variables during the determination of the optimum mathematical solution. Our method also only has one equation for calculating oxidizing T_{soft}, which is much simpler than the four equation method proposed by the afore-mentioned authors.[20] Additionally, the equations proposed in the current paper enables calculation of reducing T_{soft}, which has been proven to be important within the application of chromite pre-reduction in rotary kilns.[17]

Several authors[34–36] have proposed statistical techniques to calculate parameters that can be used in the interpretation of regression results and to determine the contributions of the different independent variables. For instance, beta weights (β) are applied to standardized variable scores in the MLR equation and can be used to interpret independent variable contribution to the regression effect. Structure coefficients (r_s) are another method that was examined by Kraha *et al.*[34] Structure coefficients are Pearson correlations between the predicted value given by the regression equation and each independent variable. A squared structure coefficient (r_s^2) gives an indication of the contribution of each independent variable to the variance given by the structure coefficient. A negative r_s value show that there is an inverse proportional correlation between the independent variable and the predicted value. Commonality coefficients can also be calculated using the SPSS programming software. Two types of commonality coefficients exist, namely unique and common coefficients. Unique coefficients reveal the amount of variance an independent variable contributes to the MLR equation on its own without sharing its contribution in predicting the dependent variable with other variables. Common coefficients reflect the contribution of an independent variable in combination with one or more independent variables. The commonality coefficients are used to give more information on the covariance between the different independent variables that could not be understood when using β weights.[36] According to Lorenzo-Seva *et al.*,[35] relative important weight (RIW) is a measure of the proportionate contribution of each independent variable to R^2, after correcting for the effects of the intercorrelation among independent variables. The sum of the RIW is equal to R^2. For the purposes of this paper, the authors mainly focused on the RIW values. All the statistical parameters that were calculated with the SPSS programming software are presented in Table II.

According to RIW values for reducing T_{soft}, K_2O content made the largest contribution to the variance, with a value of 20.8 pct. It can also be seen from the commonality coefficients that K_2O contributed 14.51 pct uniquely to the variance. Other independent values with relatively large RIW values were H (20.4 pct), P_2O_5 (12.3 pct), O (11.6 pct), and V_2O_5 (8.9 pct). From these results, it can be seen that the intercorrelation between the different variables are very complex and even though the ash components (K_2O, V_2O_5, P_2O_5, *etc.*) contributed significantly to the variance (total of their RIW values = 47.5 pct), they are not the only determining factor. It was also interesting to note that some ash species such V_2O_5 and Sr, which had very low ash compositions (below 0.33 pct), contributed significantly to the variance (8.9 and 4.7 pct RIW, respectively, in Table II). As previously stated, elements occurring in the ash could occur in a different phase as what is presented in the standard ash composition analysis (Table I). To fully understand the impact of individual species and/or combinations of species on the reducing T_{soft}, additional investigations would be required. However, this would make the scope of the current work too extensive. Therefore, deductions from previous investigations were considered. For instance, Wang *et al.*[37] indicated that V_2O_3, rather than V_2O_5, is the most likely form of V in a reducing atmosphere. The melting point of V_2O_3 2213 K (1940 °C) is significantly higher than that of V_2O_5 963 K (690 °C),[37] which at least partially explaining why the small V content contributed to a higher T_{soft}.

For the oxidizing T_{soft}, P_2O_5 had the highest RIW value of 18.4 pct. MnO and MgO had RIW of 14.3 and 13.2 pct, respectively. Combined the ash components had a RIW contribution of 79.0 pct. Considering the commonality coefficients P_2O_5 only contributes 8.8 pct uniquely, but commonly contributed 20.67 pct. MnO commonly contributed 53.35 pct, while uniquely only 0.11 pct. For the oxidizing T_{soft}, the unique contributions were relatively small. P_2O_5 had the largest unique contribution (8.8 pct), while all the other variable contributions were less than 5 pct. However, commonly (total of "common" in Table II) the ash components had a large contribution, showing that the interaction between the different ash components played a significant role in predicting AFT for an oxidizing atmosphere.

Detailed ash compositional analyses, which include trace compositions as considered thus far, are not always available to FeCr producers. Therefore, alternative MLR analyses were also conducted by only considering parameters/species obtained from the most common analyses (*i.e.*, proximate and ultimate analyses,

Table II. Statistical Parameters that Were Calculated with SPSS Software for the Interpretation of Regression Results and to Determine the Contributions of the Different Independent Variables to the Calculated AFTs

Variable	β	$r_s \cong r$	$(r_s)^2 \cong R^2_{yx}$	Unique	Common	RIW (Pct)
Red Soft Temp						
MC	2.943	0.364	0.1325	0.1134	0.0191	5.3
Ash	10.486	0.098	0.0097	0.1808	− 0.1712	7.1
C	14.367	0.41	0.1677	0.1847	− 0.0169	8.1
H	4.231	0.568	0.3222	0.2075	0.1148	20.4
O	3.168	0.552	0.3037	0.1516	0.1521	11.6
K_2O	− 1.138	0.504	0.2532	0.1451	0.1082	20.8
P_2O_5	0.556	0.385	0.1477	0.1481	− 0.0004	12.3
V_2O_5	0.263	0.161	0.0258	0.0197	0.006	8.9
Sr	0.707	0.257	0.0658	0.0502	0.0156	4.7
SO_3	− 0.389	0.039	0.0015	0.0465	− 0.0449	0.8
Ox Soft Temp						
MC	− 0.476	0.269	0.0724	0.0265	0.0459	3.4
FC	− 0.81	− 0.409	0.1673	0.0125	0.1548	6.5
H	− 0.084	0.576	0.3323	0.0003	0.332	11
Al_2O_3	0.516	0.199	0.0397	0.0484	− 0.0087	10.1
K_2O	− 1.122	0.208	0.0432	0.1107	− 0.0675	7.6
MgO	− 1.379	− 0.417	0.1741	0.0448	0.1293	13.2
MnO	0.097	− 0.731	0.5346	0.0011	0.5335	14.3
P_2O_5	− 0.768	− 0.543	0.2951	0.0883	0.2067	18.4
ZrO_2	− 0.416	0.481	0.2312	0.0191	0.212	5.9
Ba	0.189	− 0.524	0.2741	0.006	0.2681	6.2
Sr	0.615	− 0.185	0.0341	0.0207	0.0133	3.5

CV, as well as S and P contents) as independent parameters. Such optimized MLR equations are indicated in Eqs. [4] and [5].

$$\begin{aligned} T_{soft(reducing)} = {} & 5.1644E4 + (-4.4774E2 \times MC) + (-5.0252E2 \times Ash) + (-5.7204E2 \times S) + \\ & (-4.9658E2 \times C) + (-3.8675E2 \times H) + (-8.2477E2 \times N) \\ & + (-5.2977E2 \times O) \end{aligned} \quad [4]$$

$$\begin{aligned} T_{soft(oxidizing)} = {} & 4.9162E4 + (-4.7869E2 \times MC) + (-4.7767E2 \times Ash) + (-4.0485E2 \times VM) + \\ & (-3.7872E2 \times FC) + (8.1854E0 \times CV) + (-9.6356E1 \times C) + \\ & (-4.1131E2 \times N) \end{aligned} \quad [5]$$

The above-mentioned optimized MLR equations had RMSE differences between the calculated and experimental reducing and oxidizing T_{soft} of 39.3 and 41.4 K, respectively. Therefore, these values are less accurate than those calculated with Eqs. [2] and [3]; however, they are still very useful as coarse-grained estimates of reducing and oxidizing T_{soft}.

C. *Sessile Drop Analysis of Chromite, Composite Pellet Mixtures, and Pellet Components*

Ringdalen *et al.*[24] used three points to define different stages of melting and/or reduction of manganese ores during sessile drop tests, *i.e.* (a) initiation of melting that is defined as the temperature at which liquid became visible on the surface of the ore; (b) completion of melting, when the ore appeared to be completely liquid; (c) start of reduction, when the first gas bubbles were evolved from the sample. None of the afore-mentioned temperatures can be directly correlated with the T_{soft} determined with AFT, which was used in Section III–B as a possible indication of the initiation of damring formation. Therefore, for the purpose of this study it was decided to consider the sessile drop test temperature at which any sign of deformation occurred, as an indication of possible damring formation. This can be in the form of bubbling, lifting, movement, rounding of corners, *etc*. Figures 6, 7, and 8 present example images of how deformation was detected during the sessile drop tests for ores, composite pellet mixtures, and the bentonite clay, respectively.

Table III presents the deformation temperatures derived from the sessile drop tests for all the samples considered. There are several important deductions that can be made from these results, within the context of this paper. The deformation temperatures of all the ores ranged between 1738 K and 2029 K (1465 °C and

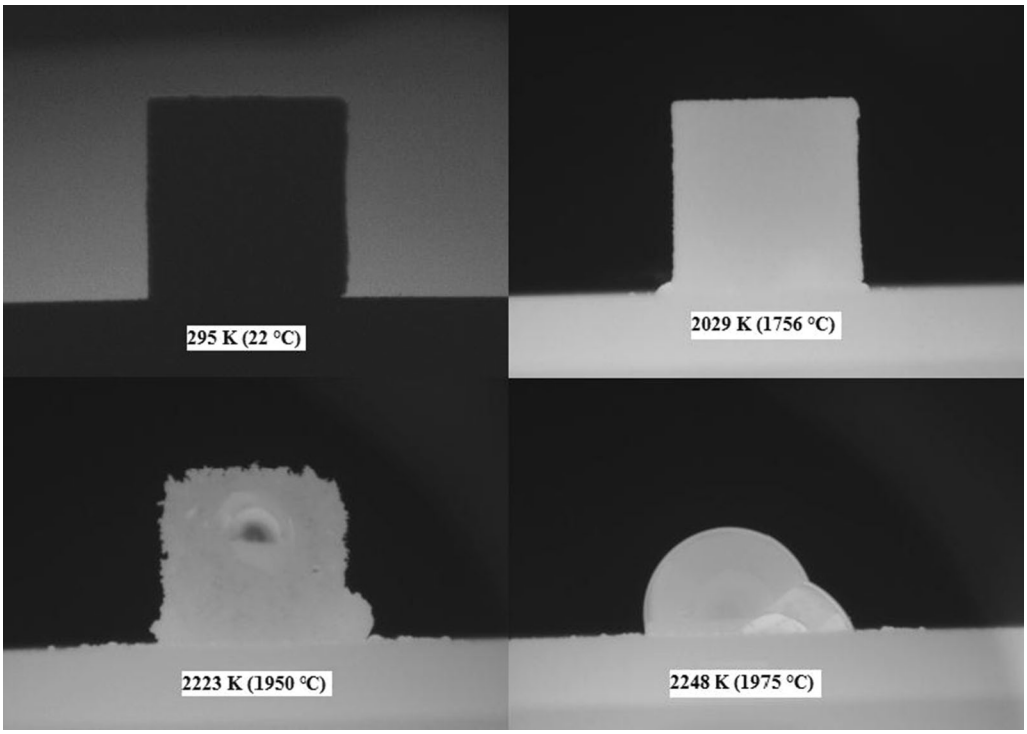

Fig. 6—Sessile drop test images of Kroondal metallurgical grade chromite ore. The first sign of deformation was visible at 2029 K (1756 °C) in the form of softening of the pellet bottom. At 2223 K (1950 °C), the sample continued to soften to the point where it was considered to be melted, which was at 2248 K (1975 °C), at which point the sample took a spherical shape.

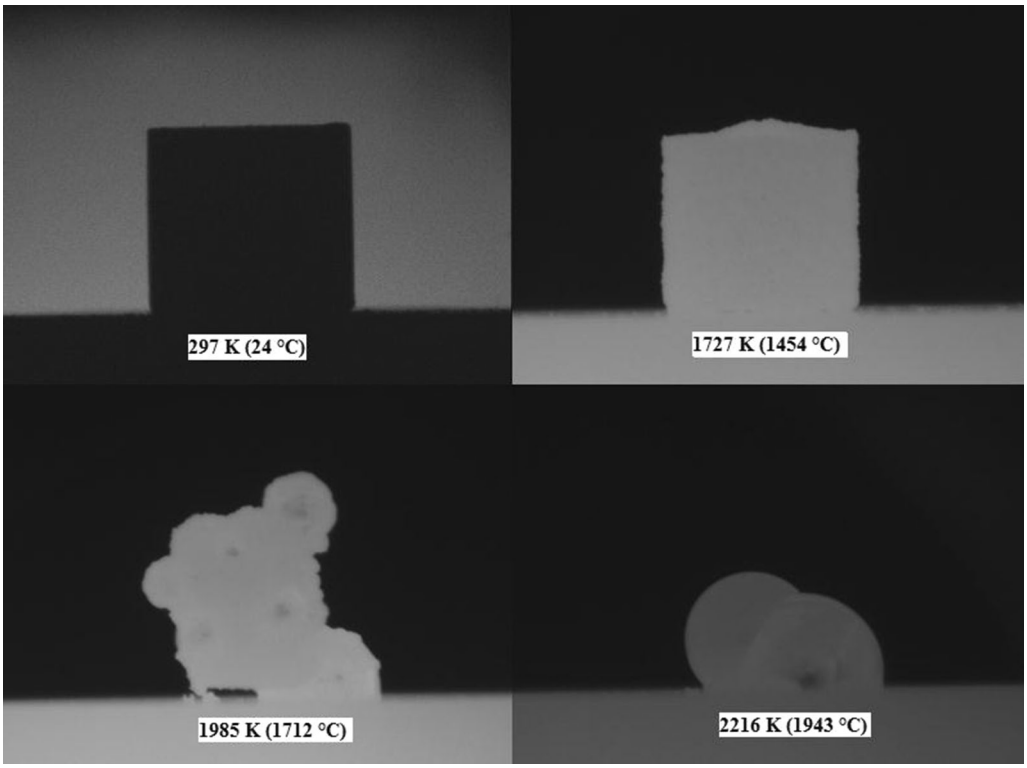

Fig. 7—Sessile drop test images of composite pellet mixture (containing Kroondal metallurgical grade ore). The first sign of deformation occurred at 1727 K (1454 °C). The sample continued to deform as can be seen at 1985 K (1712 °C) until the melting point was reached where the sample took a spherical shape, which was at 2216 K (1943 °C).

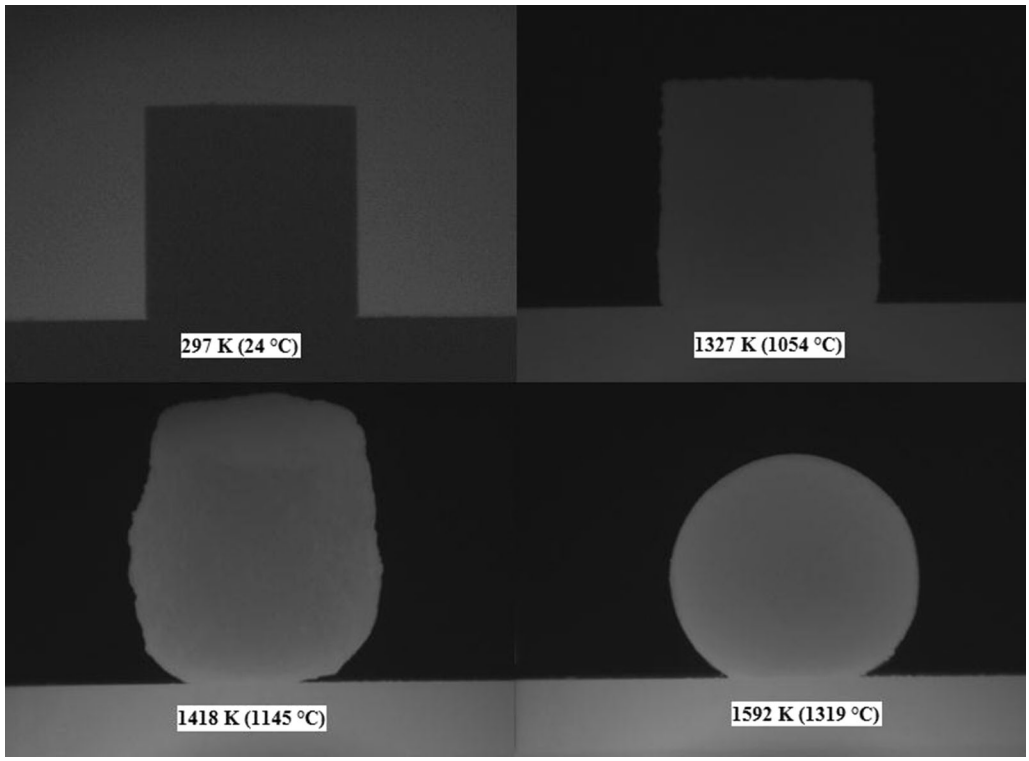

Fig. 8—Sessile drop test images of bentonite clay. The clay started swelling at 1327 K (1054 °C), at 1418 K (1145 °C) the edges started rounding, and at 1592 K (1319 °C) the sample was completely melted as it took a spherical shape.

Table III. Temperatures of Deformation of the Different Ores, Composite Pellet Mixtures, and Pellet Components According to the Sessile Drop Tests

	First Point of Deformation	Description
Ore		
DRB ECD	1951	lifting at bottom left corner
DRB MetC	1773	bottom lifting up
Helena	1843	bottom right corner lifting up
Kroondal	2029	bottom left corner softening
MMG	1739	bubble on right upper corner
UG2	1917	bubbling at the top
TWF	1901	lifting at bottom left corner
Pellet Ore Mixtures		
DRB ECD mix	1739	small bubble in middle
DRB met conc mix	1712	bubble on left
Helena mix	1689	lifting at the bottom
Kroondal mix	1727	lifting at the top
MMG mix	1730	bubbles on top and left
UG2 mix	1734	lifting
TWF mix	1646	lifting at the right corner
Nkomati anthracite	1519	bubbling on the left side
Clay	1328	bubbling edges

1756 °C), which are significantly higher than the typical maximum temperature of the pellets being pre-reduced in a chromite pre-reduction rotary kiln, *i.e.*, 1573 K (1300 °C). It is therefore unlikely that the ores alone will contribute to damring formation. The composite pellet mixtures had significantly lower deformation temperatures, which ranged from 1646 K to 1739 K (1373 °C to 1466 °C), than the ores alone. However, these temperatures were still above the typical maximum pellet pre-reduction temperature. Therefore, limited contribution to damring formation can be expected from composite pellets. Fragmentation of composite pellets (pellet breakdown) due to various reasons (*e.g.*, too high moisture content of green pellets, too fast heating in

heating chambers prior to rotary kiln) can release small amounts of reductants and/or clay which can contribute to damring formation, since the deformation temperatures of these materials were 1529 K and 1327 K (1256 °C and 1054 °C), respectively. The UG2 ore and the UG2 containing composite pellet mixture did not have the lowest deformation temperatures, when compared with the other metallurgical grade chromite ores and the correlating composite pellet mixtures. The commonly held industry perception that UG2 ore will lead to quicker and/or more excessive damring formation is therefore not true.

D. *Surface Analysis of Damrings*

In order to augment the results derived from the AFT and sessile drop tests, and associated statistical processing thereof, actual damrings were also considered. Several damring fragments that were broken out of a pre-reduction kiln during a shutdown were polished without the addition of resin to avoid carbon contamination and examined with SEM-EDS. In Figure 9, a SEM micrograph of a cross-sectional polished representative specimen is presented. From this micrograph, it is evident that the damrings consisted of lighter colored particles (elements with higher atomic numbers) that are bonded together with a darker colored matrix (elements with lower atomic numbers). Average EDS analyses of the lighter colored particles (points 1, 2, and 3 in Figure 9) and darker areas (points 4, 5, 6, and 7) are indicated in Table IV. From these results, it can be deducted that the lighter colored particles are mainly pellet fragments, since the Cr (24.6 wt pct) and Fe (16.0 wt pct) contents, and Cr/Fe ratio (1.54) resembled typical South African metallurgical grade chromite ore.[38] The small amount of C present in these particle can possibly originate from the carbon reductant included in the composite pellet mixture. This C can be present as free C or as part of metal carbides that form during pre-reduction. In contrast, the darker matrix, which surrounded the afore-mentioned pellet fragments, only contained trace amounts of Cr and Fe. However, this matrix contained a significant amount of Si that is the most prevalent PF coal ash element (Table I). Also, this darker matrix contained very high concentrations of C, which is indicative of unburned PF coal. Such high C contents will not be possible if the matrix was dominated by the clay binder and/or the gangue minerals included in the composite pellets.

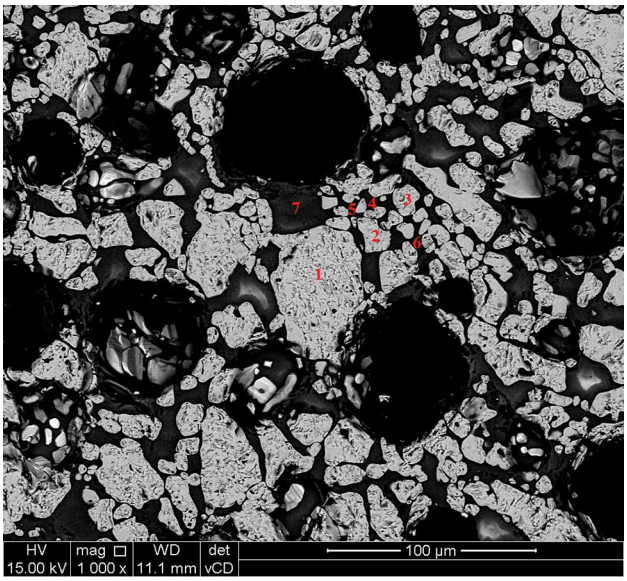

Fig. 9—SEM micrograph of a polished section of damring fragment broken out of a chromite pre-reduction rotary kiln. Numbers 1 to 7 indicate areas that were analyzed with EDS.

IV. CONCLUSIONS

As far as the authors could assess, this is the first study published in the peer-reviewed public domain that assesses the possible contribution of carbonaceous PF ash, chromite ore, as well as composite pellet mixtures to damring formation in chromite pre-reduction rotary kilns.

It was proven that the oxidizing and reducing AFTs of some carbonaceous PF were below the typical maximum temperature of pre-reduced pellets in a chromite pre-reduction process, *i.e.*, 1573 K (1300 °C). However, for the pellets to be heated to approximately 1573 K (1300 °C), the actual PF flame temperature must be significantly higher. Therefore, PF ash was identified as the most likely source of damring formation. This does not imply that damrings consist exclusively of PF ash. In reality, damrings contain > 30 wt pct Cr_2O_3. This significant Cr content, combined with the afore-mentioned result, implies that the PF ash is the "glue" that binds chromite particles originating from composite pellet fragments and/or disintegrated pellets together. However, the different carbonaceous materials evaluated in this study had significantly different AFTs.

Table IV. Average EDS Analyses (Weight Percent) of Lighter (Areas 1, 2, and 3) and Darker Areas (Areas 4, 5, 6, and 7) in the Micrograph (Figure 9) of a Cross-Sectional Polished Damring Fragment

Areas	C	O	Na	Mg	Al	Si	K	Ca	Ti	V	Cr	Fe	Total
1,2,3	8.28	39.41		5.04	6.5	0.26					24.58	15.92	100
4,5,6,7	36.73	42.5	0.15	0.54	3.21	13.84	0.28	0.91	0.56	0.18	0.16	0.96	100

Therefore, if ferrochrome producers want to limit damring formation, AFTs have to be specified as selection criteria for procurement of PF. Currently, only proximate analyses and cost considerations are used to select PFs. If determining AFTs is not practical, the MLR equations (Eqs. [2] and [3]) derived in this study can be used to estimate the oxidizing and reducing T_{soft}. An important future prospective would be to investigate the influence of independent variables included in the afore-mentioned optimum MLR equations, as well as the interaction between species and ash species with the clay binder and the silicate gangue.

Sessile drop tests proved that chromite ores will not contribute significantly to damring formation. Composite pellet mixtures, containing both a carbonaceous reductant and a clay binder, had lower deformation temperatures than the ores alone. However, these deformation temperatures were still above the typical maximum temperature of pre-reduced pellets in a chromite pre-reduction process. Therefore, limited contribution to damring formation is expected from composite pellets. However, pellet fragmentation could release carbonaceous reductant ash and clay binder particles, both of which had much lower deformation temperatures. It was also proven that UG2 ore does not necessarily contribute more to damring formation than metallurgical grade chromite ore. Each ore and composite pellet mixture has to be evaluated separately to assess its possible contribution to damring formation.

SEM-EDS analyses of actual damrings proved that the damrings consisted of chromite pellet fragments, which were bonded together with a matrix mainly originating from the PF coal ash, which supported the earlier conclusions.

ACKNOWLEDGMENTS

The financial assistance of the National Research Foundation (NRF) toward the PhD studies of Y. van Staden is hereby acknowledged. Opinions expressed and conclusions arrived at are those of the authors and are not necessarily to be attributed to the NRF. The authors would also like to acknowledge the South African Research Chairs Initiative of the Department of Science and Technology (Coal Research Chair Grant No. 86880) for financial support provided for material characterization analyses. The support from the Norwegian Research Council through the project ''Metal production – education, competence and research'' (261692/H30) is also acknowledged for encouraging and funding cooperation between South Africa and Norway, as well as funding from the Research Project 233825/E30 CORALSEA (Chrome Oxide Reduction – an Atomic Level modelling and Spectrographic Experimental Approach) and by the SFI Metal Production (Centre for Research-based Innovation, 237738).

OPEN ACCESS

REFERENCES

1. S.E. Haggerty: *Rev. Miner. Geochem.*, 1991, vol. 25, pp. 355–416.
2. M. Riekkola-Vanhanen: *Finnish Expert Report on Best Available Techniques in Ferrochromium Production*, Helsinki, 1986.
3. Y.R. Murthy, S.K. Tripathy, and C.R. Kumar: *Miner. Eng.*, 2011, vol. 24, pp. 375–80. https://doi.org/10.1016/j.mineng.2010.12.001.
4. D.S. Rao, S.I. Angadi, S.D. Muduli, and B.D. Nayak: *At Miner. Process. Eng. Ed.*, 2010, vol. 51, pp. 2–6.
5. J. Daavittila, M. Honkaniemi, and P. Jokinen: *J. S. Afr. Inst. Min. Metall.*, 2004, vol. 104, pp. 514–49.
6. W. Biermann, R.D. Cromarty, and N.F. Dawson: *J. S. Afr. Inst. Min. Metall.*, 2012, vol. 12, pp. 301–08.
7. O. Naiker and T. Riley: *Proceedings of the Southern African Pyrometallurgy Conference*, Johannesburg, South Africa, March 2006, pp. 297–306.
8. C. Takano, A.P. Zambrano, A.E.A. Nogueira, M.B. Mourao, and Y. Iguchi: *ISIJ Int.*, 2007, vol. 47, pp. 1585–89. https://doi.org/10.2355/isijinternational.47.1585.
9. S. McCullough, S. Hockaday, C. Johnson, and N.A. Barcza: *Proceedings of 12th International Ferroalloys Congress*, Helsinki, June 2010, pp. 249–62.
10. O. Naiker: *Proceedings of 11th International Ferroalloys Congress*, New Delhi, India, February 2007, pp. 112–19.
11. J.P. Beukes, S.P. Du Preez, P.G. van Zyl, D. Paktunc, T. Fabritius, M. Päätalo, and M. Cramer: *J. Cleaner Prod.*, 2017, vol. 165, pp. 874–89. https://doi.org/10.1016/j.jclepro.2017.07.176.
12. G.T.M. Mohale, J.P. Beukes, E.L.J. Kleynhans, P.G. van Zyl, J.R. Bunt, L.R. Tiedt, A.D. Venter, and A. Jordaan: *J. S. Afr. Inst. Min. Metall.*, 2017, vol. 117, pp. 1045–52. https://doi.org/10.17159/2411-9717/2017/v117n11a9.
13. N.F. Dawson and R.I. Edwards: *Proceedings of 4th International Ferroalloys Congress*, Sao Paulo, Brazil, August 1986, pp. 105–13.
14. R.C. Nunnington and N.A. Barcza: *Proceedings of 5th International Ferroalloys Congress*, New Orleans, USA, March 1989, pp. 55–68.
15. P. Weber and R.H. Eric: *Miner. Eng.*, 2006, vol. 19, pp. 318–24. https://doi.org/10.1016/j.mineng.2005.07.010.
16. B. Neizel, J.P. Beukes, P.G. Van Zyl, and N.F. Dawson: *Miner. Eng.*, 2013, vol. 45, pp. 115–20. https://doi.org/10.1016/j.mineng.2013.02.015.
17. E.L.J. Kleynhans, J.P. Beukes, P.G. Van Zyl, P.H.I. Kestens, and J.M. Langa: *Miner. Eng.*, 2012, vol. 34, pp. 55–62. https://doi.org/10.1016/j.mineng.2012.03.021.
18. E.L.J. Kleynhans, J.P. Beukes, P.G. van Zyl, R.J. Bunt, N.S.B. Nkosi, and M. Venter: *Metall. Mater. Trans. B*, 2017, vol. 48, pp. 827–40. https://doi.org/10.1007/s11663-016-0878-4.
19. M.V. Nel, C.A. Strydom, H. Schobert, J.P. Beukes, and J.R. Bunt: *Fuel Process. Technol.*, 2014, vol. 124, pp. 78–86. https://doi.org/10.1016/j.fuproc.2014.02.014.
20. Y.P. Liu, M.G. Wu, and J.X. Qian: *Thermochim. Acta*, 2007, vol. 454, pp. 64–68. https://doi.org/10.1016/j.tca.2006.10.026.
21. S. Chakravarty, A. Mohanty, A. Banerjee, R. Tripathy, G.K. Mandal, M.R. Basariya, and M. Sharma: *Fuel*, 2015, vol. 150, pp. 96–101. https://doi.org/10.1016/j.fuel.2015.02.015.
22. E.C. Winegartner and B.T. Rhodes: *J. Eng. Power.*, 1975, vol. 97, pp. 395–406. https://doi.org/10.1115/1.3446018.

23. S. Gaal, D. Lou, S. Wasbø, B. Ravaray and M. Tangstad: *Proceedings of 11th International Ferroalloys Congress*, New Delhi, India, February 2007, pp. 247–57.
24. E. Ringdalen, S. Gaal, M. Tangstad, and O. Ostrovski: *Metall. Trans. B*, 2010, vol. 41B, pp. 1220–29. https://doi.org/10.1007/s11663-010-9350-z.
25. J. Safarian, L. Kolbeinsen, M. Tangstad, and G. Tranell: *Metall. Trans. B*, 2009, vol. 40B, pp. 929–39. https://doi.org/10.1007/s11663-009-9294-3.
26. S.P. Du Preez, J.P. Beukes, and P.G. Van Zyl: *Metall. Mater. Trans. B*, 2015, vol. 46, pp. 1002–10. https://doi.org/10.1007/s11663-014-0244-3.
27. A.D. Venter, J.P. Beukes, P.G. Van Zyl, E.G. Brunke, C. Labuschagne, F. Slemr, R. Ebinghaus, and H. Kock: *Atmos. Chem. Phys.*, 2015, vol. 15, pp. 10271–80. https://doi.org/10.5194/acp-15-10271-2015.
28. N.R. Awang, N.A. Ramli, A.S. Yahaya, and M. Elbayoumi: *Atmos. Pollut. Res.*, 2015, vol. 6, pp. 726–34. https://doi.org/10.5094/APR.2015.081.
29. E.L.J. Kleynhans, B.W. Neizel, J.P. Beukes, and P.G. Van Zyl: *Miner. Eng.*, 2016, vol. 92, pp. 114–24. https://doi.org/10.1016/j.mineng.2016.03.005.
30. Sentula mining: *Nkomati Anthracite (Pty) Ltd*, http://www.sentula.co.za/?page_id=28, accessed 15 Aug 2017.
31. J.C. van Dyk and M.J. Keyser: *J. S. Afr. Inst. Min. Metall.*, 2005, vol. 105, pp. 1–6.
32. W.J. Song, L.H. Tang, X.D. Zhu, Y.Q. Wu, Z.B. Zhu, and S. Koyama: *Energy Fuels*, 2009, vol. 24, pp. 182–89. https://doi.org/10.1021/ef800974d.
33. K. Thirumalai, A. Singh, and R. Ramesh: *J. Geol. Soc. India*, 2011, vol. 77, pp. 377–80. https://doi.org/10.1007/s12594-011-0044-1.
34. A. Kraha, H. Turner, K. Nimon, L.R. Zientek, and R.K. Henson: *Front. Psychol.*, 2012, vol. 3, pp. 1–16. https://doi.org/10.3389/fpsyg.2012.00044.
35. U. Lorenzo-Seva, P.J. Ferrando, and E. Chico: *Behav. ResMethods*, 2010, vol. 42, pp. 29–35. https://doi.org/10.3758/BRM.42.1.29.
36. L.L. Nathans, F.L. Oswald, and K. Nimon: *Pract. Assess. Res. Eval.*, 2012, vol. 17, pp. 1–19.
37. Z. Wang, J. Bai, L. Kong, Z. Bai, and W. Li: *Energy Fuels*, 2013, vol. 27, pp. 7303–13. https://doi.org/10.1021/ef401651w.
38. L.A. Cramer, J. Basson, and L.R. Nelson: *J. S. Afr. Inst. Min. Metall.*, 2004, vol. 104, pp. 517–27.